

Universidade Federal de Minas Gerais
Escola de Engenharia
Programa de Pós-Graduação em Engenharia Elétrica

Detecção e Localização de Distúrbios Transitórios em Linhas de Transmissão de Energia Utilizando Sensores sem Fio

Dênio Teixeira Silva

Tese de Doutorado apresentada ao Programa de Pós-Graduação em Engenharia Elétrica da Universidade Federal de Minas Gerais, como requisito parcial para obtenção do título de Doutor em Engenharia Elétrica.

Orientador: Prof. Dr. Julio Cezar David de Melo (UFMG)

Co-Orientador: Prof. Dr. José Luiz Silvino (UFMG)

Belo Horizonte, Dezembro de 2010

Universidade Federal de Minas Gerais
Escola de Engenharia
Programa de Pós-Graduação em Engenharia Elétrica

Detection and Location of Transient Disturbances in Power Transmission Lines Using Wireless Sensors

Dênio Teixeira Silva

Thesis presented to the Graduate Program in Electrical Engineering of the Federal University of Minas Gerais in partial fulfillment of the requirements for the degree of Doctor in Electrical Engineering.

Advisor: Prof. Dr. Julio Cezar David de Melo (UFMG)

Co-Advisor: Prof. Dr. José Luiz Silvino (UFMG)

Belo Horizonte, December 2010

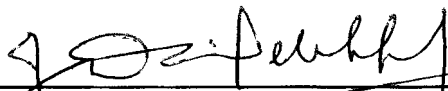
"Detecção e Localização de Distúrbios Transitórios Em Linhas de Transmissão de Energia Utilizando Sensores Sem Fio"

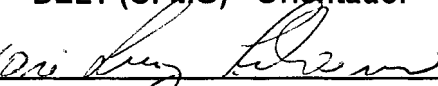
Dênio Teixeira Silva

Tese de Doutorado submetida à Banca Examinadora designada pelo Colegiado do Programa de Pós-Graduação em Engenharia Elétrica da Escola de Engenharia da Universidade Federal de Minas Gerais, como requisito para obtenção do grau de Doutor em Engenharia Elétrica.


Aprovada em 22 de dezembro de 2010.

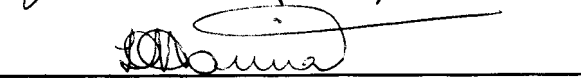
Por:

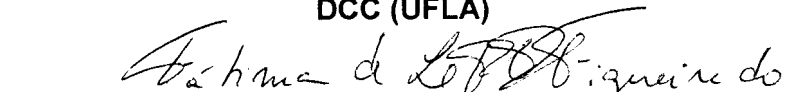

Prof. Dr. Julio Cezar David de Melo
DELT (UFMG) - Orientador


Prof. Dr. José Luiz Silvino
DELT (UFMG) - Co-Orientador


Prof. Dr. Porfirio Cabaleiro Cortizo
DELT (UFMG)


Prof. Dr. José Osvaldo Saldanha Paulino
DEE (UFMG)


Prof. Dr. Luiz Henrique Andrade Correia
DCC (UFLA)


Profa. Dra. Fátima de Lima Procópio Duarte Figueiredo
DCC (PUC-Minas)

À

Leila, minha mulher,
Raphael e Bárbara, nossos filhos,
Joaquim e Elizabete, meus pais.

Agradecimentos

Agradeço à minha mulher Leila e aos meus filhos Raphael e Bárbara pelo apoio e paciência, aos professores Julio Cezar e Silvino pela orientação e ao Centro de Desenvolvimento da Tecnologia Nuclear (CDTN) pelo suporte institucional.

Resumo

Este trabalho apresenta uma aplicação de sensores sem fio em linhas de transmissão de energia para detectar e localizar distúrbios transitórios impulsivos causados por descargas atmosféricas diretas na linha e curtos-circuitos nas fases. As descargas diretas e os curtos-circuitos produzem correntes transitórias de grande magnitude e com alta taxa de variação de corrente. A corrente de retorno da descarga atmosférica que atinge diretamente o cabo pára-raios circula através do cabo e das torres em direção ao solo. O curto-circuito produz uma corrente transitória que induz uma tensão significativa no cabo pára-raios. Da mesma forma, a descarga direta na fase induz uma tensão significativa no cabo pára-raios. A tensão induzida no cabo pára-raios produz uma corrente transitória com alto valor de pico que circula através do cabo pára-raios e nas torres em direção ao solo. Sensores sem fio, instalados no topo das torres, podem medir essas correntes. A componente transitória das correntes é maior nas torres próximas ao ponto onde ocorreu a descarga direta ou o curto-circuito. Esse comportamento é utilizado para localizar o distúrbio transiente. Cada sensor mede o pico de corrente transitória e o pico da taxa de variação da corrente que circula nas torres. Somente os sensores próximos ao distúrbio medem valores significativos de corrente nas torres. Essas medidas são digitalizadas pelos sensores e enviadas através de uma rede sem fio para um computador de localização. Nesse computador, essas medidas são analisadas através de um programa de localização para identificar se o distúrbio transitório é uma descarga direta ou um curto, para localizar o vão onde ocorreu o distúrbio transitório, e para avaliar a potência no caso de uma descarga direta.

Uma questão importante para a operação de sensores sem fio, estudada nesta tese, é como fornecer energia aos sensores sem utilizar células fotovoltaicas e baterias, que precisam de manutenção periódica. É apresentada uma proposta de utilização da corrente de 60 Hz induzida nos cabos pára-raios para fornecer energia aos sensores, substituindo as células fotovoltaicas, e também para o uso de super capacitores, substituindo as baterias.

Abstract

This work presents an application of wireless sensors in power transmission lines to detect and locate impulsive transient disturbances caused by direct lightning strokes to the line and short circuits. Direct stroke and short circuit on phases produce transient currents of great magnitude and high rate of change. The return current of the lightning stroke to shield wire flows through the wire and through the towers to earth and a short-circuit produces a transient current that induces a significant voltage along the shield wire. Accordingly, a direct stroke to phase cable induces a significant voltage in the shield wire. This induced voltage produces a current with high peak value that flows through the wire and through the towers to earth. Wireless sensors installed on top of the towers, can measure these currents flowing in the towers. The transient component of the currents is greater in the towers close to the stroke or to the position of the short-circuit. This behavior is used to locate the transient disturbance. Each sensor measures the peak value of the transient current, and the peak value of the rate of change of current, but only the sensors close to the disturbance measure significant values of the current in the shield wires. These analog measurements are converted into binary data by the sensors and sent via a wireless network to a computer. In this computer, the values of the measurements are analyzed by the location software to identify whether the transient disturbance is a direct stroke or a short-circuit, to locate the span where the transient disturbance occurred, and to evaluate the power in case of a direct stroke.

An important issue covered in this work is how to supply energy to sensors without using photovoltaic cells and batteries, which need periodic maintenance. In this regard, a method is presented to use the 60 Hz steady state current induced in the shield wires to supply power to the sensors, substituting the photovoltaic cells, and the use of super capacitors to replace the batteries.

Contents

Resumo	i
Abstract.....	iii
Abbreviations.....	ix
List of Figures.....	xi
List of Tables	xv
Chapter 1	
Introduction.....	1
1.1 The problem.....	1
1.2 The motivation	1
1.3 The objectives	2
1.4 The solution	3
1.5 The results.....	3
1.6 Text organization	4
Chapter 2	
General Concepts.....	5
2.1 Transient disturbances.....	5
2.2 Lightning strokes	5
2.3 Lightning location systems	8
2.4 Fault location systems.....	10
2.5 Modeling of transmission line towers and cables	13
2.6 The Rogowski coil.....	14
2.7 The wireless networks.....	15
2.7.1 Network architecture overview.....	15
2.7.2 IEEE wireless standards	21
2.7.3 Network topologies.....	27
2.7.4 Types of wireless Networks.....	29
2.7.5 Ad hoc routing protocols	30
2.7.6 The AODV protocol operation	32
2.7.7 Wireless Sensor Networks (WSNs)	33
2.8 Transmission range of radio.....	34
2.8.1 Radio attenuation in free space.....	34
2.8.2 Weather attenuation.....	36
2.8.3 The role of antennas in the transmission range.....	37

Chapter 3	
Detection and location of transient disturbances using wireless sensors.....	43
3.1 Detection and location of direct strokes.....	43
3.1.1 Direct lightning stroke detection and location.....	44
3.1.2 Evaluating the severity of the lightning stroke.....	46
3.2 Short-circuit fault detection and location.....	47
3.2.1 Voltage induced on shield wires.....	48
3.2.2 Voltages and currents induced by the short-circuit current.....	51
3.2.3 Behavior analysis of the transient currents.....	54
3.2.4 Using the transient currents to locate the fault.....	55
Chapter 4	
Detection and location system.....	59
4.1 The block diagram of the sensor.....	59
4.2 The wireless sensor network.....	62
4.3 The location processing computer.....	62
4.4 Security considerations.....	64
4.5 Recommendations for the product engineering of the wireless sensors.....	64
4.6 Operation of wireless sensor networks in power transmission lines.....	65
4.7 The linear topology and the alternative paths in the network.....	67
4.8 Data transmission and routing in the linear topology.....	69
4.8.1 Data transmission through the network.....	69
4.8.2 Behavior analysis of routing protocols in linear topology.....	72
4.8.3 The flooding protocol.....	73
4.9 Channel allocation.....	74
4.10 Clock synchronization.....	75
4.11 Selection of the transceiver technology.....	76
4.12 The transmission range of the wireless sensors.....	78
4.13 Power harvesting from shield wires to the wireless sensors.....	78
4.13.1 Currents induced in shield wires.....	78
4.13.2 Power supplied by current transformers.....	81
Chapter 5	
Results.....	85
5.1 Simulations of direct lightning strokes to overhead power transmission lines.....	85
5.1.1 Simulations of lines with one shield wire.....	86
5.1.2 Simulations of lines with two shield wires.....	89
5.1.3 Stroke location processing.....	93
5.1.4 Evaluation of the results of stroke simulations.....	95

5.2 Simulations of short-circuits faults	95
5.2.1 Fault location processing	98
5.2.2 Evaluation of the results of fault simulations	98
5.3 Identification of the type of transient disturbance.....	98
5.4 Simulations and measurements of steady state currents induced in the shield wires.....	99
5.4.1 Simulation of the steady state induced currents.....	99
5.4.2 Measurements in a power transmission line	103
5.4.3 Evaluation of the results of simulations and field measurements	104
5.5 Simulation of routing protocols in linear topology	104
5.5.1 Network simulator configuration.....	105
5.5.1.1 HTR protocol.....	106
5.5.1.2 OLSR protocol.....	106
5.5.1.3 AODV protocol.....	107
5.5.2 Simulations	107
5.5.3 Analysis of the results of network simulations	113
5.5.4 Simulation of a WSN on branched power transmission lines.....	114
5.5.5 Evaluation of the results of simulations of a WSN on branched OPTLs.....	115
5.6 Transmission range calculations and measurements.....	116
5.6.1 Field measurements and path loss budget.....	118
5.6.2 Evaluation of the results of calculations and measurements.....	121
Chapter 6	
Conclusions and future work	123
6.1 Conclusions.....	123
6.2 Future work.....	124
Bibliography.....	125
Appendix A	
The parameters of the fault simulation	135
Appendix B	
The parameters of the direct stroke simulation (one shield wire).....	137
Appendix C	
The parameters of the direct stroke simulation (two shield wires).....	141
Appendix D	
The integrator of the fault simulation	143

Abbreviations

AC	Alternating Current
ANATEL Agency)	Agência Nacional de Telecomunicações (National Telecommunications Agency)
AODV	Ad hoc On Demand Distance Vector
ATP	Alternative Transient Program
CEMIG	Companhia Energética de Minas Gerais
CSMA/CA	Carrier Sense Multiple Access with Collision Avoidance
CT	Current Transformer
CTS	Clear-to-Send
DC	Direct Current
DCF	Distributed Coordination Function
DIFS	Distributed Interframe Space
DSDV	Destination-Sequence Distance Vector
DSR	Dynamic Source Routing protocol
DSSS	Direct Sequence Spread Spectrum
DYMO	Dynamic MANET On-demand
EMC	Electromagnetic Compatibility
EPRI	Electric Power Research Institute
FH	Frequency Hopping
FTP	File Transfer Protocol
GPS	Global Positioning System
HTR	Hierarchical Tree Routing
HTTP	Hyper Text Transfer Protocol
HWMP	Hybrid Wireless Mesh Protocol
IEEE	Institute of Electrical and Electronics Engineers
IETF	Internet Engineering Task Force
IP	Internet Protocol
ISM	Industrial, Scientific and Medical
ITU-R	International Telecommunication Union - Radio Communication Sector
LAN	Local Area Networks
LCC	Line/Cable Constants

LLC	Logical Link Control
LLS	Lightning Location System
LOS	Line of Sight
MAC	Media Access Control
MANETs	Mobile Ad hoc NETworks
MSC	Message Sequence Chart
MTBF	Mean Time Between Failures
NAV	Network Allocation Vector
NS	Network Simulator
OLSR	Optimized Link State Routing
OPGW	Optic Ground Wire
OPTL	overhead power transmission lines
OSI	Open Systems Interconnection
PAN	Wireless Personal Area Network
PDU	Protocol Data Unit
PV	PhotoVoltaic
RREP	Route Reply Packet
RREQ	Route Request Packet
RTS	Request-to-Send
SDL	System Description Language
SIFS	Short Interframe Space
SMTP	Simple Mail Transfer Protocol
SNR	Signal-to-Noise Ratio
TCP	Transmission Control Protocol
TORA	Temporally-Ordered Routing Algorithm
TTL	Time to Live
UDP	User Datagram Protocol
VPN	Virtual Private Network
WAN	Wide Area Networks
WLAN	Wireless LAN
WMAN	Wireless Metropolitan Area Network
WSN	Wireless Sensor Network

List of Figures

Figure 2.1 - Return stroke current measured at Morro do Cachimbo research station.	7
Figure 2.2 - Tower with shield wires.	8
Figure 2.3 - Lightning location system (LLS).....	9
Figure 2.4 - Direction finder antenna, B is the magnetic flux generated by the lightning, θ is the angle between coil direction and the hit position.	10
Figure 2.5 - Two terminal impedance-based fault location method.	11
Figure 2.6 - Two terminal travelling waves fault location method.....	12
Figure 2.7 - Measurement of current using Rogowski coil, $i(t)$ is the current being measured, $v(t)$ is the coil voltage, and K is a constant.	14
Figure 2.8 - The OSI model	16
Figure 2.9 - Internet communication layers.	18
Figure 2.10 - The types of information formats and the flow of information between the layers.	19
Figure 2.11 - Stack of IEEE 802.x standards	22
Figure 2.12 - 802.11 and 802.15.4 services.	22
Figure 2.13 - ZigBee layers	23
Figure 2.14 - Basic access mechanism	24
Figure 2.15 - The problem of the hidden terminal (B)	25
Figure 2.16 - RTS/CTS mechanism	26
Figure 2.17 - 802.11 channels	27
Figure 2.18 - 802.15.4 channels	27
Figure 2.19 - Network topologies.	28
Figure 2.20 - Nearly linear topology and the equivalent mesh topology.	29
Figure 2.21 - Infra-structured wireless network.	30
Figure 2.22 - Infra-structured wireless network.	30
Figure 2.23 - Some common Ad Hoc routing protocols.	31
Figure 2.24 - The operation of the AODV protocol	33
Figure 2.25 - The first Fresnel zone.	35
Figure 2.26 - The elevation angle of the antenna and the difference in the tower levels.	37
Figure 2.27 - Obstruction of the signal in case of a failure one sensor on the top a hill.	38
Figure 2.28 - Dipole antenna.....	38
Figure 2.29 - Irradiation diagrams of the dipole antenna	39

Figure 2.30 - Some types of collinear antennas.	40
Figure 2.31 - Irradiation diagrams of the collinear array of three dipole antennas	40
Figure 3.1 - Direct lightning stroke currents, i_1 and i_2 are the currents that flow to ground through the nearest towers, i_1' and i_2' are the residual currents that flow to the next towers.	44
Figure 3.2 - Position of the sensor on the top of the tower.	45
Figure 3.3 - Genscape wireless monitoring system	48
Figure 3.4 - Equivalent circuit for the induction of voltage on the shield wires: I_{phase} is the current on the phase cable, Z_m is the mutual impedance, Z_t is the impedance of the tower, Z_s is the impedance of the shield wire, R_g is the tower grounding resistance, V_m is the induced voltage, I_m is the induced current, V_{phase} is the phase voltage, and Z_L is the load impedance.	49
Figure 3.5 - The equivalent circuit for the evaluation of the induced voltages and currents on the shield wire and towers. Z_T is the tower impedance plus the grounding resistance, Z_W is the wire impedance, V_m is the induced voltage, I_n is resulting induced current.	50
Figure 3.6 - Line-to-ground fault currents before (a) and after (b) the short-circuit position; Voltage induced on the shield wire before (c) and after (d) the short-circuit position.	51
Figure 3.7 - Details of the edges of the transient currents and the induced voltages of Figure 3.6.	52
Figure 3.8 - Currents in the shield wire and in the towers near the fault position, I_{S1} to I_{S7} are the shield wire currents, I_{T1} to I_{T6} are the tower currents, Z_f is the short-circuit impedance, I_f is the short-circuit current (T1 to T6 are the identifications for tower 1 to tower 6).	53
Figure 3.9 - Waveforms of the transient currents in the shield wire and towers according to Figure 3.8.....	54
Figure 3.10 - Equivalent circuit for the high frequency induction in the shield wire, Z_t e Z_s are the surge impedances of tower and shield wire, respectively, R_g is the tower grounding resistance, V_m is the induced voltage.	55
Figure 3.11 - Position of the sensor on the top of the tower (a), detail of the tip of the tower (b), and the detail of the coil (c).....	56
Figure 4.1 - Block diagram of the wireless sensor.	60
Figure 4.2 -current induced by the fault.	61
Figure 4.3 - Overview of the wireless network communication of the detection and location system.	62
Figure 4.4 - The location processing computer.	63
Figure 4.5 - Proposal for the sensor case.	65
Figure 4.6 - Convention for the node range.	67

Figure 4.7 - Linear topology (a) and mesh topology (b) the dashed line circle around the source node indicates the range of the radio transceiver (equal for every node).	68
Figure 4.8 - The alternative path at the end of the network	68
Figure 4.9 - MSC diagram of the data transmission process.	70
Figure 4.10 - Message types and fields.	71
Figure 4.11 - The SDL diagram of the flooding process.	73
Figure 4.12 - Message format with address fields.	74
Figure 4.13 - Allocation of 802.11 channels for 12 transmission lines, the numbers indicate the channels.	75
Figure 4.14 - The path of the sync messages.	76
Figure 4.15 - The equivalent circuit of the shield wire and towers to evaluate the distribution of currents: Z_T is the tower and grounding impedance, Z_{ER} and Z_{EL} are the equivalent resistances to the right and to the left of the span, respectively, V_m and I_n are the voltage and current induced.	80
Figure 4.16 - The current transformer and apparatus installed on shield wire, I_m is the current induced in the shield wire.	81
Figure 4.17 - The CT equivalent circuit, R_{sec} and L_m are the secondary resistance and inductance of the CT, respectively, I_m is the induced current and N is the number of turns of the secondary of a window type CT.	81
Figure 4.18 - Power supply circuit.	82
Figure 4.19 - The output voltage of the power supply (a), the output of the PWM (b), and the current at the secondary of the current transformer (c). V_{reg} , V_{op} , and I_{sec} refer to the labels in Figure 4.18.	84
Figure 5.1 - The stroke positions, span lengths and footing resistances used in the simulations.	86
Figure 5.2 - Simulated currents of a direct lightning stroke to the top of tower 4.	87
Figure 5.3 - Simulated currents of a direct lightning stroke to the middle of the span, between towers 4 and 5.	87
Figure 5.4 - Simulated currents for a lightning stroke to phase cable, close to tower 4.	89
Figure 5.5 - The stroke points used in the simulations.	90
Figure 5.6 - Currents of a direct stroke to shield wire 1 in tower 3.	91
Figure 5.7 - Currents of a direct stroke to shield wire 1 at the middle of the span, between towers 3 and 4.	91
Figure 5.8 - Simulated currents for a direct stroke to phase cable, near tower 4.	93
Figure 5.9 - Positions of the phase cables and shield wire (dimensions in meters).	100
Figure 5.10 - Current transformer excitation curve.	101

Figure 5.11 - ATP saturable component: L_p , R_p , L_s and R_s are the primary inductance and resistance, and secondary inductance and resistance, respectively, R_{mag} is the magnetizing resistance, SATURA is the ATP support routine.....	102
Figure 5.12 - The current induced in the 21 th span and the CT output current.	102
Figure 5.13 - A piece of the diagram of the simulated overhead power line showing six spans and the CT: the cables are modelled by the LCC objects, the grounded resistors represent the tower grounding resistances, R_B is the burden resistor.	102
Figure 5.14 - Positions of the phase cables and shield wires, H varies for every tower (dimensions in meters).	103
Figure 5.15 - Simulation scenario.	105
Figure 5.16 - The alternative paths of the network in a power line with branches.	114
Figure 5.17 - The simulation of branches.	115
Figure 5.18 - Communication in case of a failure of one sensor.	118
Figure 5.19 - The position of antennas in the field measurements.	119
Figure 5.20 - The tower as an obstacle inside the Fresnel zone.	120
Figure A 1 - Tower dimensions (m) and the positions of the phase cables (A, B, and C) and the shield wire (S) (m).	135
Figure A 2 - The instant of the fault within the voltage cycle.	136
Figure B 1 - Tower dimensions (m) and the positions of the phase cables (A, B, and C) and the shield wire (S) (m).	137
Figure B 2 - The simulation diagram of a direct stroke to shield wire.	139
Figure B 3 – Shape of the lightning stroke current used in the simulations.	140
Figure C 1 - Tower dimensions (m) and the positions of the phase cables (A, B, and C) and the shield wires (S1 and S2) (m).	141
Figure D 1 - Current flowing in the tower and the corresponding output of the integrator...	143

List of Tables

Table 2.1 - The maximum difference between the top of towers as a function of the antenna elevation angle.....	38
Table 4.1 - 802.15.4 and 802.11 transceivers.....	77
Table 5.1 - Results for one set of simulations of a non-homogeneous power transmission line (“Tn” is the abbreviation for “tower n”, “Tn-Tn+1” means between “tower n” and “tower n+1”)......	88
Table 5.2 - Results for the simulations of a direct stroke to phase cable (shielding failure) (“Tn” is the abbreviation for “tower n”).	89
Table 5.3 - Results for one set of simulations of a non-homogeneous power transmission line (“Tn” is the abbreviation for “tower n”, “Tn-Tn+1” means between “tower n” and “tower n+1”)......	92
Table 5.4 - Results for the simulations of a direct stroke to phase cable (shielding failure) (“Tn” is the abbreviation for “tower n”, “Tn-Tn+1” means between “tower n” and “tower n+1”)......	93
Table 5.5 - Lightning stroke position estimation using the values of Table 5.3 and Table 5.4 (“Tn” is the abbreviation for “tower n”).	95
Table 5.6 - Results of the fault simulations in T4.	97
Table 5.7 - Results of the fault simulations in the middle of the span (between T4 and T5). .	97
Table 5.8 - di/dt values for different types of transient disturbances.	99
Table 5.9 - Maximum power available simultaneously from eight spans.	101
Table 5.10 - Simulation results for the maximum power available simultaneously from ten spans of the 24 km power line.	104
Table 5.11 - OLSR NS2 parameters.....	107
Table 5.12 - AODV NS2 parameters.	107
Table 5.13 - NS2 parameters of 802.11 simulations.....	108
Table 5.14 - NS2 parameters of 802.15.4 simulations.....	108
Table 5.15 - Common parameters of the simulation.....	109
Table 5.16 - Results for the simulations with 250 nodes.	110
Table 5.17 - The results of worst case simulations.	112
Table 5.18 - Results of simulations of branches.	115
Table 5.19 - Transmission range calculation.	117
Table 5.20 - Transmission range calculation with 5.8 dBi antennas.....	117
Table 5.21 - Range calculation for the components of Table 4.1.	118
Table 5.22 - Calculation of received power with the parameters of the field measurements.	120

Table 5.23 - Path loss budget with 5.8 dBi antennas. 120

Chapter 1

Introduction

Accidental outages of electric power transmission lines have significant social and economic impacts in large areas, causing losses of various types. Each of these lines can carry power to several cities or even several states. Besides, large energy systems are interconnected and a problem with one transmission line can propagate to other lines causing problems in cascade. The outages are caused by short-circuits in the phase cables, disruptions of cables or lightning discharges that hit the power line directly.

1.1 The problem

Direct lightning strokes to power transmission lines are the main cause of faults [1]. Therefore, it constitutes a major problem for power distribution companies. It is of great relevance to determine if the cause of the power outage is a direct stroke or a short-circuit caused by other events like fire or trees. There is scientific and technological interest in low cost systems to identify, quickly and accurately, the incidence of direct strokes to the transmission line and locate the stroke point. Thus it will be possible to begin immediate corrective actions and effective preventive actions. Because the lines crosses great extensions of territory in regions that are often inhospitable, such a system allows a great reduction in the time wasted in the preventive or corrective actions.

1.2 The motivation

If the lightning stroke position is known with precision, in case of a line fault it is possible to do the repairing faster, reducing significantly the outage time. Even if the lightning stroke does not cause a power outage, it is important to detect it, locate the hit position and evaluate its power. With this information, it is possible to evaluate if there was damage to the power line that may cause a failure later, and to perform the necessary preventive maintenance. Therefore, the development of a lightning stroke location system with these characteristics is an important contribution to the power system management.

If the stroke location system has the additional feature of short-circuit fault location, the location system is more complete and useful. Besides, the usefulness is increased if the system can detect and locate short-circuit that do not cause a fault.

The known operational fault location systems perform the location through measurements at the ends of the transmission line and do not detect directly the lightning strokes to lines that caused an outage. There are few publications about direct stroke to power line location systems [2][3][4] and the existing operational systems combine a Fault Location System with a Lightning Location System (LLS) to perform the event correlation [5]. These systems do not detect the direct strokes nor the short-circuits that do not cause power outage.

1.3 The objectives

Events such as lightning and faults caused by fire and other phenomena can be monitored effectively and in real time by sensors distributed along the power transmission line, on the top of the towers, with communication via radio for transmitting data to a collection point. The sensors can be provided with local processing capacity that allows great flexibility in data collection, functioning as a network of "smart" sensors. The intelligent sensors can be equipped with a processor, memory, analog to digital converters, sensors and communication devices that allow making, storing and processing measurements, and running communication protocols, through which they can communicate more efficiently for data transmission. Technological developments and the spread of microcontrollers and wireless technologies made it feasible to create a low cost system for identification and location of direct strokes to transmission lines and short-circuit faults, by using intelligent sensors.

The goal of this work is to evaluate the feasibility of and to propose a system for detection and location of direct strokes and short-circuits (transient disturbances) in overhead power transmission lines (OPTL). In this work the whole system is studied and the main issues of the system are addressed:

- a) How to detect the direct strokes and short-circuits with the sensors;
- b) How to locate the events;
- c) How to transport the information collected by the sensors to be processed;
- d) How to process the information to detect and locate de transient disturbances.

1.4 The solution

The result of this work is a method to detect and locate direct lightning strokes and short-circuit faults in overhead power transmission lines using sensors on the top of the towers. The detection is performed by the measurement of induced currents in shield wires using wireless sensors that send these measurements to be processed by a computer at one of the ends of the transmission line. The wireless sensors are the nodes of a wireless network that transports the information to be processed. The transient disturbances are located by the computer after processing the information about the currents in the shield wires received from each sensor close to the disturbance. This work includes the analysis and the proposal of a low maintenance solution to supply power to the sensors without using photovoltaic (PV) cells and batteries, using the continuous power available in the shield wires.

1.5 The results

The method to detect and locate direct lightning strokes and the method to locate short-circuit faults was evaluated using simulations that showed their feasibility and accuracy. The operation of the wireless sensor network was simulated to verify the behavior of the high number of sensors operating in the peculiar linear topology. The field measurements showed the feasibility to use the well known wireless standards in the wireless network to guarantee a reliable operation. The simulations and field measurements showed the feasibility of using the power of the shield wires to feed the sensors eliminating the PV cells and batteries and their maintenance.

The proposed system is innovative in several aspects. It detects and locates direct strokes to transmission lines as well as low impedance and high impedance short-circuits. The location is possible even when the transient disturbance does not cause a fault. The system allows the evaluation of the power of the direct stroke to the shield wire. The system can operate on parallel and branched transmission lines. The detection is performed by the local measurement of the currents circulating from shield wires to the ground through the towers which allows a good precision, independent of the line length, and the detection of high impedance short-circuits.

1.6 Text organization

The text is organized in six chapters. The first chapter is the introductory text. Chapter 2 summarizes the main concepts used in the work. Chapter 3 describes the methods proposed for detection and location of direct strokes and faults in transmission lines using wireless sensors. Chapter 4 describes the proposed system to locate the transient disturbances. Chapter 5 presents the results to show the feasibility of the proposed methods and system. Chapter 6 is the conclusion with considerations about the results, the importance of the work, and the proposal of future works to complement or supplement the work presented.

Chapter 2

General Concepts

2.1 Transient disturbances

The power systems disturbances are mainly classified as steady-state and transient phenomena [6]. The transients induced by direct strokes to overhead power lines and the transients caused by short circuit faults are two important transient disturbances that can cause power outage with several consequences.

The direct lightning strokes to power transmission lines are the main cause of faults, representing about 65% of the events according to international statistics. In our state, Minas Gerais, Brazil, with high keraunic level, the faults in power transmission caused by lightning strokes represent 70% of events (20% being permanent), according to the state power company CEMIG (Companhia Energética de Minas Gerais) [1]. The direct strokes to phase cables can establish high overvoltages between phase conductor and earth. The overvoltage can cause the insulator failure and an electric arc between the conductor and the tower creating a short circuit path from phase conductor to ground [7]. The direct strokes to the shield wire of overhead power transmission lines produces high value of transient currents flowing in the shield wires and towers and corresponding high surge voltage on the top of the tower which can damage the insulators.

The short circuit faults can occur between one or more phases and ground, and between phases. Other causes of short-circuits are the fall of towers and the proximity of trees to cables. The calculations from CEMIG [8] show that the resistance of short circuits caused by strokes is low, between 0 and 10 Ω . In case of short circuits caused by fire, the resistance is between 10 and 70 Ω . In case of short circuits caused by trees, the resistance is above 70 Ω .

2.2 Lightning strokes

A typical storm cloud, called cumulonimbus, has an average diameter of 10 km, and its top can reach up to 20 km and the base height is between 1 and 3 km. The lightning stroke can occur between the cloud and the ground, between clouds, or from the cloud to the air. The

most common are the cloud-to-cloud. Cloud-to-ground strokes are the most important due to the greater extent of the problems but represents less than 25% of the total. Approximately 90% of cloud-ground discharges are negative, i.e. the lower region of the cloud base is loaded negatively, inducing positive charges on the ground [9].

The phenomenon of atmospheric discharge consists of several steps. In case of negative cloud-to-ground type, first the cloud with the base charged with negative charges induces a positive charge in the ground establishing a great potential difference between its base and the ground (several megavolts). Under certain conditions, the electric field inside the base of the cloud reaches values above the dielectric strength of the air (3 MV/m). This condition creates an ionized channel of plasma with several tens of meters, known as stepped leader. This stepped leader moves toward the ground in straight segments with spacing of approximately 50 m in time intervals of the order of 1 μ s [9]. When the stepped leader is close to the ground (hundreds of meters), there is the formation of an intense electric field between the front of the stepped leader and the ground with induction and consequent formation of positive discharges from the ground up, called upward leaders. With the meeting between the upward leaders and the stepped leader, there is the formation of the main discharge channel called return stroke with upside direction and possessing speed above 108 m/s, with average rise time of 10 μ s and average duration of 100 μ s [10]. The abrupt local expansion of the air due to intense channel discharge temperature causes the phenomenon called thunder.

In 80% of cases, after the first return stroke there are a series of subsequent return strokes. The first stroke and the unique stroke have similar characteristics. In case of subsequent strokes, they have different characteristics from the first stroke [11].

Return stroke currents have high peak values, with an average value of 31 kA [11] and can reach magnitudes greater than 200 kA. The average value obtained in searches carried out by CEMIG was 48 kA at Morro do Cachimbo research station [12]. Figure 2.1 shows a measured return stroke current at Morro do Cachimbo research station [13].

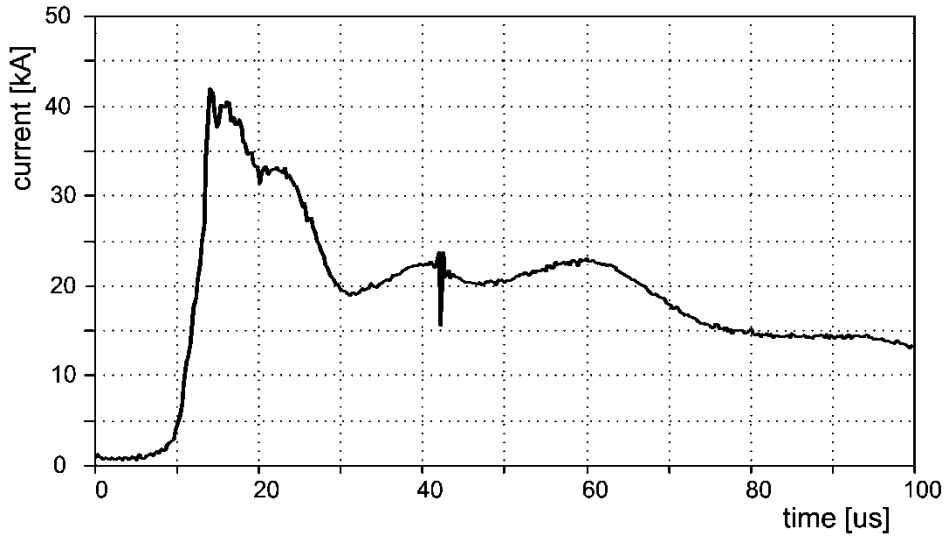


Figure 2.1 - Return stroke current measured at Morro do Cachimbo research station [13].

There is a higher probability of the main discharge channel to be formed on high metallic structures like the cables and towers of a power transmission line [11]. The shield wires are installed above the phase cables, on the top of the towers, and are electrically connected to the structure of the steel towers to protect the phase cables against lightning strikes. The towers are grounded and therefore the shield wires have a path to ground through the towers. If the lightning downward leader, in the path to earth, enters the attractive radius of the shield wire of a power transmission line, it will hit the wire with high probability [14]. Therefore the lightning strikes the shield wire in most cases, instead of striking the phase cables. The return stroke current flows in the shield wires and to ground through the towers, reducing the risk of a power outage (Figure 2.2).

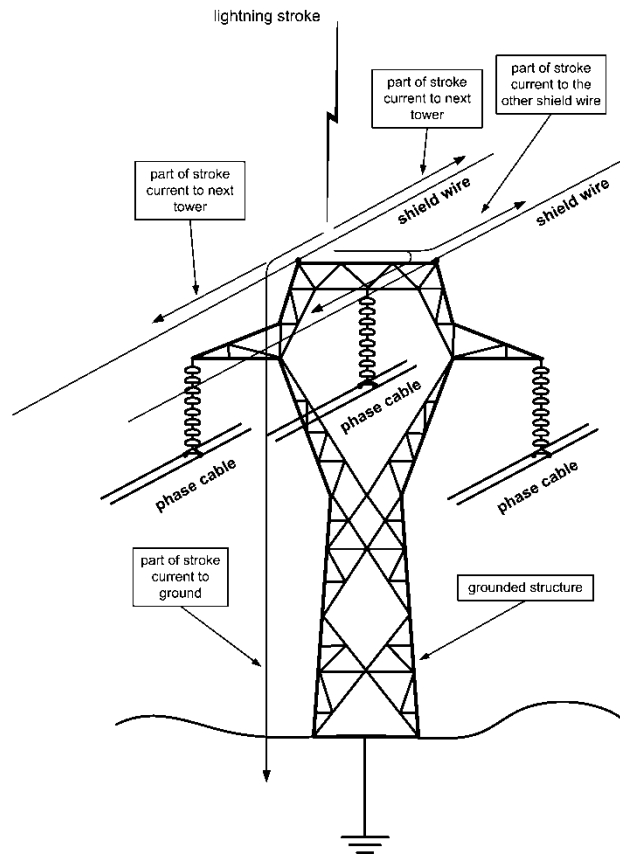


Figure 2.2 - Tower with shield wires.

2.3 Lightning location systems

The main cause of faults in the power transmission and distribution system is the lightning discharges. There are systems used by the Electric Distribution Systems to detect and locate the lightning strokes over a geographic region. The lightning location systems (LLS) perform the location of lightning through special sensors that capture the electromagnetic field through terrestrial stations, distributed in the region of monitoring [9]. The system consists of detection stations and a processing station. Figure 2.3 illustrates the system.

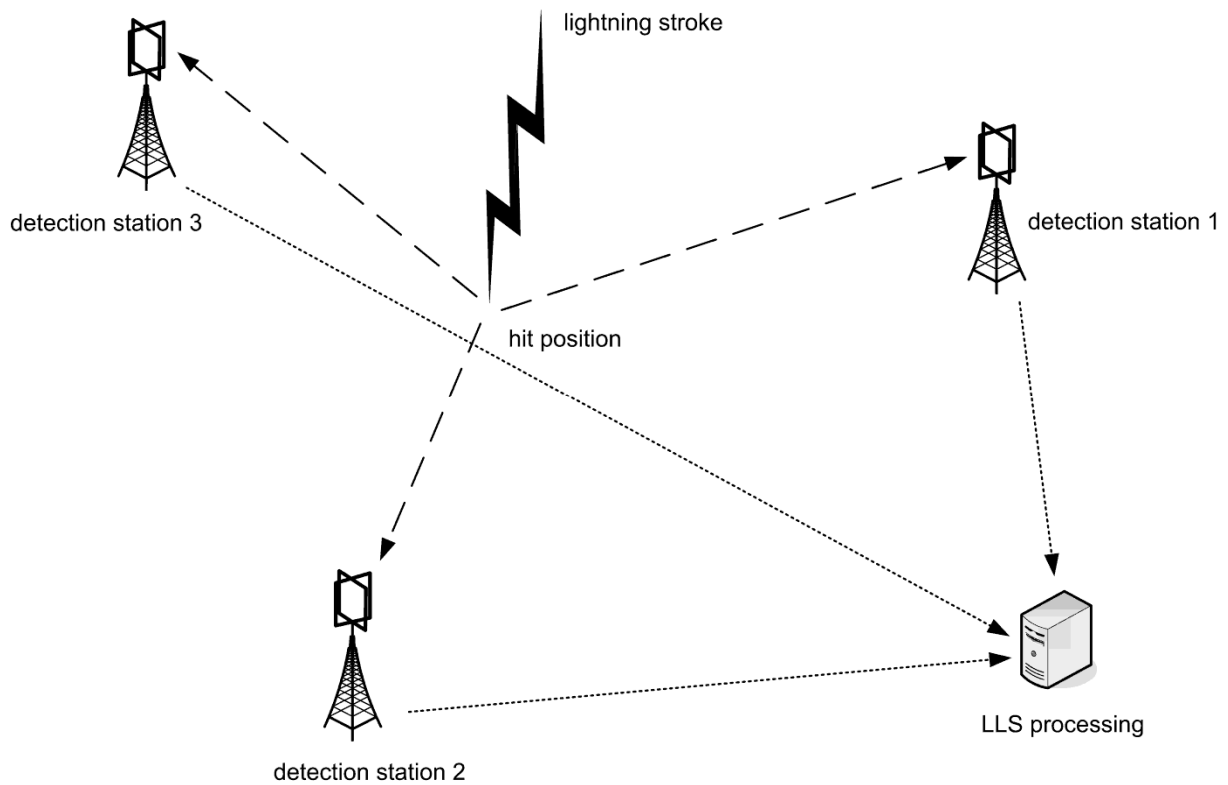


Figure 2.3 - Lightning location system (LLS).

There are two types of systems to locate the lightning: direction finding system and time of arrival system. In the method of direction finding, detection stations have a device which is basically an antenna consisting of two coils orthogonal to each other. The magnetic field of the lightning strike crosses these coils and produces a voltage in each coil. The relationship between these voltages determines the angle between the magnetic field and the turns of the coils. Positioning the two coils of each station in one known direction such as North-South and East-West directions turns it possible to determine the direction of the lightning (Figure 2.4). With three stations it is possible to triangulate the location of the hit point of the lightning strike.

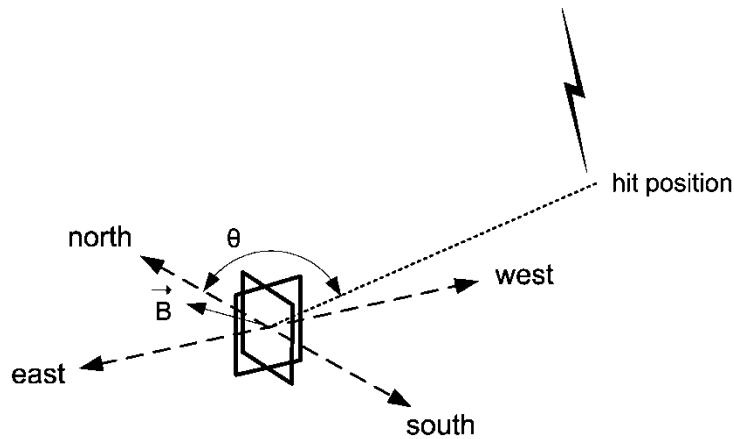


Figure 2.4 - Direction finder antenna, B is the magnetic flux generated by the lightning, θ is the angle between coil direction and the hit position.

The Time of Arrival system uses a different approach to locate the lightning stroke. The detection stations record the time of arrival of the electromagnetic field generated by the lightning. The differences between the time records of three or more stations are used to locate the hit position. There is a hyperbole associated to the difference of time between two stations which is the geometric place of hit positions that would result in the same time difference of arrival time between these two stations. The intersection of these hyperboles determines the hit position.

The location accuracy of these systems is of the order of several hundred meters [15].

2.4 Fault location systems

The fault locations systems usually perform the location of the fault using terminals installed at the ends of the transmission line to gather information from the phase cables. Two of the most used fault location systems are the impedance-based systems and the travelling wave systems [16]. The system can use one terminal at the end of the line, or two terminals, one at each end. The two terminal systems are more accurate than one terminal systems.

Two-terminal fault location techniques based on impedances usually use the following approach. The fault is at location m of the line from Bus G and $(1-m)$ from Bus H (Figure 2.5) [16].

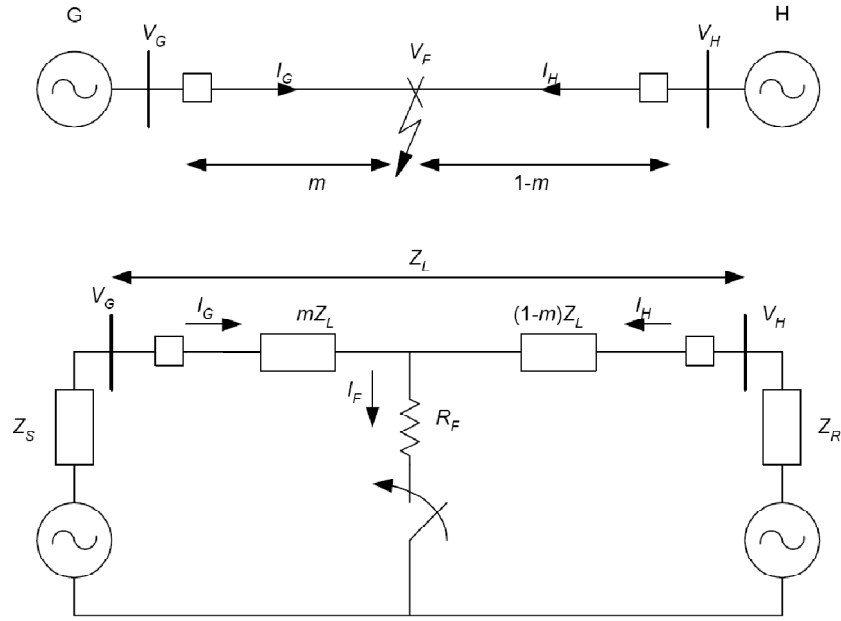


Figure 2.5 - Two terminal impedance-based fault location method [16].

V_F is the voltage at the fault. The bus voltages and currents are as indicated in the figure. Use of voltage/current relationships in all three phases (A, B, and C) yields the results shown in Equation (2.1) and Equation (2.2):

$$(V_{GF})_{abc} = m Z_{Labc} (I_{GF})_{abc} + V_F \quad (2.1)$$

$$(V_{HF})_{abc} = (1-m) Z_{Labc} (I_{HF})_{abc} + V_F \quad (2.2)$$

V_F is the fault voltage on the fault resistance R_F , V_{GF} and V_{HF} are the bus voltages in fault condition, I_{GF} and I_{HF} are the line currents in fault condition, m is the distance to the fault position, and Z_{Labc} is the line impedance. Subtracting the two equations to eliminate the unknown V_F results in Equation (2.3):

$$(V_{GF})_{abc} - (V_{HF})_{abc} = m Z_{Labc} (I_{GF})_{abc} + (m-1) Z_{Labc} (I_{HF})_{abc} \quad (2.3)$$

This equation can be solved for the real m , and the phase values can be substituted with the symmetrical components. The state power company CEMIG has a two terminal system with location accuracy of 2% of the line length that have located fault resistances up to 110 Ω [8].

Two-terminal fault location techniques based on travelling waves usually use the following approach [17]. Faults in a transmission line generate transient travelling along the line as waves composed of a series of frequencies ranging from few kilohertz to several

megahertz. These traveling waves have a front wave with fast rise time and a relatively slow fall time. The waves travel at speeds close to the light, from the point of failure toward the terminal points at buses *A* and *B* of the line as illustrated in Figure 2.6.

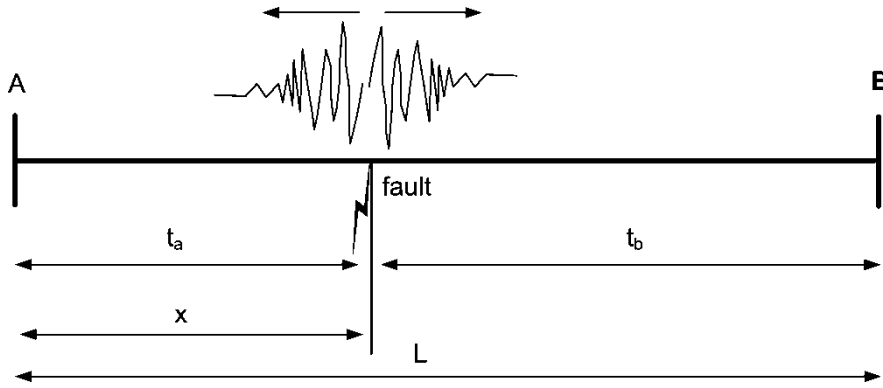


Figure 2.6 - Two terminal travelling waves fault location method.

A and *B* are the buses at the end of the power line with a length *L* and the fault occurs at the distance *x* from bus *A*. t_a and t_b are the propagation time of the transient waves generated by the fault to the buses *A* and *B*, respectively. The waves are not limited to the transmission line where the fault occurred. They propagate through the adjacent electrical system with descending amplitude, as a result of the combined effects of line impedance and successive reflections. The fault location by traveling waves is based on the precise determination of the moment when the wave fronts pass through known points, usually substations located at the terminal points of the transmission line. Knowing the instant of time when the wave front arrives to terminals *A* and *B* of the transmission line (t_a and t_b) and starting from the length of the line (*L*), it is possible to determine the location of the fault from the terminal (*x*) by the formula:

$$x = \frac{L + k c (t_a - t_b)}{2} \quad (2.4)$$

where *c* is the speed of light (299.792.458 m/s) and $k = 0.95$ to 0.99 is a reduction factor which depends on some particularities of transmission line. The location accuracy is higher than the accuracy of impedance based systems, being less than 1% from real position in tests reported in [18]. Commercial equipment from ISA Sri has an accuracy of 1000 m [19]. Fault resistances up to 200 Ω can be located with traveling waves systems [20].

2.5 Modeling of transmission line towers and cables

The modeling of the power transmission lines is essential for the simulations performed in this work. To model a power line it is necessary to model the towers and the cables.

The towers are represented in the simulations by their surge impedance which has a critical role in the determination of the rise of potential at the top of the towers under lightning and transient fault conditions. Besides, the surge impedance of towers and cables determines the lightning and fault currents flowing through the towers. The rise of potential at the top of the towers can lead to back-flashover across the insulator strings.

Tower surge impedance determination includes both theoretical calculations and experimental measurements with models and full-scale towers. Experimental methods include the direct method [21] and the time-domain reflectometry method [22]. In the direct method the current is injected in the tower top and the ratio of the measured voltage and current records is calculated. In time-domain reflectometry method the tower impulse response of small-scale models is measured and analytical expressions are used for the calculation of the surge impedance based on traveling wave theory. Theoretical studies for predicting the surge characteristics of towers have been performed in the time domain by solving the electromagnetic field equations analytically [23][24][25]. The IEEE suggests a method to calculate the tower surge impedance [26], used in this work, based on the equation proposed by Chisholm et.al. [25]:

$$Z_0 = 60 \ln \left[\cot \left(\frac{1}{2} \tan^{-1} \left(\frac{R_{\text{avg}}}{h_1 + h_2} \right) \right) \right] \quad (2.5)$$

$$R_{\text{avg}} = \frac{r_1 h_2 + r_2 (h_1 + h_2) + r_3 h_1}{h_1 + h_2} \quad (2.6)$$

where:

Z_0 =tower surge impedance

r_1 =tower top radius (m)

r_2 =tower midsection radius (m)

r_3 =tower base radius (m)

h_1 =height from base to midsection (m)

h_2 =height from midsection to top (m)

We have also used the equation proposed in [25] for towers with conical shape:

$$Z_0 = 60 \ln \left(\sqrt{2} \frac{\sqrt{h^2 + r^2}}{r} \right) \quad (2.7)$$

where Z_0 is the tower surge impedance, h is the height of tower and r is the radius of the tower base.

Modeling of cables is a well-known theme whose treatment is well defined in the literature. The Alternative Transient Program (ATP), used to perform the simulations of the power transmission lines [27] in this work, have line and cable support routines to simulate accurately the cables of a power transmission line. These routines are based on well-known and widely used theories well documented in [28] and simulate the cables for steady state 60 Hz analysis and for higher frequency transient analysis. There are several case studies showing that the simulation results using the ATP program and the line and cable support routines are close to the field measurements [28][29][30].

2.6 The Rogowski coil

The measurement of the transient currents can be carried out by a Rogowski coil which is a coil with turns equally distributed along a non magnetic core. The return wire goes back concentrically to avoid the external fields produced by external currents near the coil (Figure 2.7). The placement of the coil is very easy due to the construction of the coil in an open ring shape that is mechanically closed around the conductor of the current to be measured.

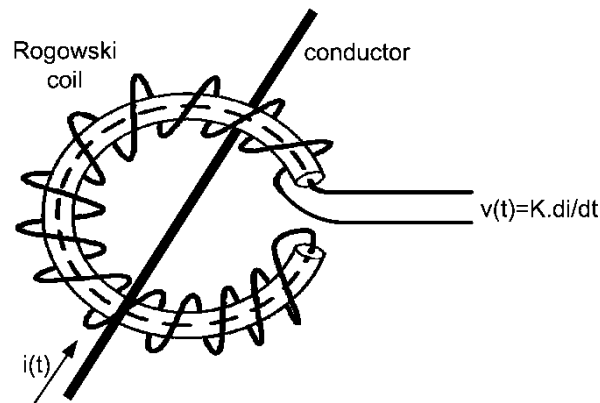


Figure 2.7 - Measurement of current using Rogowski coil, $i(t)$ is the current being measured, $v(t)$ is the coil voltage, and K is a constant.

The Rogowski coil voltage ($v(t)$) is proportional to the rate of change of the current by the constant K , which depends on the construction characteristics of the coil:

$$v(t) = K \frac{di}{dt} = -\mu_0 \frac{N}{l} A \frac{di}{dt} \quad (2.8)$$

where μ_0 is the vacuum permeability, N is the number of turns, l is the mean length of the toroid and A is the area of the turn. Integrating the voltage $v(t)$, we obtain an output voltage, $v_{out}(t)$, proportional to the original current $i(t)$ by the time constant RC of the integrator:

$$v_{out}(t) = \frac{1}{RC} \int v(t) dt = \frac{1}{RC} \mu_0 \frac{N}{l} Ai(t). \quad (2.9)$$

The most important characteristics of a Rogowski coil are large bandwidth, large range (from amperes to kiloamperes), good linearity (non-magnetic core), no saturation, easy installation, and galvanic isolation between the primary circuit and the measuring circuit [31]. The Rogowski coils are usually used to measure the stroke currents in the towers of lightning research stations [9].

2.7 The wireless networks

2.7.1 Network architecture overview

Modern communication networks are based on an architecture model of communication whose organization is a stack with at most seven communication layers. Each layer performs a specific function, offers services to the upper layers and has a protocol used to perform the services. The protocols define the set of rules for the format and meaning of data exchanged between two entities at a specified layer [32]. This stack model is based on the Open Systems Interconnection (OSI) reference model [33] and is useful to understand the role of each layer involved in networked communication systems (Figure 2.8).

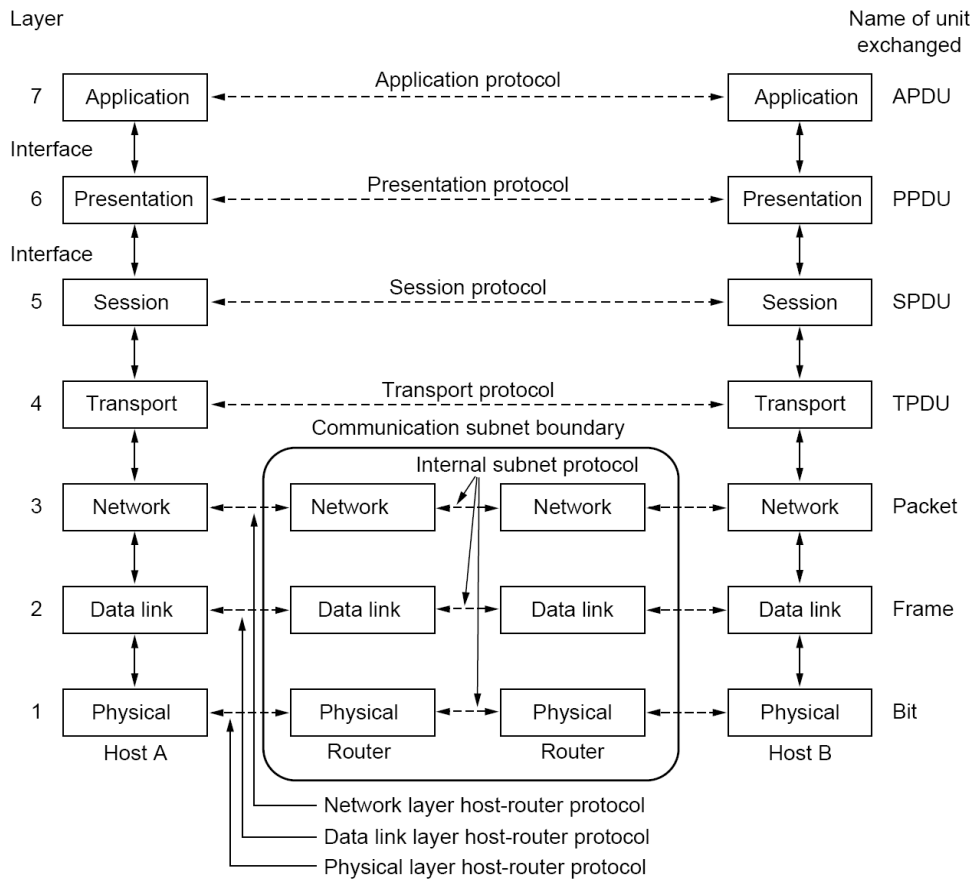


Figure 2.8 - The OSI model [32].

Figure 2.8 shows that the lower layers entities perform a node-to-node communication. The hosts in the Local Area Networks (LANs) and the routers in the LANs and in the Wide Area Networks (WAN) use the physical, link and network layers to communicate. Equipments like switches in the Local Area Networks (LAN) and wireless access points in the Wireless LANs use the physical and data link layers to communicate. The model shows that the communication between the upper layers (transport, session, presentation and application) is end-to-end (source and destination) [32].

The application layer is the upper layer and is the closest to the software application and to the end user. This layer interacts with software applications that implement a communicating component. Application layer functions typically include the procedure of identification of communication partners, determining resource availability, and synchronizing communication [32]. Examples of application layer protocols are the Simple Mail Transfer Protocol (SMTP), File Transfer Protocol (FTP), Hyper Text Transfer Protocol (HTTP) and Terminal Network Protocol (telnet) used in the Internet [32].

The presentation layer provides independence from differences in data representation (e.g., encryption) by translating from application to network format, and vice versa. The presentation layer works to transform data into the form that the application layer can accept [32].

The session layer establishes, manages and terminates connections between applications. The session layer sets up, coordinates, and terminates conversations, exchanges, and dialogues between the applications at each end. It deals with session and connection coordination. Examples of session layer protocols are the Windows NetBIOS protocols [34].

The transport layer is responsible for error-free data delivery and in the proper sequence, flow control, multiplexing and error checking and recovery. Flow control manages data transmission between devices so that the transmitting device does not send more data than the receiving device can process. Multiplexing enables data from several applications to be transmitted onto a single physical link. Error checking involves the use of mechanisms for detecting transmission errors, while error recovery involves the action of requesting the retransmission of the data when errors occur [32]. The transport protocols used on the Internet are TCP (Transmission Control Protocol) and UDP (User Datagram Protocol). For certain applications the transport protocol may not be necessary. Some functions of this layer can be implemented in the application layer, or in the application. In this case, if a reliable service is necessary, the application has to implement error checking and recovery.

The network layer provides switching and routing technologies creating logical paths for transmitting data from node to node. Routing and forwarding are functions of this layer, as well as addressing, internetworking, error handling, congestion control and packet sequencing. The network protocol used on the Internet is the IP (Internet Protocol) protocol [32].

The data link layer provides reliable transit of data across a physical network link. In this layer, data packets are encoded and decoded into bits. It provides transmission protocol acknowledge and management and handles errors in the physical layer, flow control and frame synchronization [32].

The Institute of Electrical and Electronics Engineers (IEEE) has subdivided the data link layer into two sublayers: Logical Link Control (LLC) and Media Access Control (MAC). The Logical Link Control (LLC) sublayer manages communications between devices over a

single link of a network. LLC is defined in the IEEE 802.2 specification and supports both connectionless and connection-oriented services used by higher-layer entities. IEEE 802.2 defines a number of fields in data link layer frames that enable multiple higher-layer entities to share a single physical data link [35]. Besides, the LLC enables the upper layers to use different MAC layers, like the TCP/IP protocols in the wireless routers that use both the 802.3 Ethernet MAC [36] and 802.11 MAC [37]. The Media Access Control (MAC) sublayer of the data link layer manages upper layer access to the physical network medium. The IEEE MAC specification defines MAC addresses, which enable multiple devices to uniquely identify one another at the data link layer.

The standard of physical layer defines the electrical, mechanical, procedural, and functional specifications for activating, maintaining, and deactivating the physical link between communicating network systems. Physical layer specifications define characteristics such as voltage levels, timing of voltage changes, physical data rates, maximum transmission distances, and physical connectors. Physical layer implementations can be categorized as either LAN or WAN specifications. This layer conveys the bit stream (electrical impulse, light or radio signal) through the network at the electrical and mechanical level. Examples of LLC and MAC layers are the ones specified in IEEE 802.3 (Ethernet), IEEE 802.11b (Wireless LAN), and IEEE 802.15.4 (Wireless PAN) [38] standards.

The TCP/IP protocol suite has five layers (Figure 2.9). Usually, the application layer includes the functions of presentation and session layers, if necessary. Cryptography, a typical function of presentation layer, is partially implemented in the MAC layer of IEEE wireless standards.

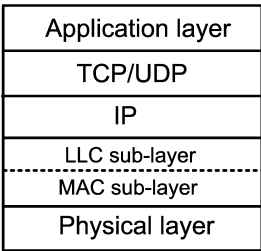


Figure 2.9 - Internet communication layers.

The data and control information that are transmitted through internetworks takes a variety of formats known as Protocol Data Unit (PDU). The most common terms used to refer to these PDU formats include frames, packets, segments, and messages. Figure 2.10 shows

these formats associated to the corresponding layer. The dashed line shows the real flow of the information data between the application layers of two equipments communicating in the network.

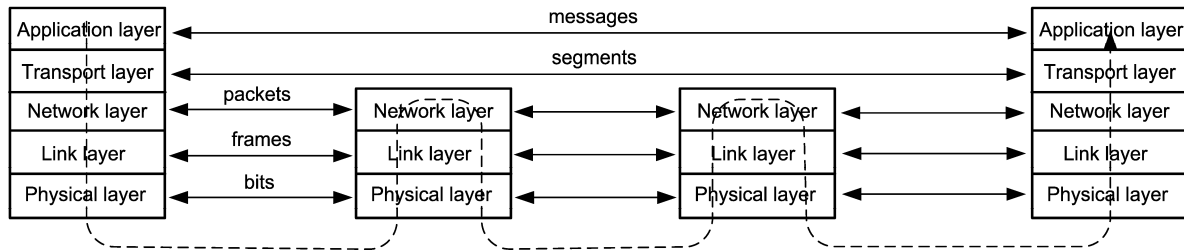


Figure 2.10 - The types of information formats and the flow of information between the layers.

A message is the application layer PDU whose source and destination are application layer entities. A segment is the transport layer PDU whose source and destination are transport layer entities. A packet is the network layer PDU whose source and destination are network layer entities. A frame is the link layer PDU whose source and destination are data link layer entities. A PDU is composed of a header (and possibly a trailer) and upper-layer data. The header and trailer contain control information intended for the corresponding layer entity in the destination system. Data from the upper-layer entity is encapsulated between the header and trailer of the PDU. At the physical layer the information is transported by bits, the smallest logical unit of information in the network.

Data delivery services on the network can be divided into reliable services and unreliable services. In reliable services, there are mechanisms to ensure that the data sent by the source node will arrive without errors at the destination node. The source node is notified that the data was received, or that the network could not accomplish the delivery of data to the destination because of network problems. TCP transport layer of the Internet is an example of implementation of this type of service. These mechanisms are not implemented in the unreliable services. The source node sends the data and there is no guarantee of delivery of the data to the destination. The UDP protocol of the Internet is an example of implementation of this type of service.

On the other hand, the services can be characterized as being either connection-oriented or connectionless. In the connection-oriented services the entity must first establish a connection with the desired service in the peer entity before transferring any data. In the connectionless service the entity can send the data without establishing a connection first.

Connection-oriented service has three phases: connection establishment, data transfer, and connection termination. During connection establishment, the end nodes may reserve resources for the connection. The end nodes also may negotiate and establish certain criteria for the transfer, such as a window size used in the connections. The data transfer phase occurs when the data is transmitted over the connection. During data transfer, most connection-oriented services will monitor for lost packets and resend them. The layer that implements the service is generally also responsible for ordering the packets in the right sequence before passing the data to the upper layer in the communication stack. When the transfer of data is complete, the end nodes terminate the connection and release resources reserved for the connection.

In general, connection-oriented services provide some level of delivery guarantee, whereas connectionless services do not, therefore the connection oriented protocols are used to implement a reliable service. The connectionless protocols are usually used to implement an unreliable service but it is possible to have a connectionless reliable service, known as confirmed datagram. Connection-oriented network services have more overhead than connectionless ones.

An example of connection oriented protocol in the transport layer is the TCP protocol. An example of connectionless protocol in the transport layer is the UDP protocol. The connection oriented protocols are implemented in the upper layers (from transport to application layers) while the connectionless protocols can be implemented in every layer. An example of connectionless network protocol is the IP protocol of Internet. The connectionless protocol data unit is known as datagram. IP uses datagram packets and UDP uses datagram segments.

The network addressing can be divided in three types: unicast, broadcast and multicast. Unicast packets are sent from node to node. The communication is from a single node to another single node. There is one device transmitting a message destined for one receiver. Broadcast packets are sent from one node to all other nodes in a given address range. The broadcast can reach all nodes on the network or all nodes inside a range of addresses in network, known as a subnet. Multicast enables a single node to communicate with a specific set of nodes. This allows for communication that resembles a conference call.

2.7.2 IEEE wireless standards

The Institute of Electrical and Electronics Engineers (IEEE) has produced the series of standards 802.X, which encompassed the wired Local Area Network (LAN), the Wireless LAN (WLAN), Wireless Metropolitan Area Network (WMAN), and Wireless Personal Area Network (PAN). The scope of IEEE 802 is the two lower network layers, the physical and the link layers. The wireless network standards supported by the industry are 802.11 (WLAN), 802.15 (WPAN) and 802.16 (WMAN). These standards specify the physical layer and the MAC layer services defining how each network node communicates with other node exchanging frames. The IEEE 802.2 link layer control (LLC) [35], is used with these MAC layers as an interface with the upper layers like the IP and the TCP/UDP Internet layers.

IEEE 802.16 [39], known as WiMax because of the alliance formed to certify the 802.16 products, is a specification for fixed broadband wireless metropolitan access networks (WMANs). It is a long-range technology which can reach up to 50 km in line-of-sight at data rates up to 70 Mbps.

The 802.15 standard defines three specifications for WPAN: the 802.15.1 for the Bluetooth technology [40]; the 802.15.3 for high rate WPAN [41]; and the 802.15.4 for low rate WPAN [38]. The 802.15.1 is best suited for connecting PDAs, cell phones and PCs in short intervals. The 802.15.3 standard has a high bandwidth up to 55 Mbps and low transmission range, like Bluetooth, and is suite for short-range multimedia streaming. The 802.15.4 is the standard of choice to be used on most Wireless Sensor Networks (WSNs). The physical layer technologies used in 802.15.4 has good performance against noise and interferences. The transmission range is high, of the order of kilometers as we show later, especially in the 868/915 MHz bands.

The 802.11 [37] is a well proven standard, also known as Wi-Fi because of the alliance formed in 1999 to certify interoperability of wireless Local Area Network (LAN) products based on IEEE 802.11 specification. The 802.11 standard is by far the most widely used wireless technology. It is used practically on all WLANs which is at most part of an infrastructured network. Nevertheless, the specification includes Ad hoc mode of operation which enables the equipments to operate as nodes of Ad hoc wireless networks. The 802.11 Ad hoc networks are used to provide wireless connectivity to notebooks, PDAs and

smartphones over a wide area. Like 802.15.4, 802.11 have good performance against noise and interferences because of the use of similar technologies in the physical layer.

The wired and the wireless networks can use the same transport and network layers, usually TCP/UDP and IP, respectively, and the same 802.2 LLC sublayer. Only the MAC sublayer and physical layer are different at each wired or wireless technology (Figure 2.11) [35].

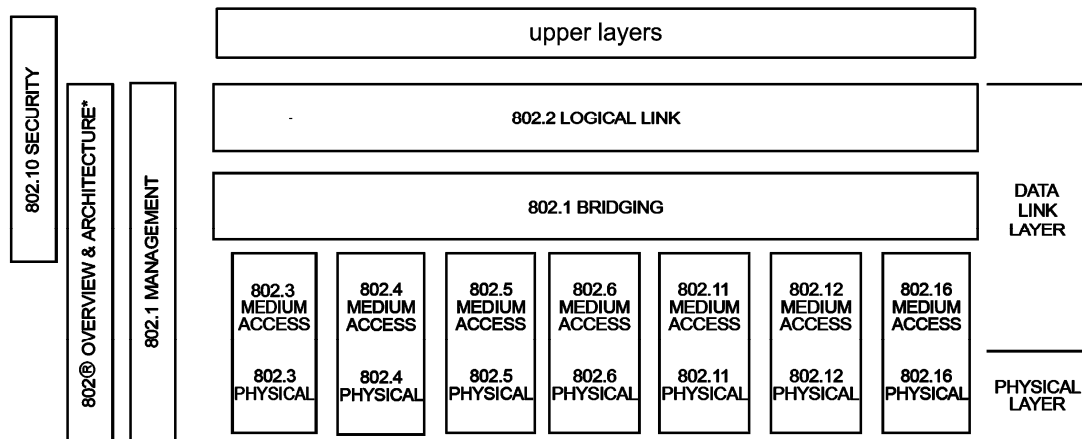


Figure 2.11 - Stack of IEEE 802.x standards [35].

Figure 2.12 shows the IEEE 802.x standards. There are three possible physical layers technologies for 802.11: Frequency Hopping (FH), Direct Sequence Spread Spectrum (DSSS) and infrared light. There is only one physical layer technology used in 802.15.4, the DSSS. DSSS is a transmission technique that has good performance against noise and interferences. The communication at physical layer of these wireless standards is half-duplex. Each network node transmits or receives, not both at the same time.

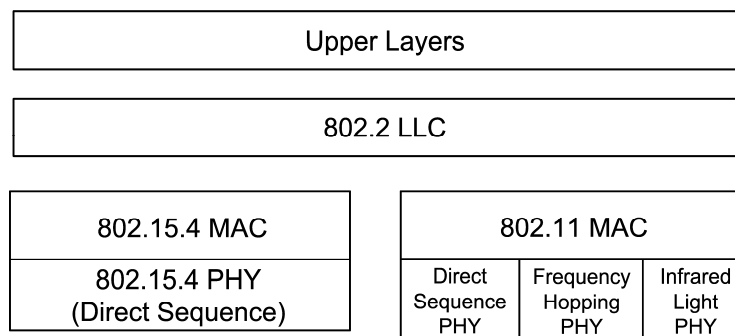


Figure 2.12 - 802.11 and 802.15.4 services.

The Zigbee alliance has defined a communication layer stack to be used with 802.15.4 MAC layer which includes the network layer, the routing protocol and the infrastructure of

the application layer [42]. In the ZigBee specification there is no transport layer. ZigBee was primarily designed for the wide ranging automation applications and to replace the existing non-standard technologies. Figure 2.13 shows the ZigBee layers [8].

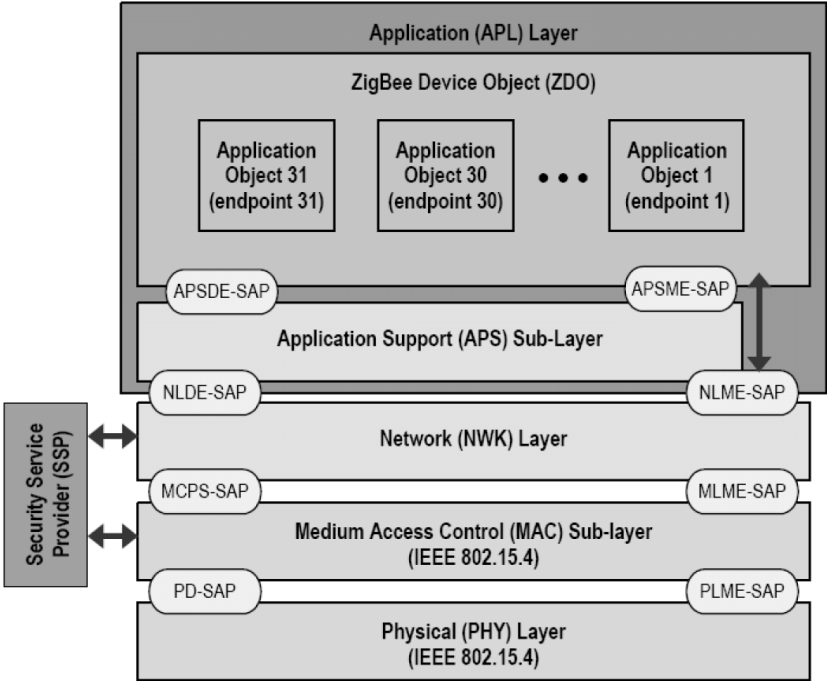


Figure 2.13 - ZigBee layers [8].

The MAC layers of the wireless standards like 802.11 and 802.15.4 have an access mechanism to begin the transmission in an orderly manner. The basic access mechanism is the Carrier Sense Multiple Access with Collision Avoidance (CSMA/CA) with random exponential backoff [43]. It is referred in the 802.11 standard as the basic access mechanism of the Distributed Coordination Function (DCF) [37] (Figure 2.14). With this mechanism, whenever a network node has some packet to transmit, it monitors the activity of the channel. If the channel is idle for a period greater than the time between frames DIFS (Distributed Interframe Space), the node transmits the packet. Otherwise, it monitors the channel until it is idle for a period of time equal to DIFS. Then the node starts a random duration counter (backoff) before starting transmission, trying to minimize the probability of a new collision.

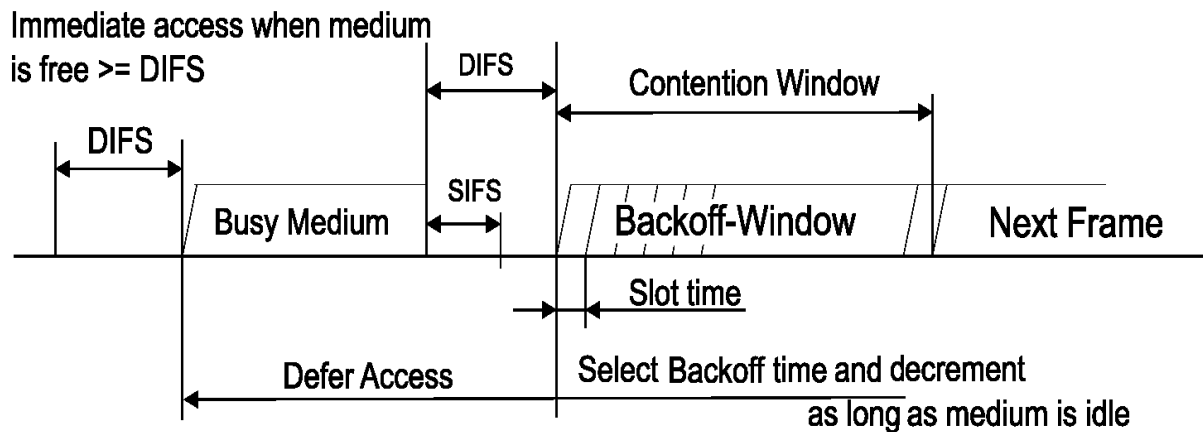


Figure 2.14 - Basic access mechanism [37].

For a single node do not monopolize the channel, it starts the counter whenever two or more packages were transmitted. The nodes have no way to detect whether there was a collision or not because they are unable to transmit and listen to the channel simultaneously [43]. Then, an Acknowledge Frame (ACK) is sent by the destination node immediately after a short period of time called Short Interframe Space (SIFS) whenever a packet is received without error. If an ACK is not received after a pre-defined period of time, there was a collision or a loss of packet and the source node reschedules the transmission according to the size of the window of backoff.

The 802.11 has two modes of operation: the mode described above called basic mode, and the reservation mode [43]. The reservation mode is intended to resolve a problem known as hidden terminal (Figure 2.15). Because of the transmission ranges, node A and node C cannot listen to each other. If they transmit at the same time to node B their frames could be corrupted.

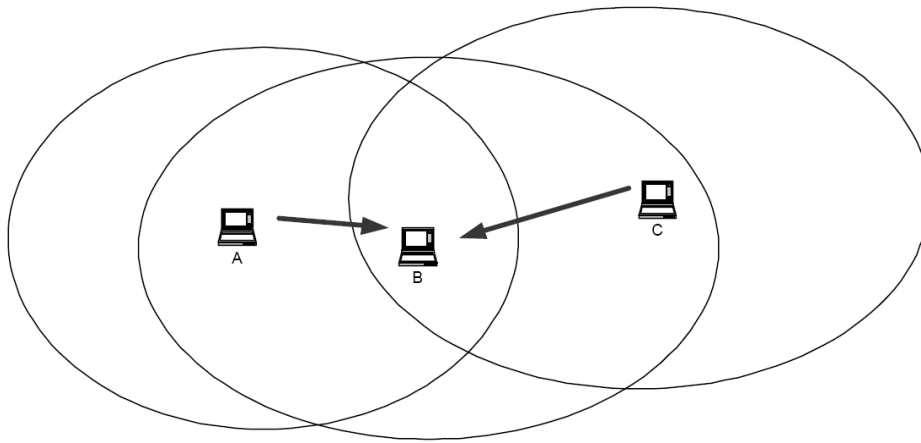


Figure 2.15 - The problem of the hidden terminal (B) [43].

In the reservation mode, each node after detecting that the channel is free for a time equal to DIFS, and after following the rules of backoff described previously, sends a Request-to-Send (RTS) instead transmitting the data. This frame contains the length of the data packet that is addressed to the destination node. If the target node receives this RTS correctly, it waits a time equal to SIFS and sends a frame called Clear-to-Send (CTS) indicating that the node that have done the request may send the data. After a time equal to SIFS, the node that received the CTS starts its transmission. A station can operate simultaneously in these two modes of operation. The RTS/CTS frame informs the size of the payload that the station requested. As the channel is a broadcast channel, stations who receive the RTS/CTS may use this information to update their Network Allocation Vector (NAV). The NAV is a value that indicates to a station the amount of time that remains before the medium will become available. This way, stations that do not participate in the data exchange do not have to listen to the channel all the time. They listen only when the timer equal to NAV expires. Therefore, the NAV is a virtual carrier sensing mechanism. This mechanism is shown in Figure 2.16.

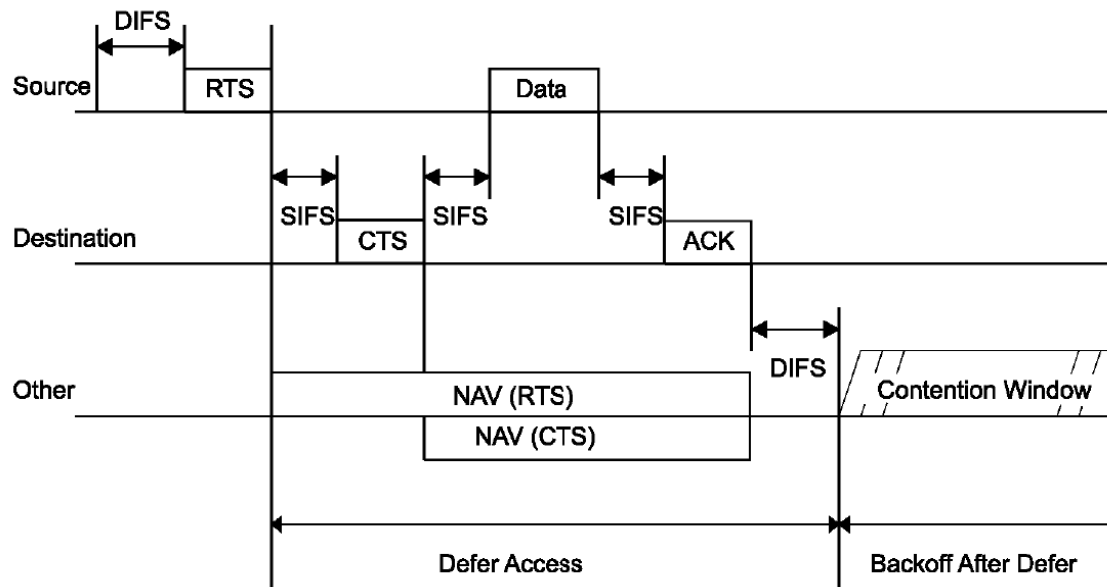


Figure 2.16 - RTS/CTS mechanism [37].

The radio frequencies allowed for use in wireless networks are the frequencies of ISM (Industrial, Scientific and Medical) bands, defined by ITU-R (International Telecommunication Union - Radio Communication Sector), which do not require special licensing for operation. The ranges 433.05–434.79 MHz, 902–928 MHz, 2.4–2.5 GHz, and 5.725–5.875 GHz are the most used. Lower frequencies allow higher transmission range, because they are less attenuated, but are more susceptible to fading (unwanted reflections on obstacles) that degrades the signals. As the sensors will operate in open environments, without buildings nearby, the problems of fading are small. IEEE 802.11 uses the ranges 2.4–2.5 GHz, and 5.725–5.875. The IEEE 802.15.4 uses the ranges 902–928 MHz and 2.4–2.5 GHz. The IEEE 802.11 standard has amendments to specify additional functionalities such as data rates, frequency of operation and data encoding. The most used are the amendments “a”, “b”, and “g”. The basic IEEE 802.11 and the amendments “b” and “g” operate in the 2.4 GHz band. IEEE 802.11a operates in the 5 GHz band. The basic IEEE 802.11 operates with the data rates 1 Mbps and 2 Mbps. IEEE 802.11a operates with data rates between 6 and 54 Mbps [44]. IEEE 802.11b data rates between 1 Mbps and 11 Mbps [45]. IEEE 802.11g operates with data rates between 1 Mbps and 54 Mbps [46].

For 802.11b, the spectrum is divided into 14 overlapping channels in Europe and Japan. Each channel is 22 MHz wide, and the center frequency of each channel is separated by 5

MHz (with the exception of channel 14) (Figure 2.17) [45]. To use non overlapping channels, only the channels 1, 5, 9 and 13 can be used.

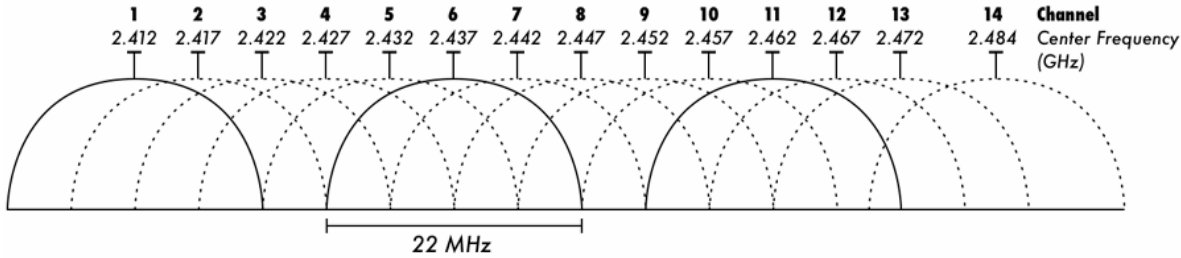


Figure 2.17 - 802.11 channels [47].

For 802.15.4, the spectrum is divided into 10 channels in 915 MHz band and 16 channels in the 2.4 GHz band (Figure 2.18) [38]. The center frequency of each channel is separated by 5 MHz (with the exception of channel 14) in the 2.4 GHz band and separated by 2 MHz in the 915 MHz band.

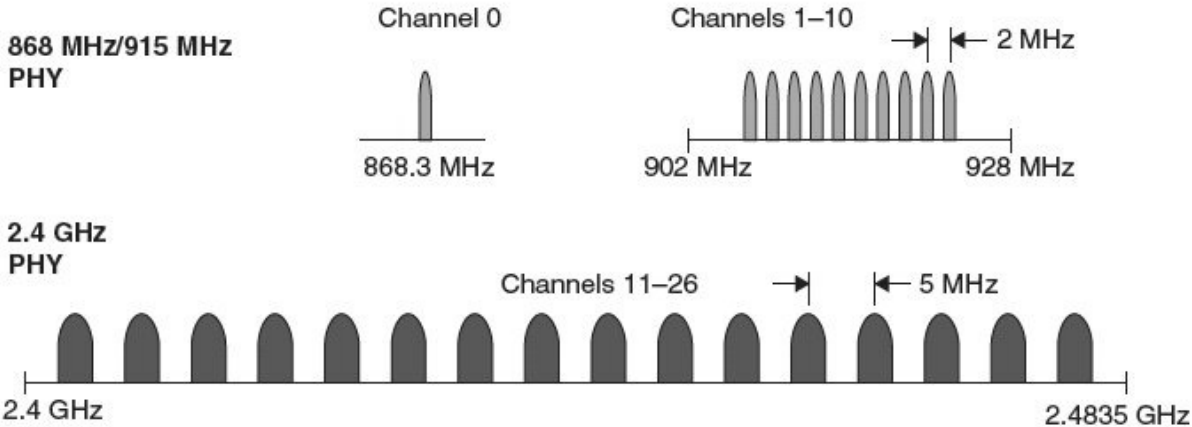


Figure 2.18 - 802.15.4 channels [48].

2.7.3 Network topologies

Network Topology is the arrangement of the nodes of the network. The network topology is determined by the mapping of the physical or logical connections between nodes graphically. There are basically five types of topology: Bus, Ring, Star, Tree, and Mesh (Figure 2.19) [49].

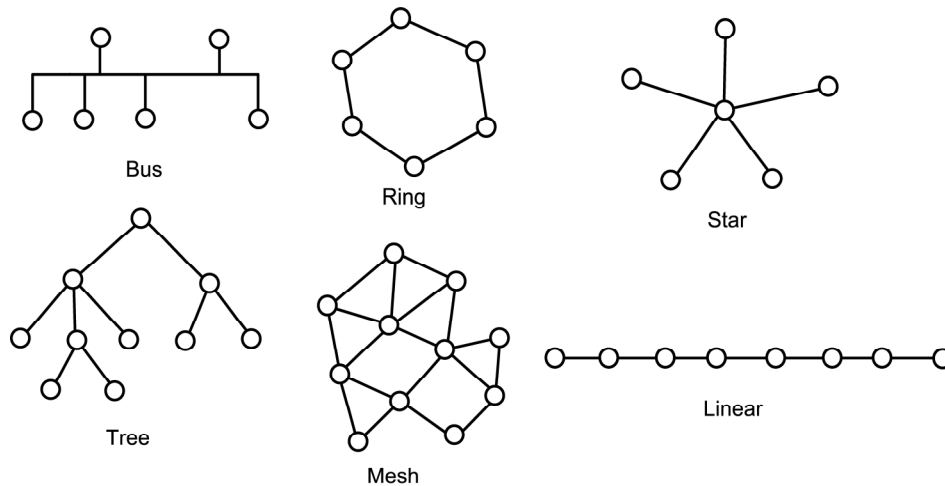


Figure 2.19 - Network topologies.

a) Bus Topology

In this topology the nodes are connected to a single common backbone. This common medium is a shared communication path for the nodes. Each node communicates directly to other node or to every node simultaneously. The shared media can be a cable like the old Ethernet 10Base2 or 10Base5, or a radio channel, like the 802.11 wireless networks.

b) Ring Topology

In this topology each node can communicate with up to two neighbors. The message travels through the ring in either clockwise or anti-clockwise direction. The FDDI and Token ring networks are examples of ring topology.

c) Star Topology

This network topology centralizes the communication in a central node responsible to forward the data to the destination node. An example of this topology is the common Ethernet network with fast Ethernet switches or hubs.

d) Tree Topology

Tree topology is basically the mixture of many star topology networks connected together using bus topology. Devices like hub or switch can be directly connected to tree bus and each hub or switch performs as root of a tree of the network nodes.

e) Mesh Topology

In this topology every node can be connect to one or more neighbor nodes without any specific structure. Each node has to operate as a router to forward the data to the destination through its neighbors. The data passed on to the network can take several paths to reach the destinations, unlike the other topologies. If every device is connected to every other device the network is called full mesh.

f) Linear topology

In the linear topology the nodes are arranged in line and every node communicates with a neighbor behind and a neighbor ahead. When the nodes are geographically arranged in line (physical linear topology), but the logical topology is mesh, the topology is called nearly linear topology. Figure 2.20 shows an example of nearly linear topology and the equivalent mesh topology. For the sake of simplicity, the nearly linear topology will be referred as linear topology in this work.

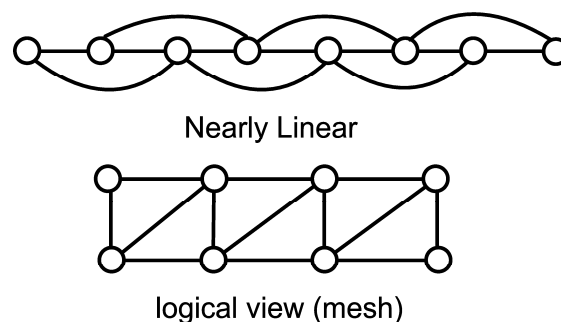


Figure 2.20 - Nearly linear topology and the equivalent mesh topology.

2.7.4 Types of wireless Networks

There are two types of wireless networks [50]. The first is the infra-structured network which operates with fixed gateways. The wireless bridges of the network are known as base stations. A wireless unit within the network connects to and communicates with the nearest base station within its transmission range. The base stations can be access points, that works like a switch or bridge, or wireless routers. The access points and wireless routers communicate with wired routers to route the packets to other networks. Typical applications of this type of network include office WLAN with IEEE 801.11 equipments (routers and access points). Figure 2.21 is an example of an infra-structured wireless network.

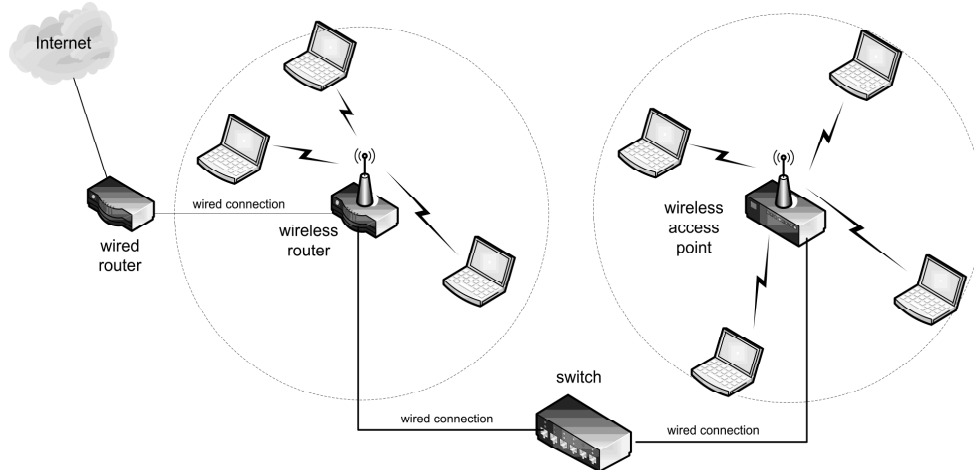


Figure 2.21 - Infra-structured wireless network.

The second type of network is a wireless network without infrastructure, commonly known as Ad Hoc network. They have no fixed routers. All nodes can be connected in an arbitrary manner. These nodes function as routers, which discover and maintain routes to other nodes in the network. The mobile wireless network used on military vehicles to change information in the battlefield is an example of Ad hoc network. In this context, every sensor is a node with routing capacity. Figure 2.22 shows an Ad hoc network of notebooks.

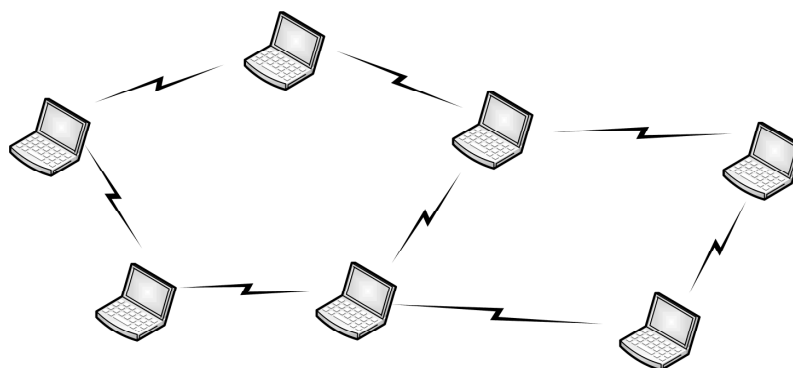


Figure 2.22 - Infra-structured wireless network.

2.7.5 Ad hoc routing protocols

The nodes in wireless network Ad Hoc networks use Ad Hoc routing protocols. These protocols were developed to work on mobile wireless networks to adapt to the changes in the topology when the position of mobile units change and still keep the units communicating. The Ad Hoc routing protocols can be classified in two main groups: table-driven protocols and source-initiated on-demand protocols [50].

Table-driven routing protocols attempt to maintain consistent, up-to-date routing information from each node to every other node in the network. Each node must maintain one or more tables to store routing information. The changes in network topology trigger the propagation of updates throughout the network in order to maintain a consistent network routing information.

The source-initiated on-demand routing protocols employ a different approach from table-driven routing. This type of routing protocol creates routes only when triggered by the source node. When a node requires a route to a destination, it initiates a route discovery process within the network. This process is completed once a route is found or all possible route paths have been examined. Once a route has been established, it is maintained until either the destination becomes inaccessible along every path from the source or until the route is no longer desired.

There are several protocols of each type [50]. Figure 2.23 shows a list of the most known Ad Hoc protocols and the classification of each one: Destination-Sequence Distance Vector (DSDV), Optimized Link State Routing (OLSR), ZigBee Routing, Ad hoc On Demand Distance Vector (AODV), Dynamic Source Routing protocol (DSR), Dynamic MANET On-demand (DYMO) and Temporally-Ordered Routing Algorithm (TORA). ZigBee Routing is considered to be a hybrid protocol because it uses two routing protocols: Hierarchical Tree Routing (HTR) which is a table driven protocol and modified AODV which is an on-demand protocol. HTR is used for nodes without routing capability and AODV is used for router nodes.

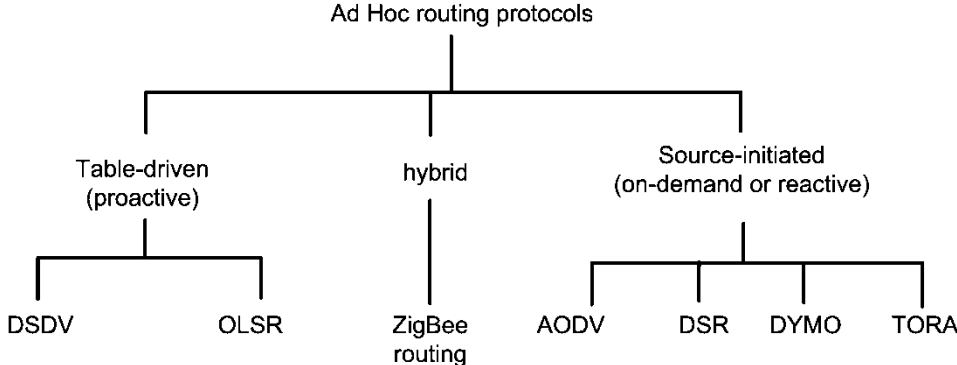


Figure 2.23 - Some common Ad Hoc routing protocols.

The IEEE 802.11s workgroup [51] is working on a standard routing protocol for mesh networks of 802.11 nodes. The routing protocol, known as Hybrid Wireless Mesh Protocol

(HWMP), combines the concurrent operation of a proactive tree-oriented approach with an on-demand distributed path selection protocol derived from the AODV. Nevertheless, the working group has not finished their work and the HWMP is not concluded. On the other hand, the Zigbee standard defined the ZRP that uses HTR and modified AODV. The AODV of ZigBee specification has modifications to minimize the overhead [52].

2.7.6 The AODV protocol operation

AODV is a well known routing protocol with good performance in the linear topology as will be shown later for the wireless sensor network operating on the power transmission lines. To find a path to the destination using the AODV protocol, the source node broadcasts a Route Request Packet (RREQ) [50]. The neighbors in turn broadcast the packet to their neighbors until it reaches an intermediate node that has valid route information about the destination or until it reaches the destination (Figure 2.24a). A node discards a route request packet that it has already received. The route request packet uses sequence numbers to ensure that the routes are loop free. The sequence numbers are also used to make sure that if the intermediate nodes reply to route requests, they reply with the latest information only. When a node forwards a route request packet to its neighbors, it also records in its tables the node from which the first copy of the request was received. This information is used to construct the reverse path for the Route Reply Packet (RREP). AODV uses only symmetric links because the RREP packet follows the reverse path of route request packet. When the destination node receives the RREQ it sends the RREP to the source node. As the RREP packet traverses back to the source (Figure 2.24b), the nodes along the path enter the forward route into their tables. If a node along the route fails, its upstream neighbor notices the failure and propagates a link failure notification message (an RREP with infinite metric) to each of its active upstream neighbors to inform them of the erasure of that part of the route. The process is repeated until the notification reaches the source which can reinitiate route discovery if needed.

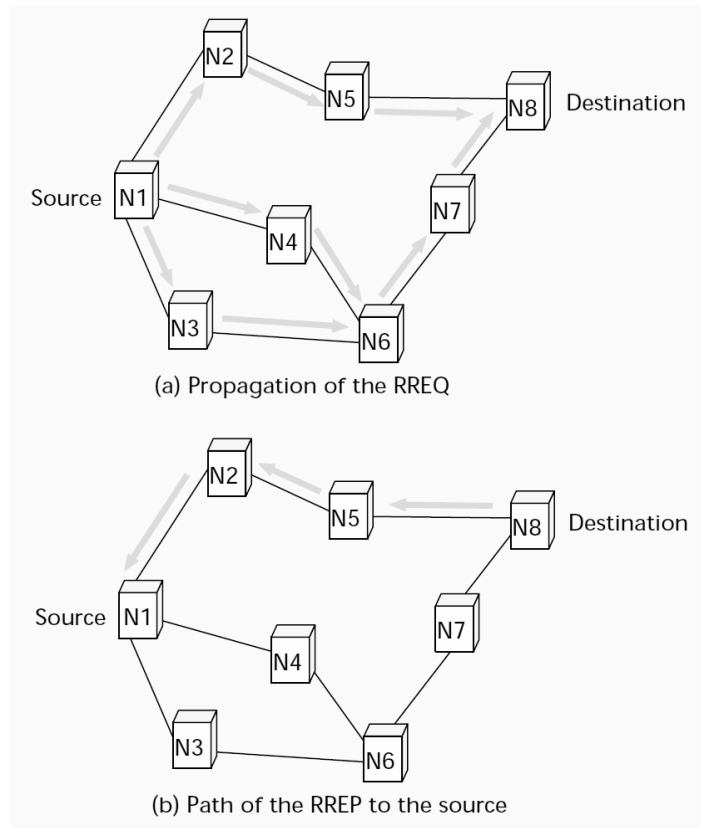


Figure 2.24 - The operation of the AODV protocol [50].

2.7.7 Wireless Sensor Networks

A wireless sensor node consists of components for sensing, computing, communication, actuation, and power supplying. These components are integrated on a single or multiple boards, and packaged in a small case. With state-of-the-art, low-power circuit and networking technologies, a sensor node powered by AA batteries can last for years with a low duty cycle working mode. A WSN usually consists of tens to thousands of such nodes that communicate through wireless channels for information sharing and cooperative processing. WSNs can be deployed on a large geographical scale for environmental monitoring and habitat study, over a battle field for military surveillance and reconnaissance, in emergent environments for search and rescue, in factories for condition based maintenance, in buildings for infrastructure health monitoring, and many other applications.

After the initial deployment (typically Ad hoc), sensor nodes are responsible for self-organizing an appropriate network infrastructure, often with multi-hop connections between sensor nodes. The onboard sensors then start collecting acoustic, visual, infrared or electromagnetic information about the environment, using either continuous or event driven

working modes. Location and positioning information can also be obtained through the Global Positioning System (GPS) or local positioning algorithms. All this information can be gathered from the sensors across the network and processed to construct a global view of the monitoring phenomena. The basic concept behind WSNs is that, despite the limitations in the capability of each individual sensor node, the aggregate power of the entire network is sufficient for the required work. This is a fundamental difference between the WSNs and the traditional wireless networks like the Wi-Fi installations in the offices, campi and public places. While the wireless technology is basically the same, the sensor nodes in the WSNs work to reach a common objective of the system, while in the traditional wireless networks the individual station nodes work to accomplish the individual objective of each user. In the context of power transmission lines, the sensor nodes have a common objective: to gather information from the line to allow the system to detect, identify and locate direct lightning strokes to the line or short-circuits in the phase cables.

2.8 Transmission range of radio

The transmission range of wireless equipments is an important issue in the network operation. The continuous and reliable operation of these equipments depends on the signal received from the neighbors. The open field operation of wireless sensors and other wireless equipments can be analyzed theoretically estimating the attenuation of the signal in line-of-sight operation.

2.8.1 Radio attenuation in free space

The power received by the wireless sensor in free space without obstacles, can be calculated by the Friis formula [53]:

$$P_r(d) = \frac{P_t G_t G_r \lambda^2}{(4\pi)^2 d^2} \quad (2.10)$$

where P_r is the power at the reception, P_t is the transmit power, G_t and G_r are the gains of transmitter and receiver antennas, respectively, d is the distance between the antennas and λ is the wavelength. With this formula, the range (d) can be calculated using the receiver sensibility as the value of the power received:

$$\log(d) = \frac{1}{20} [P_{t_{dBm}} - P_{r_{dBm}} + G_{t_{dBi}} + G_{r_{dBi}} - 20 \cdot \log(f) + 27.54] \quad (2.11)$$

where f is the frequency in MHz, dB_m means that the parameter is in dB milliwatts, and dB_i means that the gain is in dB relative to an isotropic antenna. Including a gain margin (M) in dB the value of range can be calculated by the equation below:

$$\log(d) = \frac{1}{20} \cdot [\text{Pt}_{\text{dBm}} - \text{Pr}_{\text{dBm}} + \text{Gt}_{\text{dB}_i} + \text{Gr}_{\text{dB}_i} - 20 \cdot \log(f) + 27.54 + M_{\text{dB}}] \quad (2.12)$$

The Friis formula is accurate at unobstructed Line of Sight (LOS) path at low distances. Above a critical distance, the two path model (two-ray ground reflection model) [54] is more accurate and includes a ground reflection path besides the direct path of Friis model:

$$P_r(d) = \frac{P_t G_t G_r h_t^2 h_r^2}{d^4} \quad (2.13)$$

where h_r and h_t are the height of transmitter and receiver antennas (meters), respectively. The critical distance (d_c) in meters is:

$$d_c = \frac{4\pi h_r h_t}{\lambda} \quad (2.14)$$

If the distance between the antennas is less than d_c , the Friis model must be used otherwise the two path model must be used.

To have a propagation of the signal in conditions close to the free space, the volume of the Fresnel ellipsoid (Figure 2.25) [55] between the transmitter and receiver must be free of obstructions.

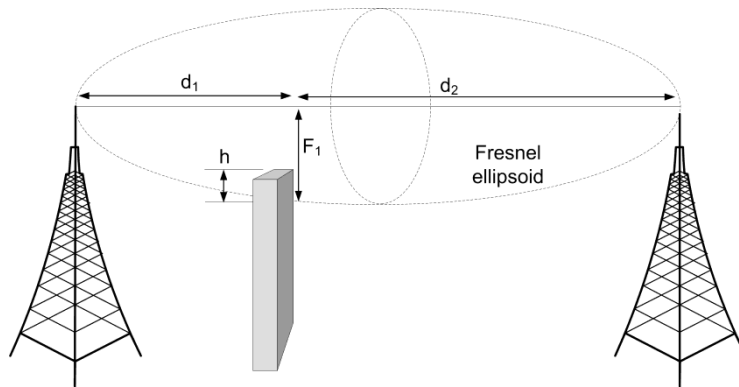


Figure 2.25 - The first Fresnel zone.

The cutting plan of Fresnel ellipsoid perpendicular to the propagation direction is the first Fresnel zone. The radius of the circle of this cutting plan is the radius of the first Fresnel zone. The radius of the first Fresnel zone (F_1) (m) at a distance d_1 from the transmitter is:

$$F_1 = \sqrt{\frac{c d_1 d_2}{f (d_1 + d_2)}} \quad (2.15)$$

where c is the speed of light (m/s), d_1 is the distance (m) from transmitter to the obstacle, d_2 is the distance from obstacle to the receiver, and f is the frequency (Hz).

The radius of the first Fresnel zone (F_1) (m) in the middle of the path is:

$$F_1 = \sqrt{\frac{c d}{4 f}} \quad (2.16)$$

If 60% or more of first Fresnel zone have no obstruction, we have the conditions close to the free space. If h is the length of the obstacle that enters the volume of the ellipsoid, the obstruction is calculated by h/F_1 . For $h/F_1=0.5$ the attenuation is 3 dB and for $h/F_1=1$ the attenuation is -40 dB for flat earth surface [55], as usually is the case for the sensors operating on OPTLs.

2.8.2 Weather attenuation

The system must operate on any weather conditions. Therefore, it is necessary to evaluate the additional attenuation of the signal caused by rain and snow. The rain attenuation (A_r), in dB/km, can be estimated by the following formula [56]:

$$A_r = K R^\alpha \quad (2.17)$$

where K and α are constants that depend on the frequency, and R is the rate of rain in mm/hr. For a heavy rain with the high rate of 250 mm/hr of water, the attenuation at 2.4 GHz is less than 0.1 dB/km. At 5.15 GHz the attenuation is 1.5 dB/km.

The snow attenuation (A_s) can be estimated by the following formula [57]:

$$A_s = 0.00349 \frac{R^{1.6}}{\lambda^4} + 0.00224 \frac{R}{\lambda} \quad (2.18)$$

where λ is wave length (m) and R is the water equivalent of snow rate (mm/hr). For a heavy snow with the high rate of 50 mm/hr of equivalent water, the attenuation at 2.4 GHz is only 0.009 dB/km and at 5.15 GHz is 0.02 dB/km.

The rain attenuation is significant above 5 MHz and snow attenuation is significant only above 30 GHz. At the frequencies of 915 MHz and 2.4 GHz they are negligible.

2.8.3 The role of antennas in the transmission range

The antenna is very important to determine the maximum range of the radio transceiver because the gain significantly affects the range of the sensor. The antenna gain is a function of its directionality. An isotropic antenna irradiates the power equally in all directions. The free space models described above consider this type of irradiation in their formulas and include the antenna gain to account for the mode of irradiation of real antennas that do not irradiate in all directions. They concentrate the power in the horizontal (azimuth) and/or vertical (elevation) plan. The higher is the directionality, the higher is the gain of the antenna.

Special attention must be paid to the installation of the sensors. Because of the high number of sensors, the installation procedure must be simple. Therefore, antennas with directionality in both the horizontal and vertical plane must be avoided because it would be necessary to align the antennas to optimize the range. The transmission lines also can change direction at angles up to 90 degrees because of the topography of the terrain. The lines may also have branches in which case a sensor has to communicate with other sensors that are not positioned in line. The choice should be for the omnidirectional antennas in the horizontal plane so that the technicians have to concern only to install the antenna in a vertical position.

The vertical plane must have an elevation angle so that the irregularities of the terrain (hills and valleys) do not affect significantly the range of the transceivers (Figure 2.26).

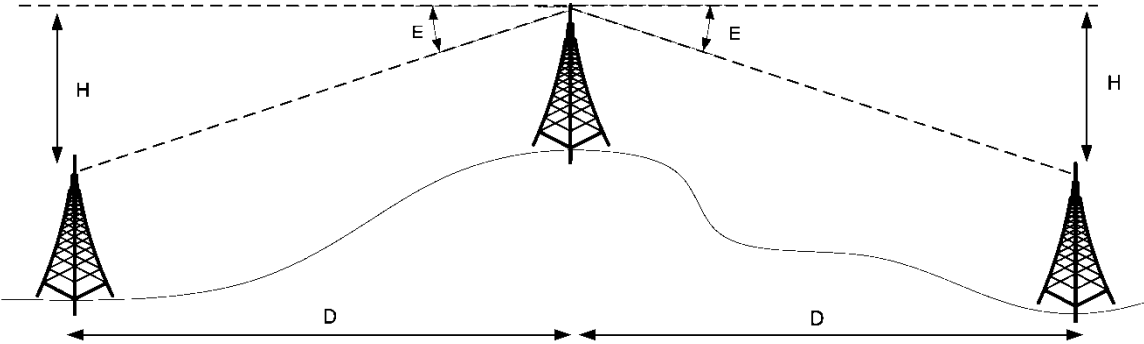


Figure 2.26 - The elevation angle of the antenna and the difference in the tower levels.

In Figure 2.26 the angle E must be at most half the elevation angle of the antenna. To keep the neighbor sensor inside the elevation angle of the antenna, the minimum value of elevation angle of the antenna (θ) can be calculated as a function of the distance between the towers (D) and the difference of the heights of the towers (H):

$$\theta = \tan^{-1}(H/D) \tag{2.19}$$

Table 2.1 shows the values of maximum values of H for some values of D and θ .

Table 2.1 - The maximum difference between the top of towers as a function of the antenna elevation angle.

θ (degrees)	D (m)	H (m)
32,5	100	64
19,0	100	34
32,5	200	127
19,0	200	69
32,5	500	319
19,0	500	172

There are common situations in mountainous regions where a sensor have line-of-sight to only one sensor at each side. In this case, if the nearest neighbor sensor is faulty, the signal reaches the next neighbor by diffraction (Figure 2.27). If the obstruction blocks the Fresnel zone completely the signal does not reach the next neighbor.

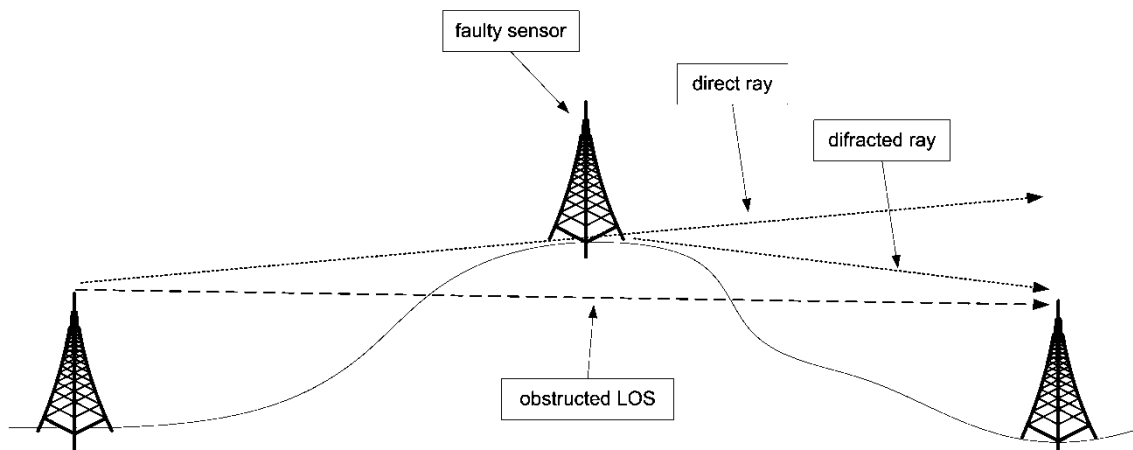


Figure 2.27 - Obstruction of the signal in case of a failure one sensor on the top a hill.

One of the simplest antennas is the half-wave dipole composed of two wires of one-quarter wavelength feed at the center (Figure 2.28).

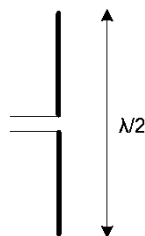


Figure 2.28 - Dipole antenna

Figure 2.29 shows the irradiation diagrams of a commercial dipole antenna. The radiation pattern is omnidirectional in the horizontal plane (360 degrees azimuth), and is directional in the vertical plane with elevation of 65 degrees, and the gain is 2.15 dBi [58].

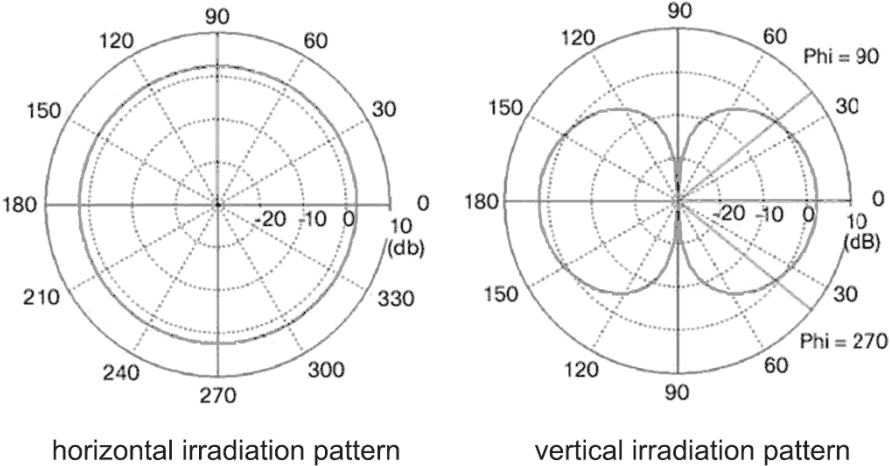


Figure 2.29 - Irradiation diagrams of the dipole antenna [58].

To have an omnidirectional antenna with higher gain, multiple omnidirectional structures (wires or other elements) can be arranged in a vertical, linear fashion. These arrangements retain the same omnidirectional pattern in the horizontal plane but with a more directional beam in the vertical plane. The power in the vertical plane is radiated in a more focused way which means higher gain than the simple dipole. This is known as a collinear array [59]. Figure 2.30 shows some types of collinear antennas. Figure 2.30a is a collinear array of dipole antennas. Figure 2.30b is a center fed collinear array of dipole antennas. Figure 2.30c is a mutually coupled array of half wave structures. Figure 2.30d is an array of half wave structures coupled with one-quarter wave stubs. Figure 2.30e is an array of half wave structures coupled with phase reversal coils.

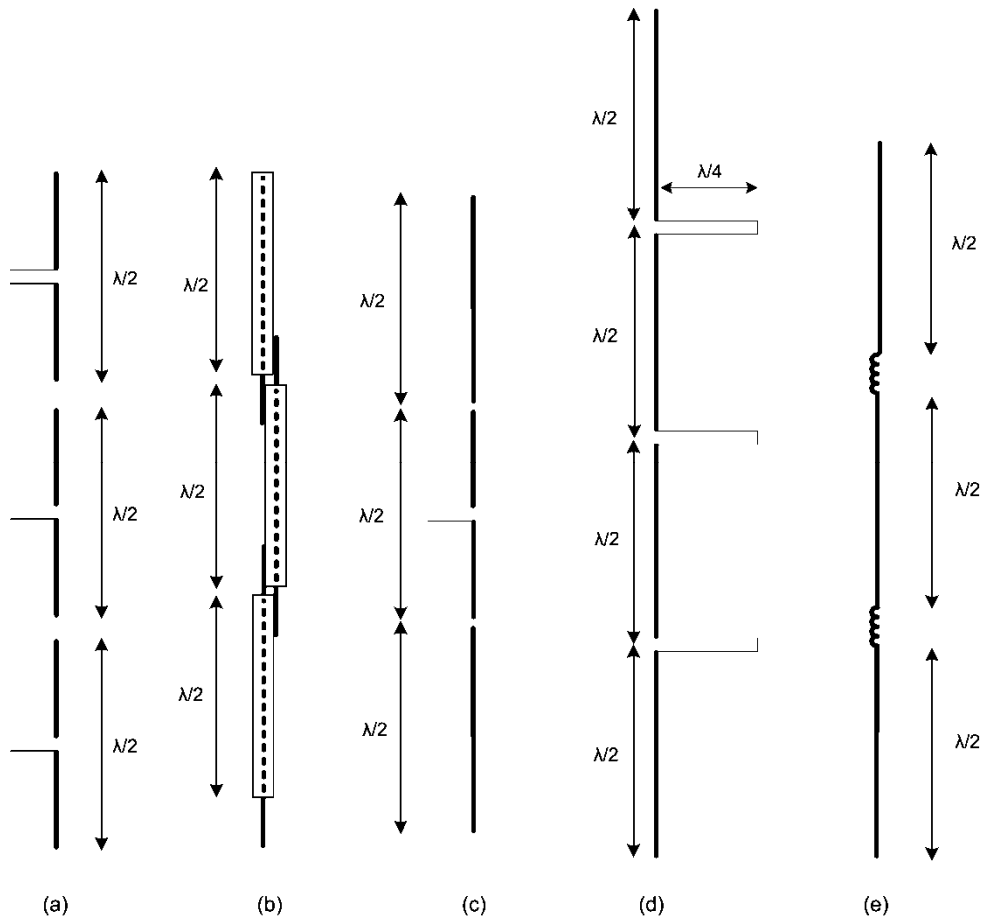


Figure 2.30 - Some types of collinear antennas.

Figure 2.31 shows the irradiation diagram of a vertical collinear array composed by three dipoles oriented along the vertical axis. The radiation pattern is omnidirectional in the horizontal plane (360 degrees azimuth), elevation of 38 degrees, and the gain of 5.8 dBi [58] obtained focusing the beam in the vertical plane.

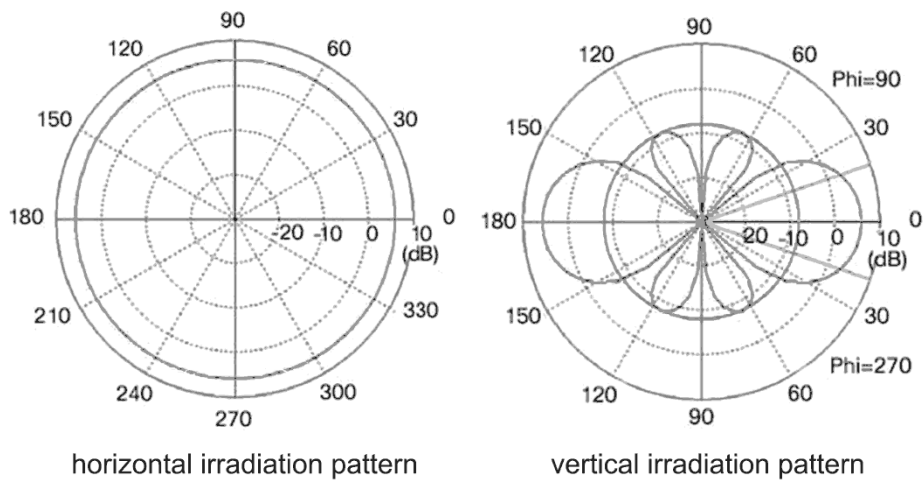


Figure 2.31 - Irradiation diagrams of the collinear array of three dipole antennas [58].

Other types of vertical collinear antennas have higher gain focusing the beam even more in the vertical plane. There are commercial collinear antennas with gain up to 12 dBi with an elevation of 7 degrees [60].

Chapter 3

Detection and location of transient disturbances using wireless sensors

At the beginning, the focus of this work was the utilization of wireless sensors to detect and locate direct strokes to overhead power transmission lines. After extensive simulations and analysis of the behavior of the currents in the shield wires and phase cables in response to transients, we advised that, besides the detection and location of direct strokes, it was also possible to detect and locate faults with the same system. Therefore, it became a more comprehensive system.

3.1 Detection and location of direct strokes

Currently, the detection and location of direct lightning strokes to OPTL is done using the information data from LLS with the fault location system information to locate lightning strokes that caused faults [5]. However, they detect only the direct stroke that caused an immediate fault. Besides, these systems cannot evaluate the power of the stroke to determine if it caused any damage to the transmission line. If the stroke current have high peak current and high di/dt , the insulators may be damaged and also the shield wire. The precision is at most equal to the precision of the fault location system.

The traditional fault location systems described earlier are unable to detect and locate every direct strokes to shield wires. The transient currents induced in the phase cables are much lower than the transient fault currents and also the rate of change of current (di/dt). Currently there is few published material about location of direct strokes to power lines. There is a method proposed to locate the strokes to power lines using the fiber optic of the Optic Ground Wire (OPGW) [2] which is applicable only to this type of shield wire. The Electric Power Research Institute (EPRI) published at December 2009 the extensive research on sensor technologies for smart transmission systems [61]. Although they have not released any details, the research includes the lightning and fault location.

We propose a new method to detect and locate direct lightning stroke to the shield wire of overhead power transmission lines using sensors distributed along the line, placed on the top of the towers [62]. With this method, it is possible to locate the stroke position with the precision of one span, and to evaluate its severity. The method can be implemented by a system that uses the technology of wireless sensors. The sensors can communicate through a wireless network with a computer that receives the data from the sensors to locate the stroke position and to evaluate the stroke severity. The installation and the maintenance of the system are easy because it does not use the phase cables.

3.1.1 Direct lightning stroke detection and location

When the lightning stroke hits the shield wire of a power transmission line, the stroke current is divided into two opposite flows (Figure 3.1). The amplitude of each flow depends on the hit position and on the impedances of the closest towers. Most of the current flows to ground through the two nearest towers, but a residual current passes to the next towers.

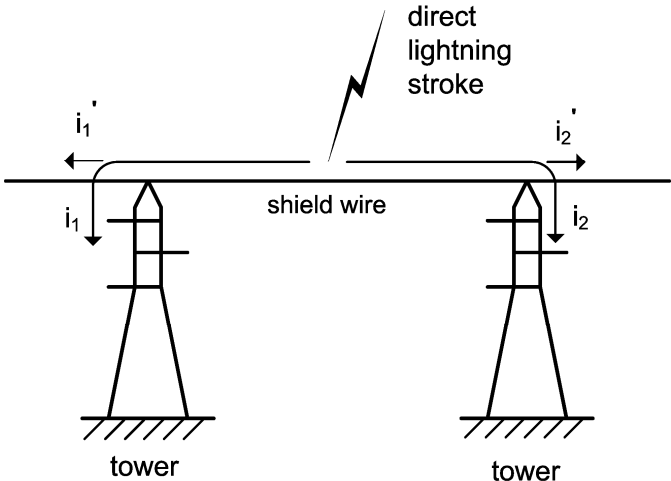


Figure 3.1 - Direct lightning stroke currents, i_1 and i_2 are the currents that flow to ground through the nearest towers, i_1' and i_2' are the residual currents that flow to the next towers.

The currents are higher in the shield wires and in the towers closest to the lightning stroke than in the wires and towers that are farther away. A straightforward way to detect a lightning that strikes the shield wire is to measure the current flowing in the path to ground, through each tower. The measurement of the current can be carried out by a Rogowski coil [31] placed on the top of the tower, around the tip of the structure where the wire is connected, or around the wire connecting the shield wire to the tower structure (Figure 3.2). The output voltage of a Rogowski coil is proportional to the rate of change of current (di/dt)

flowing through the toroid. Applying this voltage to an integrator circuit results in an output voltage proportional to the current. The integrator is usually placed close to the coil to minimize noise pickup.

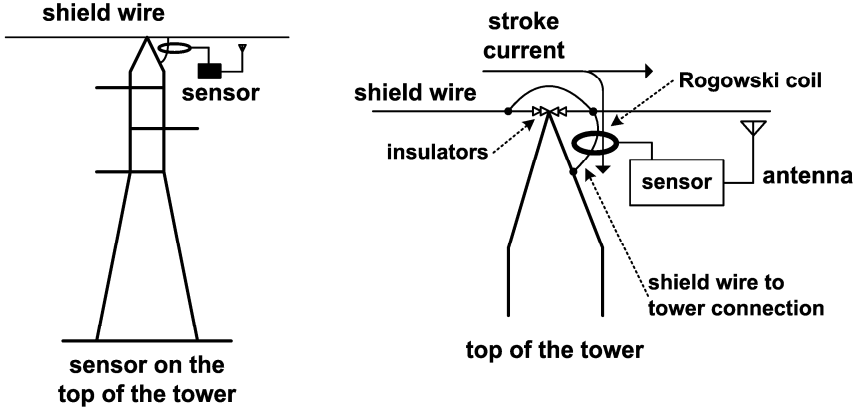


Figure 3.2 - Position of the sensor on the top of the tower.

An electronic sensor installed close to the coil can read the output voltage (proportional to the current) of the integrator, scaling it to compare to a preset threshold. When the stroke current flows through the towers nearest to the stroke point, the peak current reaches this threshold and triggers each device to do the measurement of the peak current and its di/dt. The sensors convert the output voltage into binary data to send the measurement to a computer for post processing. The devices that measure the highest peak currents are the ones closest to the stroke point. Together with the information about the current, the sensors send the time stamp of the measurement and the sensor identification to allow the process of location.

In case of a shielding failure, the lightning strikes the phase cable and is divided in two opposite flows as well. The stroke current flowing in the phase cable induces a current in the shield wires that flows mostly to the ground through the towers. The same method of detection and location of direct strike to shield wire performs well for the direct stroke to phase cable, as we show later in the simulations.

The proposed method measures the currents flowing through the towers, rather than the currents flowing in the shield wires, to allow the evaluation of direct lightning stroke severity. The method has the same precision with branched lines and parallel installations because the measurements are done at every tower and is independent of the length of the line, and can be used on Direct Current (DC) power transmission lines, as well. Extensive simulations detailed in Chapter 5 show the feasibility of the method.

3.1.2 Evaluating the severity of the lightning stroke

The evaluation of the severity of the lightning stroke is very important because it may be used to begin or not a maintenance activity for the power line. The measurement of the currents flowing through the towers, instead of measuring the currents in the shield wires, gives a direct estimation of the corresponding surge voltage on the top of the tower. With the value of the peak current and its di/dt it is possible to estimate the surge voltage if the approximate tower surge impedance and grounding resistance are known. The equation below estimates the peak voltage at the top of the tower (V_p) [63]:

$$V_p \cong (R_T + R_g) I_p + L_T \left(\frac{di}{dt} \right)_p \quad (3.1)$$

I_p is the peak value of the current flowing through the tower, $(di/dt)_p$ is peak value of the di/dt , R_g is the tower grounding resistance, R_T is tower resistance, usually negligible compared to R_g , and L_T is the tower inductance. L_T can be calculated from the tower surge impedance [63]:

$$L_T = \frac{Z_T}{v} h \quad (3.2)$$

Z_T is the tower surge impedance, which is calculated using one of known methods described earlier (Chapter 2), h is the height of tower, and v is the propagation speed of the current in the tower. The higher the measured peak current and its di/dt , the higher is the surge voltage on the top of the tower and on the insulators. The di/dt is the output of the Rogowski coil and can be measured before the integrator. The tower surge impedance can be estimated from the tower structure and dimensions, and the tower grounding resistance is usually known or estimated. With these parameters and the specifications of the insulators, the maximum safe value of surge voltage can be calculated for each tower. When the measured di/dt and the peak current are received from a sensor, they can be used to estimate the surge voltage and verify if it exceeds the maximum safe value. A warning may be issued to the operator if the value is exceeded.

Equation (3.1) gives an estimation of the value of V_p and presents an error in the calculated value which is mainly due to fact that the peak value of current and the peak value

of di/dt do not occur at the same instant. The estimated value will usually be higher the real value.

In case of a power transmission lines with two shield wires, the estimation of the stroke severity is possible if each sensor measure the currents from both wires. Otherwise, if the stroke hits one wire and the sensors measure the current only from the other wire, the current and its di/dt will be underestimated because they are smaller, as shown in the results of Chapter 5.

3.2 Short-circuit fault detection and location

There are several proposed or developed systems to locate faults on power transmission lines. The conventional systems described earlier employ methods that are very different from the proposed one. They make the measurements only at the edges of the transmission line to estimate the fault position. The systems based on travelling waves do not perform well with branched transmission lines and neither with parallel lines. This is due to the reflection of surge signals at points of sudden change in line parameters such as branching points. These systems can detect faults up to two hundred ohms. There are cases of faults up to 528Ω in high voltage transmission lines [64] that these systems cannot locate. Besides, these systems need to be well regulated and configured prior to begin operation to have good accuracy.

There are other systems based on sensors under research, like the already mentioned system from EPRI, or being operated, like the Genscape monitoring system [65] that uses wireless sensors installed below the phase cables. The sensors measure the magnetic fields generated by the phase cables using antennas (Figure 3.3) to monitor the power transmission line.

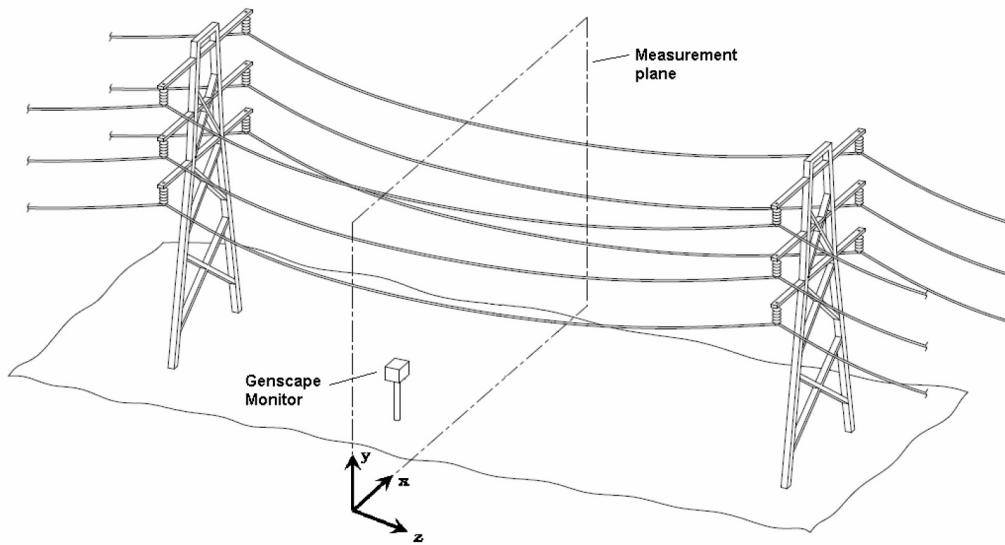


Figure 3.3 - Genscape wireless monitoring system [65].

We propose a method to locate short-circuit faults on overhead power transmission lines using sensors distributed along the line, installed on the top of the towers [66]. The fault induces transient currents in the overhead shield wire that flow partially to ground through the towers. These transient currents are greater in the towers closest to the fault position. The sensors near the fault measure these transient currents in the path to ground. Each sensor can communicate with its neighbors via embedded radio transceivers and sends the measured values to a computer using the wireless network formed by the sensor themselves. After receiving and comparing these values, the computer can locate the fault with good precision. This method facilitates the installation and the maintenance of the Fault Locator System because it does not use the phase cables. Because the method makes the measurements of the transient currents, using the sensors, close to the fault position, it is possible to detect and locate faults in a wide range of impedances. Besides, the accuracy is the same with branched lines and parallel installations and is independent of the length of the line.

The principle of operation is the same used for detection and location of direct lightning stroke to overhead power lines described earlier. The hardware to implement the location of strokes and faults is basically the same, with little modifications, and the fault location is an additional functionality added to the sensors originally conceived to detect direct strokes.

3.2.1 Voltage induced on shield wires

Several papers analyze the voltage induced by the phase currents of overhead power transmission lines on metallic gas pipelines [67] and communication cables [68] running

parallel to the phase cables. In a similar way, the currents in the phase cables induce a voltage on the shield wire.

Inductive coupling is the most important way to induce an AC voltage on a parallel wire. For this type of coupling, the voltage induced on a parallel wire by the current flowing in the cable is approximately equal to the product of the current by the mutual impedance between the two conductors:

$$V_m = Z_m I \quad (3.3)$$

where I is the current flowing in the inducing cable (Amperes), Z_m is the mutual impedance between the two parallel conductors, in ohms per kilometer, and V_m unit is given in Volts per kilometer of wire. Figure 3.4 shows the equivalent circuit for the induction of one phase in a single span power line.

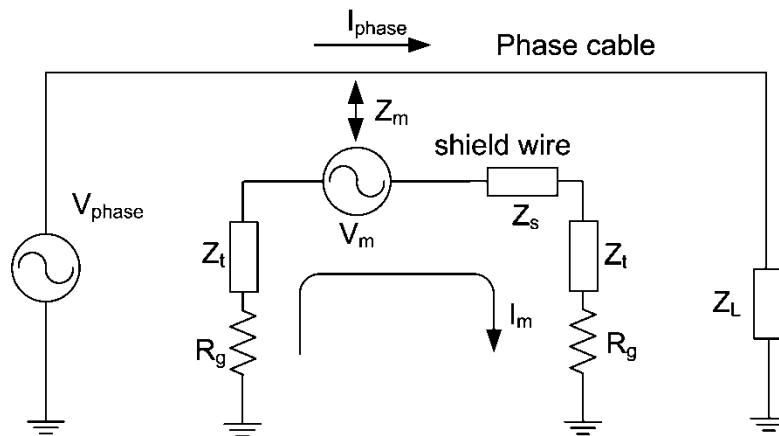


Figure 3.4 - Equivalent circuit for the induction of voltage on the shield wires: I_{phase} is the current on the phase cable, Z_m is the mutual impedance, Z_t is the impedance of the tower, Z_s is the impedance of the shield wire, R_g is the tower grounding resistance, V_m is the induced voltage, I_m is the induced current, V_{phase} is the phase voltage, and Z_L is the load impedance.

The voltage induced by the three phases on the shield wire of an overhead transmission line is equal to the sum of the products of each phase current by the mutual impedance between the phase cable and the wire:

$$V_m = Z_{mA} I_A + Z_{mB} I_B + Z_{mC} I_C \quad (\text{V/km}) \quad (3.4)$$

where I_A , I_B and I_C are the currents in phases A, B, C, respectively, and Z_{mA} , Z_{mB} and Z_{mC} are the mutual impedances between phases A, B, and C and the wire, respectively. V_m is the voltage induced per kilometer of wire. The mutual impedance (Z_m) between cables above a

homogenous earth can be computed by Carson's equations [69]. The equation below is a simplified version in which the corrections for earth return and cable resistance are ignored, as they represent roughly 1% of the value of Z_m [70]:

$$Z_m = \frac{\pi\mu_0 f}{4} + j\mu_0 f \left[6.5 - \ln \left(d \sqrt{\frac{f}{\rho}} \right) \right] \quad (3.5)$$

where f is the line frequency in Hertz, ρ is the soil resistivity in Ohm.meter, d is the distance in meters between the conductors, $j = (-1)^{1/2}$ and μ_0 is the permeability of the free space.

The mutual impedance and, consequently the induced voltage, depend on the frequency, on the distance between the cables, and on the soil resistivity. The mutual impedance increases with frequency and decreases with the distance. The frequency is the parameter that affects most the mutual impedance. The induced voltage also depends on the amplitude and balance of phase currents, and depends on the positions of the phase cables relative to the shield wire.

The current flowing in the wire between the two towers, due to the voltage induced on the wire, depends on the towers impedances, grounding resistances and the wire impedance. For the steady state currents, only the wire impedance and the towers grounding resistances are significant for the resulting current. The grounding resistance usually is higher than the wire impedance. For the high speed transient currents, the surge impedances of the wire and the towers are very significant and the wire impedance is usually greater than the tower impedance. Figure 3.5 shows the equivalent circuit for the evaluation of the induced voltages and currents on shield wire and towers.

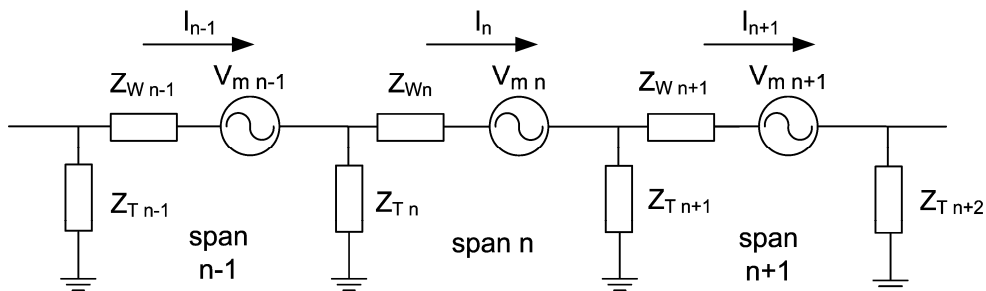


Figure 3.5 - The equivalent circuit for the evaluation of the induced voltages and currents on the shield wire and towers. Z_T is the tower impedance plus the grounding resistance, Z_W is the wire impedance, V_m is the induced voltage, I_n is resulting induced current.

3.2.2 Voltages and currents induced by the short-circuit current

To investigate the voltages and currents induced in the shield wire by the phase currents, we used the Alternative Transient Program (ATP) [27] employing the Line/Cable Constants (LCC) routine to model the cables. This routine calculates the inductive, capacitive and conductive coupling between the cables (JMarti model). There are several case studies showing that the simulation results of voltage induction using the ATP program and LCC routine is close to the field measurements [70][29].

The short-circuit current in one phase induces high voltages on the shield wire because of the high frequency components of the short-circuit transient. We have used the ATP program to simulate the voltage and current induced on the shield wire for a line-to-ground fault of low impedance (5Ω) very close to a tower, in a homogeneous transmission line (detailed in Appendix A). Figure 3.6 shows the short-circuit currents in one phase in the span before the fault position (source direction) and in the span after the fault position (load direction). Figure 3.6 also shows the corresponding voltages induced on the shield wire.

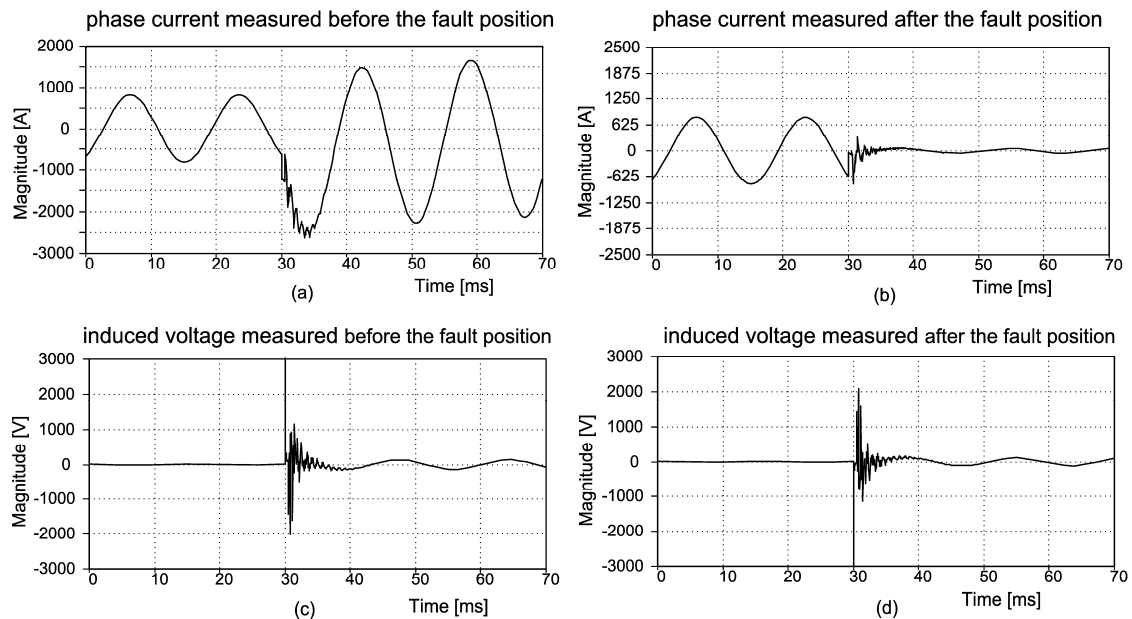


Figure 3.6 - Line-to-ground fault currents before (a) and after (b) the short-circuit position; Voltage induced on the shield wire before (c) and after (d) the short-circuit position.

The waveforms show that besides the 60 Hz induced voltage, there is a much higher transient voltage induced on the wire. The rise time and fall time of these short-circuit transients are very short. Figure 3.7 is a zoom in the waveforms of Figure 3.6 showing in

detail the edges of the waveforms. These transient voltages on the shield wires last hundreds of microseconds.

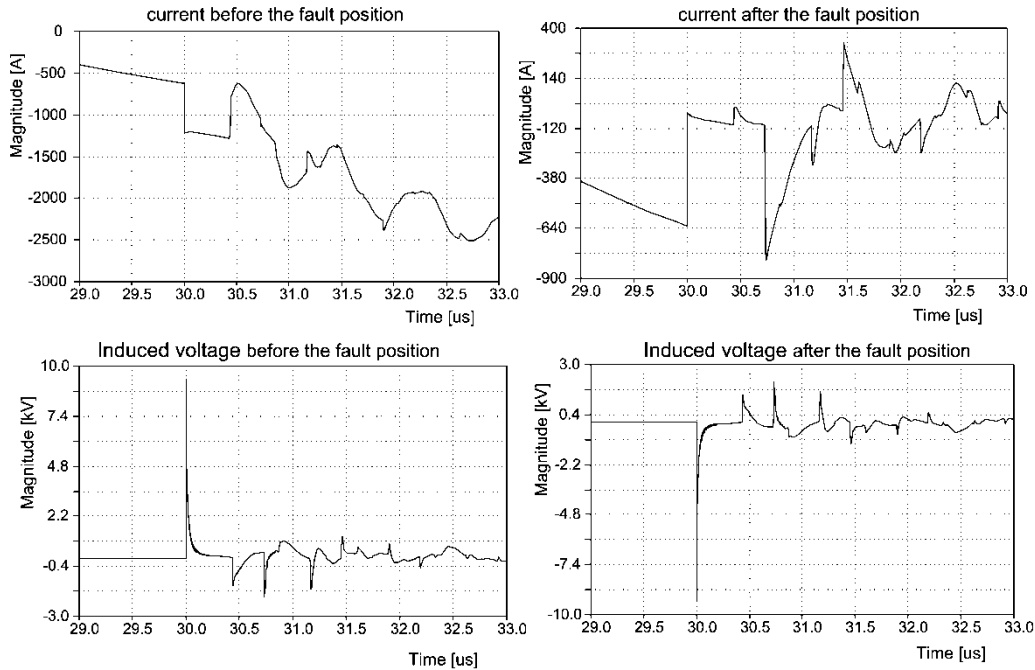


Figure 3.7 - Details of the edges of the transient currents and the induced voltages of Figure 3.6.

The fast rate of change of the current (di/dt) shown in the figures generates frequency components much higher than 60 Hz. The knee frequency (f_{knee}) of a signal, below which most of the energy concentrates, is inversely proportional to the signal rise time (t_r) [71]:

$$f_{knee} \cong \frac{0.5}{t_r} \quad (3.6)$$

For the rise time of 2 μ s, measured in the simulations, the short-circuit current has a knee frequency of 250 kHz. Because the mutual impedance increases with frequency, the transient voltage induced on the shield wire is much higher than the voltage induced by the 60 Hz current.

We analyzed the currents in the shield wire and in the towers closest to the position of the line-to-ground fault that generated the currents and voltages of Figure 3.6. Figure 3.8 shows the diagram of the segment of the transmission line near the fault and the currents simulated. The six towers where the currents were measured have the identifications T1 to T6 in Figure 3.8. The fault is very close to T4. Figure 3.9 shows the waveform of the transient currents in the shield wire in the six towers near the fault position, according to Figure 3.8. The figure shows that the tower closest to the short-circuit position is the one with the highest

current (tower 4) and the highest rate of change of current (di/dt). In the other towers, the transient currents that flow through the towers are smaller and have lower di/dt (towers 1, 2, 3, 5 and 6). The currents in the shield wire connected to these five towers have similar amplitude and waveform and cancel each other when they flow to ground through the tower. This behavior is the same in all spans that are not near the fault. Besides, between these five towers, the two towers closest to the short-circuit position have the highest transient currents (towers 3 and 5) because the currents in their segments of shield wire are less similar and the cancellation is smaller. In tower 4, the currents in the two adjacent spans are quite different and the resulting current in the tower is much higher.

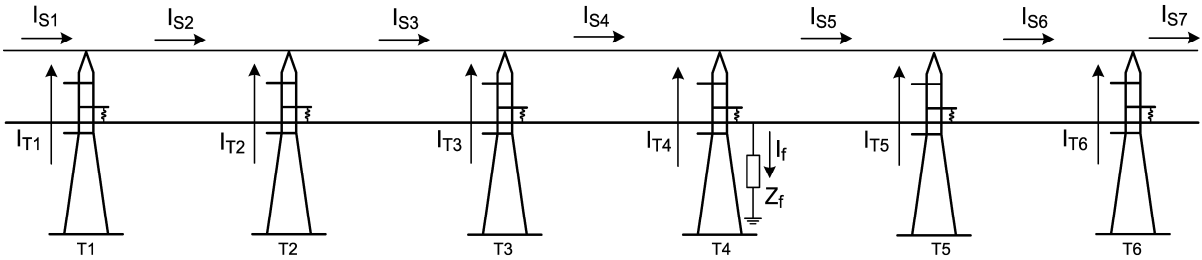


Figure 3.8 - Currents in the shield wire and in the towers near the fault position, I_{S1} to I_{S7} are the shield wire currents, I_{T1} to I_{T6} are the tower currents, Z_f is the short-circuit impedance, I_f is the short-circuit current (T1 to T6 are the identifications for tower 1 to tower 6).

In the simulations of line-to-ground faults in the middle of the span, and other intermediary positions, we observed the same behavior. In the two towers closest to the short-circuit position, the induced transient currents are higher and have a higher di/dt . In the other towers, the currents and their di/dt are lower. Other simulations showed the same behavior with other types of symmetrical and asymmetrical faults like phase-to-phase short-circuits.

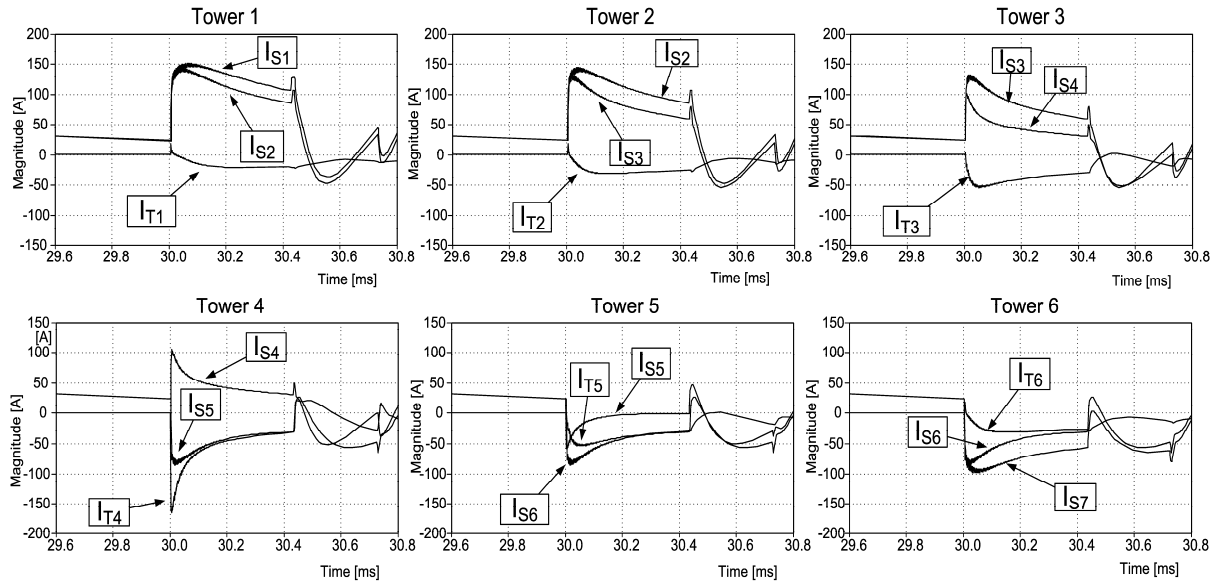


Figure 3.9 - Waveforms of the transient currents in the shield wire and towers according to Figure 3.8.

3.2.3 Behavior analysis of the transient currents

In the line-to-ground fault of Figure 3.6, the waveform of the current before the fault position travels in the phase cable in the direction of the source. The waveform of the current after the fault position travels in the phase cable in the direction of the load. In all spans, the fast rise times of the short-circuit current will induce much higher voltages and currents on the shield wires than the voltages and currents induced by the steady state phase current.

The knee frequency of the transient current of the short-circuit is in the range of hundreds of kilohertz and the spans are hundreds of meters in length. Therefore, the line surge impedances and the tower surge impedances must be taken into account to analyze the transient induced currents. In this case, the surge impedances have significant effects in the distribution of the currents in the shield wires and towers. A significant portion of the current flows to ground through the towers because the cable surge impedance ($\sim 400 \Omega$) is higher than the tower surge impedance ($\sim 150 \Omega$). For the low frequency (60 Hz) components of the induced current, the surge impedances have negligible effect, and only the tower grounding resistances are significant. Therefore, a great portion of these current flows to the shield wires in the spans adjacent to the faulted span. Figure 3.10 shows the high frequency equivalent circuit of the shield wire and towers of a homogeneous power transmission line. For the 60 Hz steady state currents and voltages, the impedances Z_t e Z_c are very low and can be neglected, only R_g is significant.

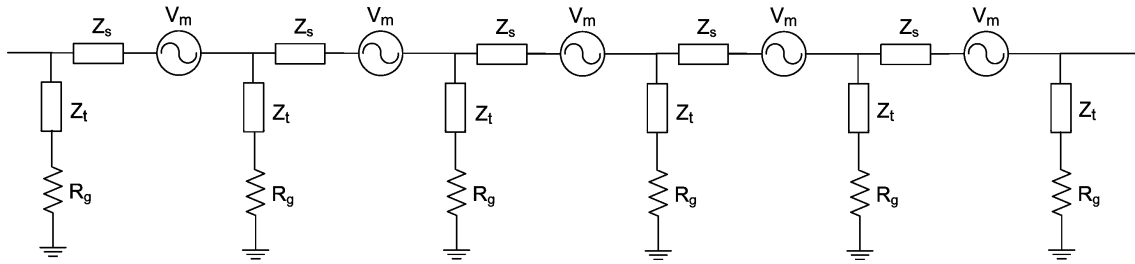


Figure 3.10 - Equivalent circuit for the high frequency induction in the shield wire, Z_t e Z_s are the surge impedances of tower and shield wire, respectively, R_g is the tower grounding resistance, V_m is the induced voltage.

Far from the fault position, the transient currents induced in the shield wires of adjacent spans have similar amplitude and waveform. These currents flow through each tower with inverted polarities resulting in the cancellation of most of the currents in the towers, and the net current is small. The cancellation is greater at the beginning of the transient, where the higher frequency components are concentrated. The farther the span, the greatest is the cancellation because the influence of the currents from the faulted span is attenuated and the transient currents in the wires of the adjacent spans are more similar.

The behavior of the currents in the shield wires closest to the fault is not the same. The induced currents are different in each wire and the net currents in the towers are much higher. This occurs because the transient portion of short-circuit current have inverse polarity in the phase cables in the direction toward source relative to the polarity in the direction toward load, as shown in Figure 3.9. Consequently, the transient voltage and transient current induced in the shield wires have inverted polarity in the faulted span and in the spans toward load, relative to the polarity in the spans toward source. The result is no cancellation or a smaller cancellation of the transient currents in the towers closest to the fault.

3.2.4 Using the transient currents to locate the fault

The simulation shows that the transient currents induced by the short-circuit fault always have amplitude and rate of change of current (di/dt) higher in the towers near the fault location. This characteristic allows the detection and location of the fault by measuring the transient induced currents flowing in the towers and comparing the measured values. The towers with the higher transient currents (or di/dt) are the ones closest to the fault position. Extensive simulations presented in Chapter 5 show the feasibility of the method.

A straightforward way to measure the transient current flowing to ground through the tower is to use a Rogowski coil placed on the top of the tower, around the tip of the structure where the wire is connected, or around the wire connecting the shield wire to the tower structure (Figure 3.11). The output voltage of the Rogowski coil is proportional to the rate of change of the current flowing through the toroid. Applying this voltage to an integrator circuit results in an output voltage proportional to the current flowing to ground (through the toroid). The integrator is usually placed close to the coil to minimize noise pickup. To integrate only the higher frequency transient current, the integrator can be implemented by a low-pass filter with corner frequency much higher than 60 Hz. The 60 Hz component of the steady state current is filtered out in the process of integration. The integration also eliminates undesired noise with frequency much higher than the frequency of fault transients (details in Appendix D).

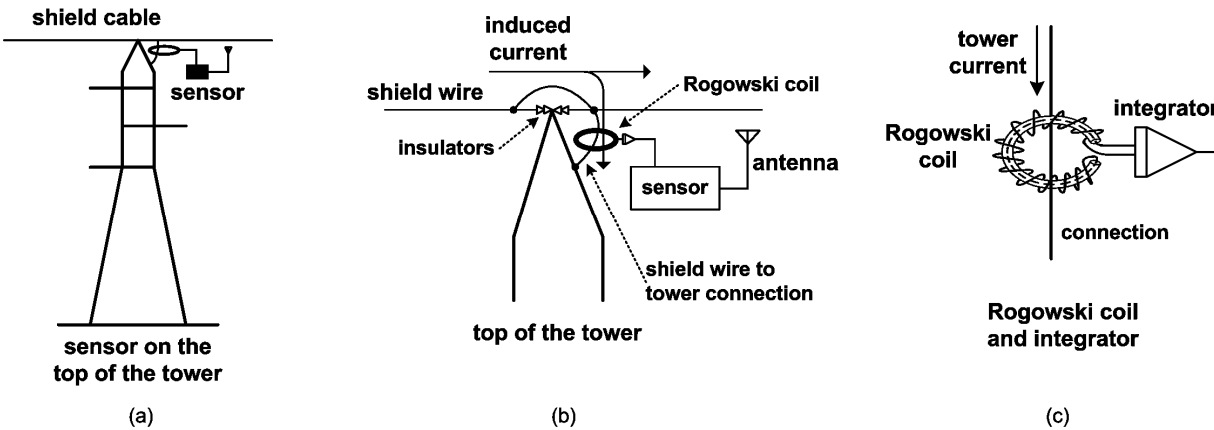


Figure 3.11 - Position of the sensor on the top of the tower (a), detail of the tip of the tower (b), and the detail of the coil (c).

An electronic intelligent sensor, placed on the top of each tower, must be triggered to read the output voltage of the integrator whenever this voltage reaches a preset threshold. The output is much higher for the transient induced current than for the steady state induced current. The sensor detects the peak value of the voltage, converts the analog measurement into binary data and sends it to a computer for processing. The sensors that measure the greatest values of the current are the ones closest to the fault. Less than a dozen sensors at each side of the fault will measure a significant value. Together with the information about the current, the sensors send the time stamp of the measurement and the sensor identification to allow the process of location. Installing one sensor at each tower allows for the detection

and location of the fault. Extensive simulations detailed in Chapter 5 show the feasibility of the method.

The method is also applicable to direct current (DC) power transmission lines. In this case, there is no Alternating Current (AC) steady state induced current, there is only the transient current induced in the shield wire.

Chapter 4

Detection and location system

The system to detect and locate the direct lightning strokes and to locate short-circuit faults must have the following components: the Rogowski coils to measure the currents; sensors to read the measured currents and send the values to the computer; a communication structure to transport the data from the sensors to the computer for processing; and a computer to process the values sent by the sensors. Batteries recharged by small solar cells may supply the power to the sensors. Another option is to use the 60 Hz steady state current induced in the shield wire. A current transformer installed around the shield wire can supply AC power to the sensor and to charge the batteries. Besides, the battery can be substituted by super capacitors to eliminate any preventive maintenance. This powering method is detailed in section 4.13.

When a direct lightning stroke hits the shield wire, or when there is a transient current in the tower induced by the short circuit current, the nearest sensors measure the peak values of the current and of the di/dt . If the peak value exceeds a preset threshold, the sensor is triggered to read them. Next, it converts the analog measurements to digital data and sends the values of the peak current, the di/dt , the time stamp and the sensor identification to a computer through the communication subsystem. The reading of the values has to be done in up to 10 ms from the beginning of the lightning stroke to release the circuits for the measurement of subsequent strokes, if any. The computer processes the information received from the sensors, estimates the fault position, or estimates the stroke position and qualify the severity of the stroke.

4.1 The block diagram of the sensor

Figure 4.1 shows a draft of block diagram of the sensor. The peak detectors are analog circuits with good transient response. After the output of the peak detector reaches a pre-defined threshold, the comparator output changes the state informing the micro-controller that the current and/or the di/dt have exceeded the minimum value. In less than 100 microseconds

the peak value of current or di/dt reaches the maximum value. The signal to be converted to digital is the stable dc voltage output of the peak detector. Therefore, a low cost low sample rate A/D can be used. The microcontroller must read the A/D output in less than 10 ms because of the subsequent strokes, in case of a direct stroke. The microcontroller reads each A/D output, stores the digital value, and resets the comparator and the peak detector to the next event. Next, the microcontroller build a message with the values read, the time stamp and the sensor identification, and passes the message to the transceiver. The transceiver sends the message through the wireless network.

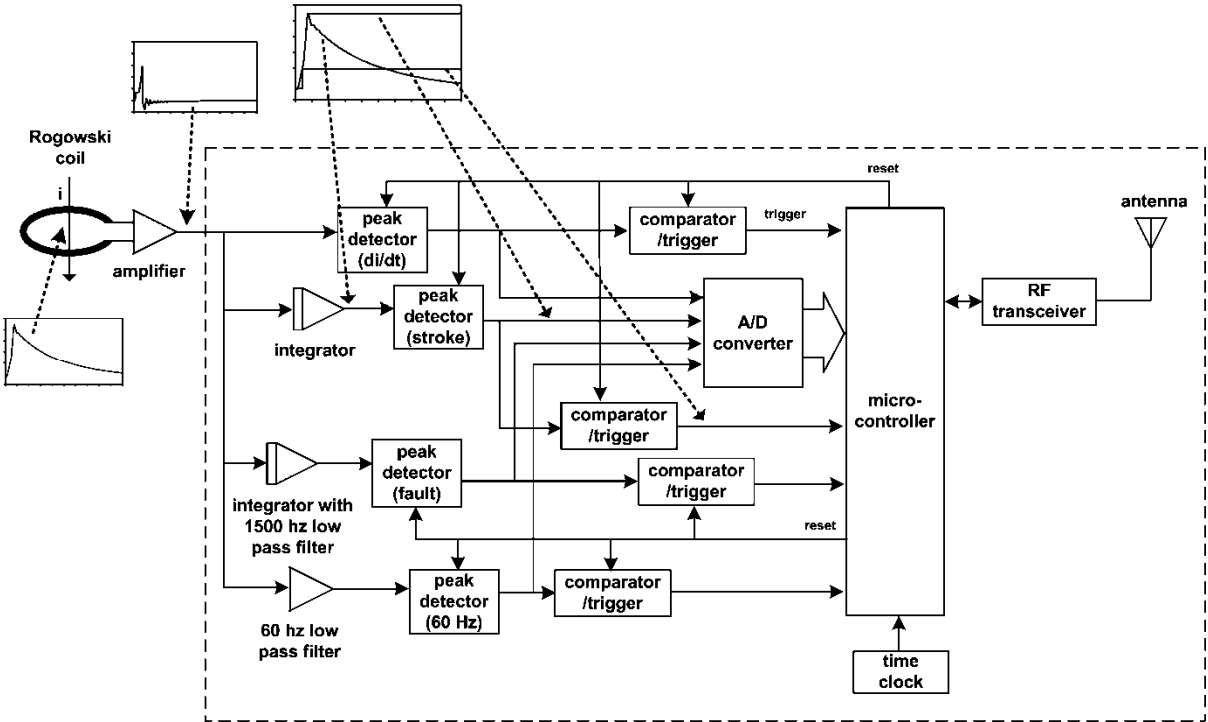


Figure 4.1 - Block diagram of the wireless sensor.

The same Rogowski coil supplies the di/dt for the current of direct strokes to shield wire, for the transient current induced by short circuits or direct strokes to phase cables, and for 60 Hz induced current. For every type of measurement there is a peak detector and a comparator/trigger circuit. The output of the peak detector is connected to one of the four channels of the A/D converter. The amplifier, integrators and filter must adjust the output voltage level to reconcile the inputs of the peak detectors and the peak detectors must adjust the level to the inputs of the A/D converter.

In the input of the first peak detector, the di/dt measurement is used for evaluation of severity of direct stroke. In the input of the second peak detector, the integrator is used to generate a voltage proportional to the stroke current.

The third peak detector is used for measurement of the currents induced by short circuit current. To integrate only the higher frequency induced transient current, the integrator is implemented by a low-pass filter with corner frequency much higher than 60 Hz. The 60 Hz component of the steady state current is filtered out in the process of integration. The integration also eliminates undesired noise with frequency much higher than the frequency of fault transients.

The fourth peak detector is used for the measurement of the currents induced by 60 Hz short circuit current. In the input of the peak detector there is a low pass filter to eliminate the transient currents with frequencies above 60 Hz. The peak value is used to determine whether the values of peak current transients were generated by direct stroke or by a short circuit. In case of a short circuit, the 60 Hz current induced in the cable shield is much higher than the steady state induced current (Figure 4.2). This information can be used to confirm the identification of high impedance short-circuits that do not cause a fault. The value of di/dt can also be used to identify the type of disturbance (detailed in Chapter 5).

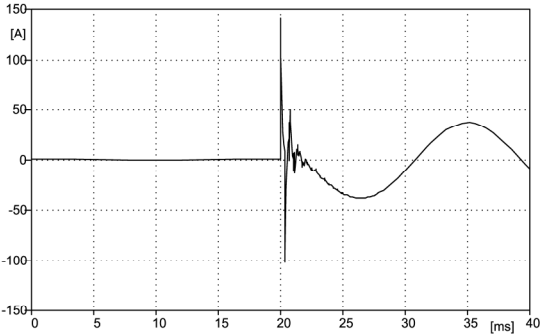


Figure 4.2 -current induced by the fault.

The sensors read and send the peak values of the four measurements (converted to digital) to the location computer. There is no local processing of the data. The function of the computer is to analyze the values and identify the type of disturbance and its location.

4.2 The wireless sensor network

To transmit the information to a computer, each sensor has to communicate through a radio frequency transceiver. The power transmission line may have the extension of hundreds of kilometers. It is not feasible to have direct radio communication between each sensor and the computer. The radio transceiver in every sensor may be an IEEE 802.11 or an IEEE 802.15.4 transceiver to convert the set of sensors into a wireless network (Figure 4.3) as will be detailed later in this Chapter. Therefore, the sensors can send the data to the computer through the network of sensors. Each sensor must retransmit the data to its neighbor until it reaches the end of the line, where the computer receives the data. Field measurements performed in this work with 802.11b routers show an outdoor line-of-sight range of 2.4 km with a 2.15 dBi antenna (detailed in Chapter 5). This range allows each sensor to communicate with several neighbors sensors giving the necessary redundancy in case of a failure of some consecutive sensors. The transceiver range analysis and the wireless sensor network operation are detailed later in this Chapter and Chapter 5.

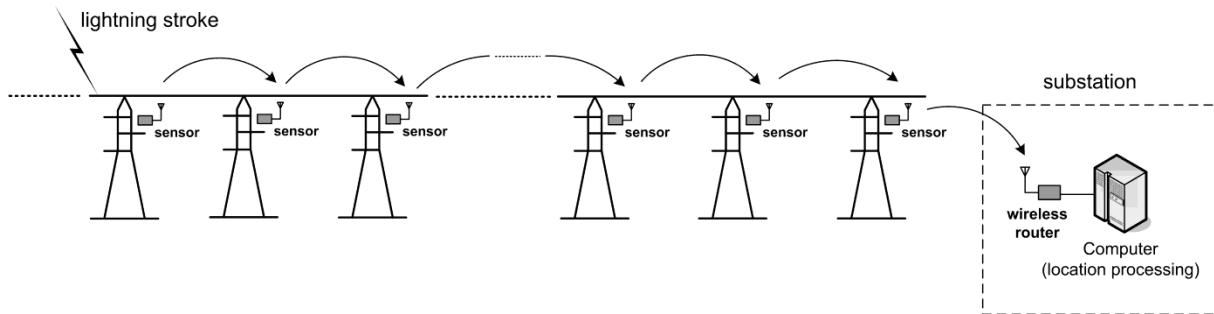


Figure 4.3 - Overview of the wireless network communication of the detection and location system.

4.3 The location processing computer

The location computer can be a small server because the processing and storage requirements are few. The most important is the reliability of the equipment. The location processing software in the location computer is simple. The process of location is straightforward. First the computer associates the tower number with the sensor identification using an internal table. Next, the computer has to order the values received by tower number, considering a time window of up to 5 milliseconds to separate the measurements of subsequent strokes. Next, it locates two or three highest values of peak currents and corresponding tower numbers to locate the stroke position or the fault position. The value of di/dt and the parameters of the towers can be used to evaluate the severity of the stroke in case

of a direct stroke to the power line. The computer receives, from every sensor, the values of four measurements of the Rogowski coil as detailed in the block diagram of the sensor: di/dt , integrated di/dt , integrated di/dt with the steady state (60 Hz) components filtered out, and di/dt with the transient components filtered out. The di/dt value of the transient is used to determine if the measurements are due to a direct stroke or to a short circuit fault and select the corresponding peak values for the transient disturbance location processing. The value of the di/dt of the 60 Hz component can be used to confirm high impedance short-circuit that do not cause a fault, and also for other purposes.

The sensor identification used to locate the tower number is the network or MAC address of the sensor. The internal table associating the tower number with the sensor address is created from the information collected during the sensors installation. Every sensor must have its address printed on the case and during the installation the technicians must annotate the address and the tower number for every sensor installed. These annotations are the source for the internal table associating sensors addresses and tower numbers.

The computer is connected to a wireless router that is the first node of the network of sensors (Figure 4.4). This router is within radio range of at least two sensors at the end of the transmission line. In addition, the computer must be connected to a modem/router that establishes a communication link with a Wide Area Network (WAN). It is a backup link through which the computer connects to the sensors on the other end of the transmission line creating an alternative path in the network as will be detailed in Section 4.7.

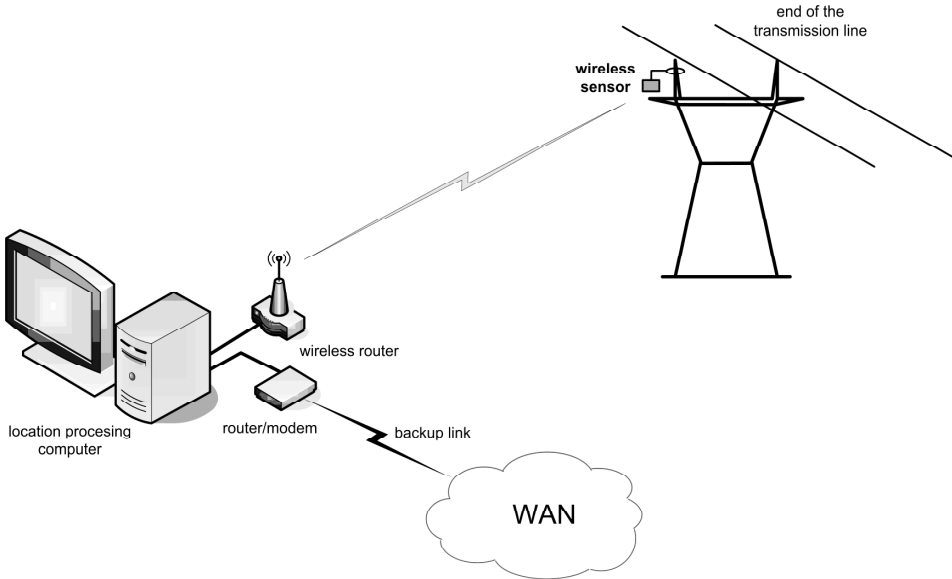


Figure 4.4 - The location processing computer.

The computer can store the information received for long periods of system operation. This information can be used for statistical analyses and evaluation of lightning performance of the transmission line.

4.4 Security considerations

All networks, especially wireless networks are susceptible to attack attempts to steal information, unauthorized access or denial of service. Security issues are well researched and proven security solutions exist against theft and misuse of information over wireless networks. The IEEE and ZigBee Alliance specify the security mechanisms for 802.11 [72] and ZigBee [73]. Moreover, the information that travels over the wireless network transmission lines are operational and have no commercial value. However, the most likely attack is the denial of service to stop the network using radio interference. Due to the length of the line, the interference on a large extension of the network is costly. Interference in one part of the network does not prevent the operation of the system because the network has an alternative route in case of failure to disrupt the network.

4.5 Recommendations for the product engineering of the wireless sensors

There are two main technical issues about the product engineering of the sensors. The first is the Electromagnetic Compatibility (EMC). The stroke currents flows through the current transformer and Rogowski coil creating high frequency electromagnetic fields that can damage the sensor circuits. The design of the sensor should prioritize the use of the techniques of EMC. The equipment must be very compact, with good electromagnetic shielding and the external cables should be avoided or reduced to the minimum length. In general, the electromagnetic compatibility techniques used to protect the electronics of tower light controllers from lightning strokes can be used to protect the sensor. Figure 4.5 is the proposal for the sensor housing.

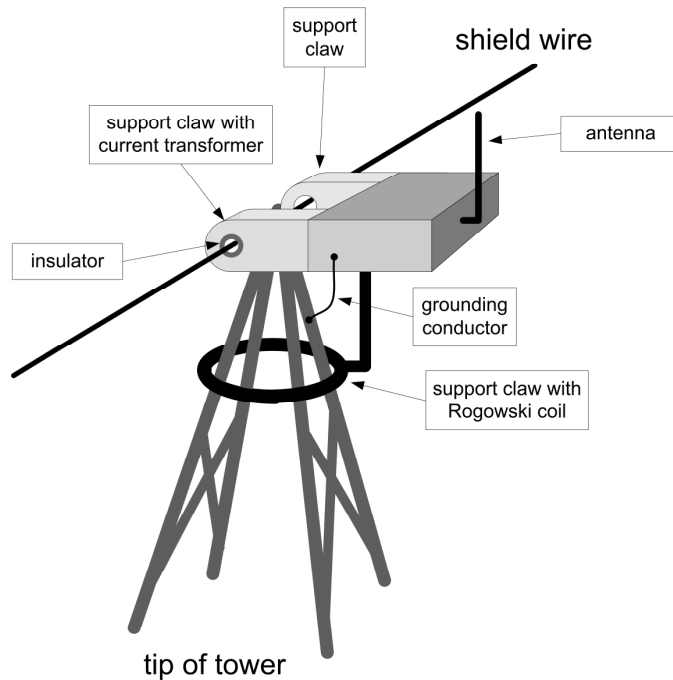


Figure 4.5 - Proposal for the sensor case.

The metal housing of the sensor must be grounded to the tower above the Rogowski coil to assure that the coil measures all the current flowing to tower grounding. The current transformer must be insulated from shield cable to ensure that all the current of the cable pass through the window of CT to supply power to the sensor. The use of the current transformer to supply power to the sensor is detailed in Section 4.13.

The second issue is the resistance to weather conditions. The sensor must support external temperatures that can reach more than 50 degrees. The sensor should be completely waterproof and withstand severe rain conditions. Moreover, it should be designed to have high MTBF (Mean Time Between Failures) to last at least a decade with minimum maintenance.

4.6 Operation of wireless sensor networks in power transmission lines

The operation of wireless sensor network for detection and location of direct strokes and short-circuits in OPTLs has some special characteristics:

- The number of sensors can be very high, in the order of thousands, because the OPTL can have several hundreds of kilometers of length and thousands of towers.

- There are no serious constraints for the transit time of data packets. The packets can take several seconds to arrive at the computer because the maintenance procedures triggered by the information sent by the sensors will take several minutes to be initiated and some hours to be completed.
- The end-to-end data traffic always flows between each sensor and the computer or in the reverse direction.
- The length of packets of application layer is small, 20 octets are sufficient for the application message plus the headers of the protocols.
- The traffic generated by the fault or direct stroke events is very small because these events occur occasionally. The main traffic is generated by the time synchronization and network management which is under control of the central system in the location processing computer.
- The topology is linear with the sensors aligned along the towers.
- The sensors are submitted to severe weather conditions and huge electromagnetic fields.
- The maintenance of most sensors is a problem because of the difficulty to access most towers. The sensors and the network must be very reliable and with very little maintenance. The network must support the failure of sensors without stopping the network.
- The sensors must send a time stamp with the values measured. The computer has to generate and send synchronization messages to every sensor.

Considering these characteristics, the main issues about the operation of WSN on OPTL are the power supply method to minimize the maintenance; the transmission range to guarantee the reliability of the network in case of failure of sensors; the behavior of routing protocol in the linear topology to guarantee the delivery of the information to be processed even with a high number of nodes; and the product engineering of the sensors to handle with the severe operation conditions.

The wireless sensors have a typical consumption below one Watt. Therefore, photovoltaic cells and batteries can supply power to these devices. The main problem with

these components is the maintenance. The OPTLs may have the length of hundreds of kilometers and the maintenance is a difficult because of the large number of sensors and the difficulty to access the towers.

The wireless sensors installed on the top of the towers must have a transmission range of several hundred meters to reach at least two neighbors at each side. This way, the failure of one sensor does not break the entire wireless network. In this work, the range of a node refers to the range at one side of the sensor. Therefore, as an example, a range of two nodes means that the node can reach four nodes in the linear topology, two at each side (Figure 4.6).

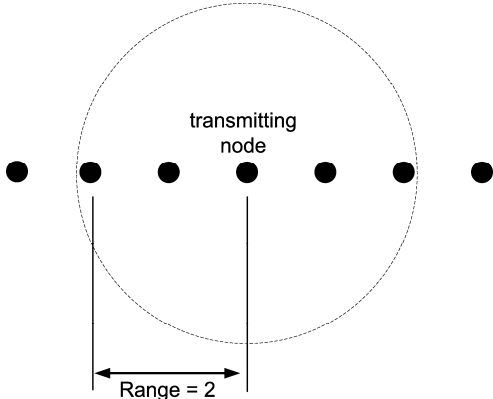


Figure 4.6 - Convention for the node range.

Because of the peculiar linear topology of the WSNs on overhead power transmission lines and the high number of sensors, the routing protocols must be tested to analyze their behavior in these special conditions.

The linear topology can be found in other applications. WSNs for monitoring of streets, roads, and gas, oil or water pipelines, are examples of networks with linear topology where the results of the analysis performed in this work have direct application [74].

4.7 The linear topology and the alternative paths in the network

The operation of the wireless Ad Hoc networks depends on every node. If several nodes fail, the routing protocol uses alternative paths bypassing these nodes to avoid the interruption of the network operation. The mesh topology creates more alternative paths for each sensor than the linear topology for the same transmission range. In the Figure 4.7, the number of nodes and their range are the same for these two topologies but the mesh topology gives more alternative paths than the linear topology because of geographic distribution of the nodes. In case of failures in several nodes, the mesh topology is less vulnerable.

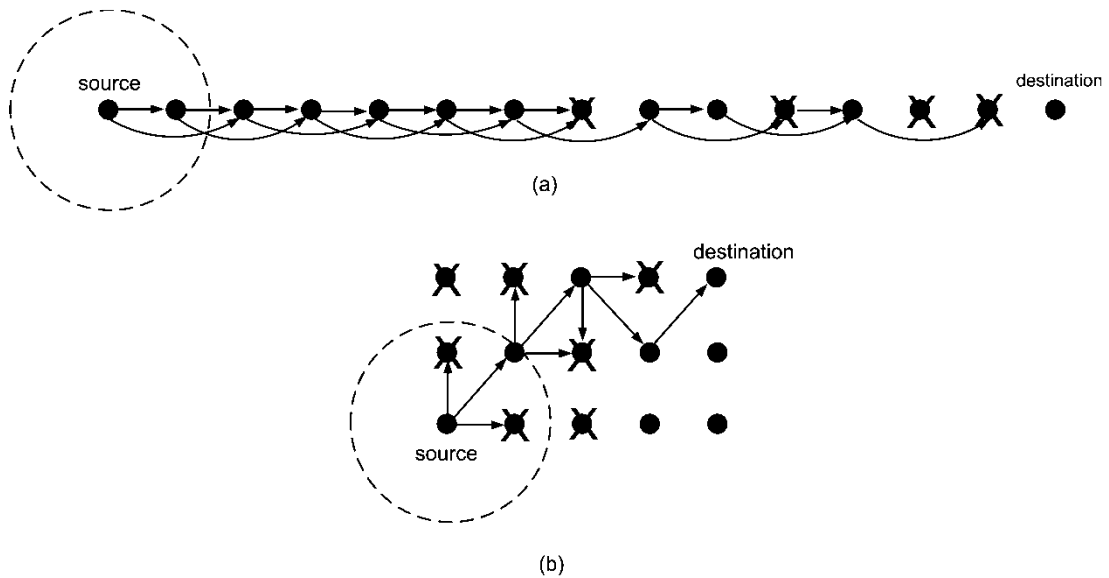


Figure 4.7 - Linear topology (a) and mesh topology (b) the dashed line circle around the source node indicates the range of the radio transceiver (equal for every node).

In the linear topology the failure of consecutive sensors can be a problem to the operation of the whole network. If all the neighbors in the range of one node fail, the network is broken into two pieces. One of these pieces does not communicate with the location computer unless there is an alternative path to the location computer on the other end the network. To have a reliable network operating on a transmission line it is necessary that the sensors have radio transceivers with the highest range. Considering the technologies of the 802.11 and 802.15.4 transceivers, and the average span length of 400 m, it is possible to have sensors with a range up to 2.5 km operating at 2.4 GHz, allowing each sensor to communicate with up to 6 neighbors. Considering the obstruction losses of intermediate towers in Fresnel zone, the transmission range is lowered. To be conservative it is better to work with a transmission range of five nodes. In case of transceivers operating in the 915MHz band, the transmission range is even higher.

Anyway, even with a high range the network is vulnerable. To have a more reliable operation it is important to have an alternative path at the other end of the network (Figure 4.8).

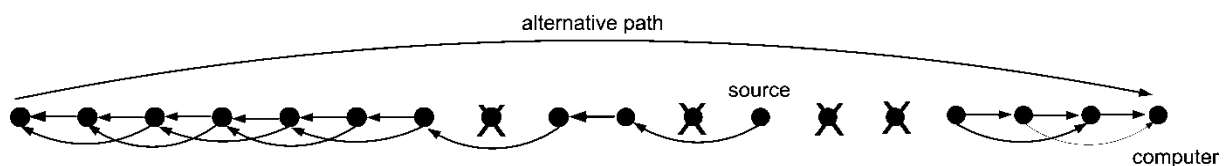


Figure 4.8 - The alternative path at the end of the network

The alternative path can be implemented by a communication link between the last node and the location computer. The link can be provided by a Wide Area Network operator, or a Virtual Private Network (VPN) through the Internet.

4.8 Data transmission and routing in the linear topology

4.8.1 Data transmission through the network

The purpose of the network is to transport the data with the values measured by the sensors to the computer for processing. The data has no significant restrictions of time of arrival, but the service of data delivery must be reliable. The data can be sent using messages at application layer routed through the network by simple unconfirmed datagrams at the network layer (connectionless service). Connection oriented services have an unnecessary overhead for this type of application because every node sends only one message. It is important to note that the LLC layer can perform a reliable node-to-node communication. Using datagrams at network layer, the message service at the application layer must be reliable. In the proposed system, a simple 2-way handshake with end-to-end confirmed messages and retry counter works well because the data delay restrictions are loose. This reliable service at the application layer must have the following sequence of events: the message is sent; each message triggers a timer to wait for an acknowledgement (ACK) message; if the ack message does not arrive within a predefined time, the message data is retransmitted. This process can be repeated until an ACK message arrives or the maximum number of retries is reached. The receiver acknowledges every message received, even if the message was already received. The data messages should have a field with a sequence number to allow the confirmation of the message and the control of repeated messages, at the receiver. Figure 4.9 is the Message Sequence Chart (MSC) diagram [75] of this process.

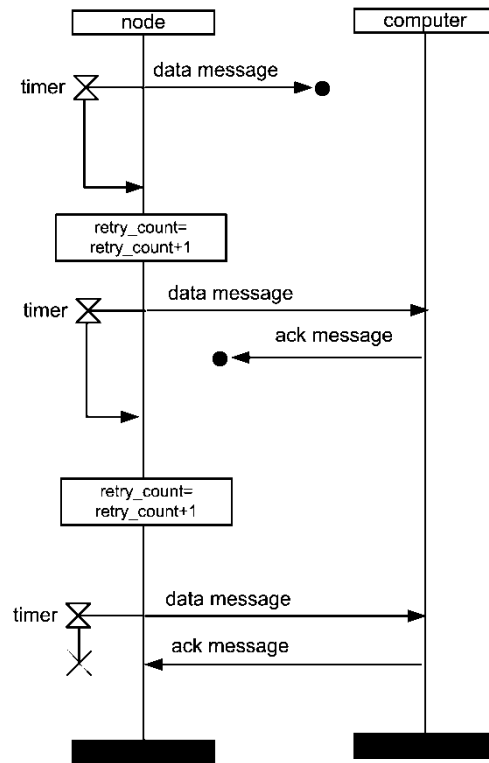


Figure 4.9 - MSC diagram of the data transmission process.

The sensor sends the data in formatted message at the application layer with the appropriate fields to allow the destination sensor to identify and process the data. The format of the message should include the required fields to allow the destination node to identify the type of message and to confirm its reception with an acknowledgement message. The data message is confirmed with an ACK message. Two other types of messages are necessary, the time sync message to synchronize the clock of the sensors and the “keep alive” message for simple network management (detection of faulty sensors). Figure 4.10 shows the types of messages and their fields.

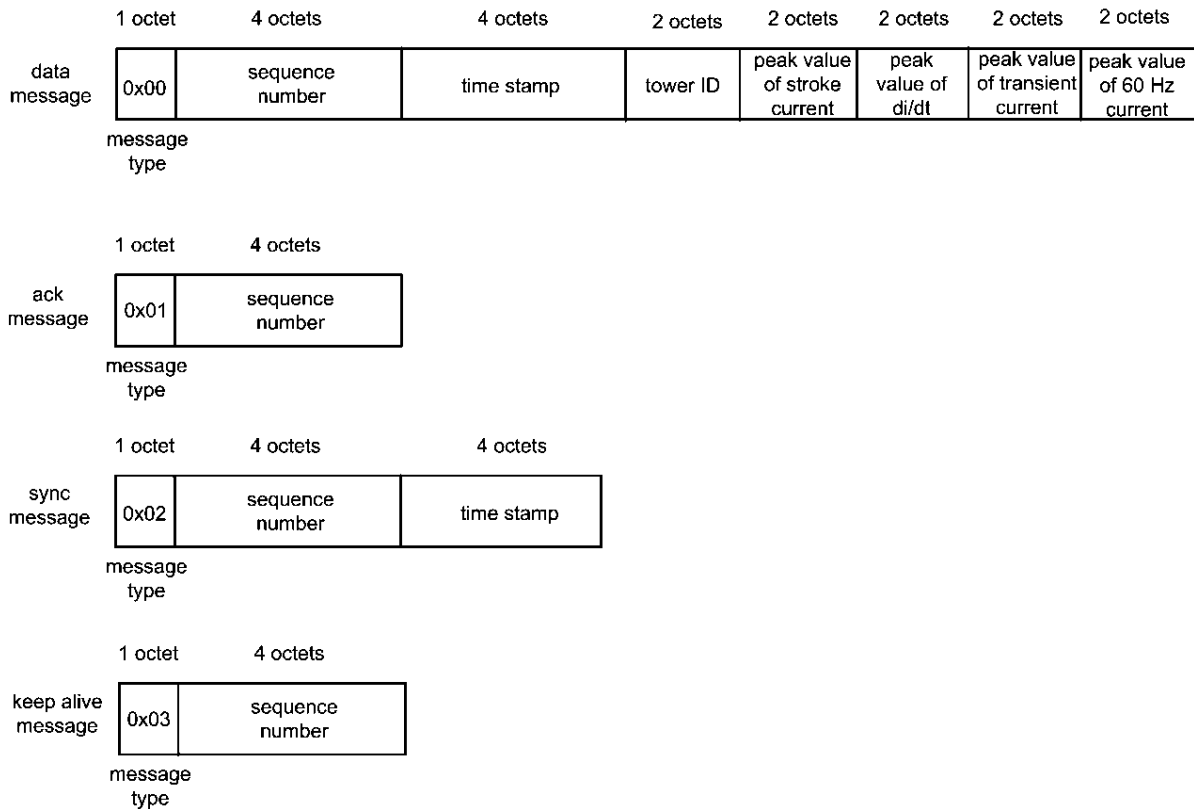


Figure 4.10 - Message types and fields.

The sequence number allows each node to identify whether the message has already been received (repeated message) and allows the destination node to send the confirmation message (ACK message) to the source node.

The “keep alive” message is used to identify the faulted sensors. Every sensor has to send periodically “keep alive” messages to the computer to inform that the sensor is “alive”. If a sensor stops to send the messages, after a timeout the location computer warns the operator about a defective sensor.

The application message is encapsulated in a network packet like the UDP of the TCP/IP stack with the source address of the local node and the destination address of the location computer. The network packet is used to take the message to the destination through the network using the frames of the MAC layer to perform the hop by hop forwarding.

Data messages are confirmed by the location computer but the time sync messages and the “keep alive” messages are not confirmed. Besides, the “keep alive” messages uses unicast address to reach the location computer and the sync messages use the broadcast address to reach every sensor.

4.8.2 Behavior analysis of routing protocols in linear topology

The topology of the wireless sensor network composed by the sensors on the top of the towers is linear. It is not a typical arrangement of nodes. Besides, the number of sensors can be very high. In Brazil, with a large territory extension, the power transmission lines can extend to several hundreds of kilometers. More than one thousand of sensors may be installed on these lines. The high number of sensors and the linear topology can impact the behavior of routing protocols and the data delivery from the sensors to the location processing computer. There are several papers about simulations of routing protocols with up to some hundreds of sensors in mesh and star topologies. A small number of papers analyze the linear topology limiting the analysis up to a few hundreds of nodes [76]. The behavior of these routing protocols in the linear topology with several hundreds of sensors is analyzed in this work because there is not known publications about this network configuration.

To evaluate the behavior of the routing protocols in the linear topology with high number of nodes, we have done several simulations, presented in Chapter 5, using the Network Simulator NS2 [77]. The protocols selected to be preliminarily evaluated were the ones that are available and ready to be used on several hardware platforms.

Most 802.11 equipments do not have routing protocols because they are usually used in infrastructured networks. However, the open source firmware based on Linux, OpenWrt, is available compiled for several hardware platforms, including, routers, access points, modules and chip sets. The firmware can be configured to work in Ad Hoc mode and there are implementations of OLSR and AODV available. The open source firmware DD-Wrt also implements the OLSR protocol. For the IEEE 802.15.4/Zigbee transceivers, the manufacturers implement the ZigBee routing protocol specified by the ZigBee alliance. Besides, the routing protocols AODV and OLSR are listed by the Mobile Ad hoc NETWORKS (MANETs) workgroup of the Internet Engineering Task Force (IETF) [78].

The availability of the AODV and OLSR protocols in the OpenWrt framework for 802.11 nodes, and HTR and AODV protocols in the hardware implementations of ZigBee nodes, simplify the software design of the sensor. Therefore, the following combinations of transceiver technology and routing protocols were considered to be used in the network:

- a) IEEE 802.11 with AODV

- b) IEEE 802.11 with OLSR
- c) IEEE 802.15.4 with HTR
- d) IEEE 802.15.4 with AODV

4.8.3 The flooding protocol

Besides evaluating these routing protocols, the behavior of a simple technique to forward the packets from source to destination, known as flooding, was analyzed. The implementation of this technique is very simple and does not impact the software design of the sensor. Technically, the flooding is not a routing protocol, but for the sake of simplicity it will be referred as a routing protocol in this work.

The flooding is a technique to make the message arrive at its destination by flooding the network with broadcast messages that are received and retransmitted by each node. At some point, the destination node will eventually receive the message. In large mesh networks this technique is very inefficient, but in the linear topology it can work well because of the linear characteristic of this topology. Figure 4.11 is the System Description Language (SDL) diagram of the flooding process in each node.

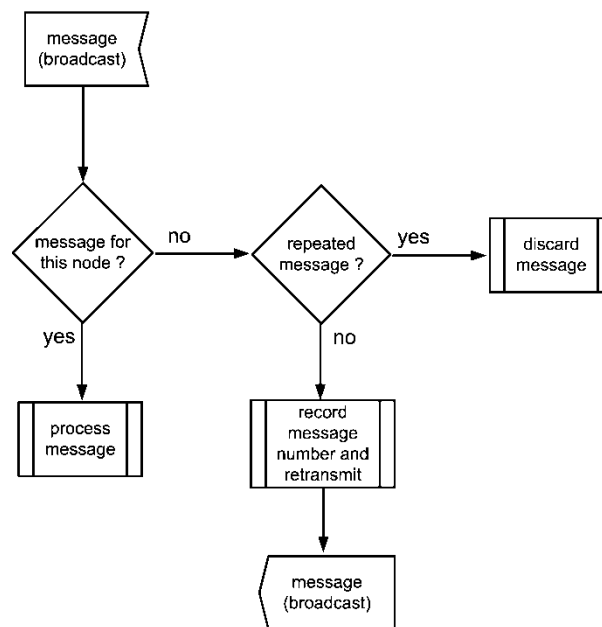


Figure 4.11 - The SDL diagram of the flooding process.

The messages are broadcasted to every node inside the transceiver range. Each node that receives a message checks if the message has already been received. In this case, the message is discarded. On the other hand, the message is forwarded using the broadcast

address. The linear topology allows the use of this technique. The packets flow naturally from source to each of the edges of the power line because these are the only paths available. The computer is located in one these edges. Besides, on the other edge it is possible to have a backup communication link connecting the last node of the transmission line to the computer. This link establishes a redundant path in the network in case of failure of several consecutive nodes.

Using the flooding protocol, the application layer passes the messages to the network layer which send the messages using the network broadcast address. The broadcast address of the network layer is mapped to the broadcast address of the MAC layer. The end-to-end addressing and the routing are performed by the application layer, and not by the network layer. Besides, the application layer itself performs the simple routing process of the flooding technique detailed in Figure 4.11. The format of the messages must include the source and destination node addresses to perform the end-to-end addressing. Figure 4.12 shows the application layer message with the address fields.

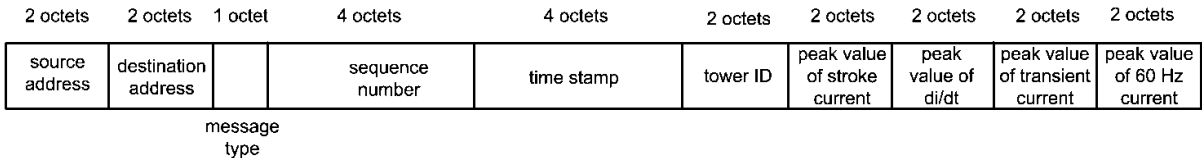


Figure 4.12 - Message format with address fields.

The network layer does not play any role in the communication process using the flooding protocol because no routing algorithm is used and the network layer uses only broadcast addresses. The end-to-end addressing is done at the application layer, and not at the network layer. Therefore, it is possible to eliminate the network layer. The application can pass the messages directly to the MAC layer to transmit the frames with the MAC broadcast address. It works the same way as using the network layer.

4.9 Channel allocation

In each substation, several OPTLs arrive. These lines are very close to each other in the neighborhood of substation. Besides, there are parallel lines of tens of kilometers in the power transmission corridors. To minimize the radio interference between the networks of each line, it is necessary to make a channel allocation plan. If the sensors use 802.15.4 transceivers there are 10 non-overlapping channels in the 915 MHz band and 14 in the 2.4 GHz band. Each line

must use a different channel. If the sensors use 802.11 transceivers, there are 14 overlapping channels and only four non-overlapping channels. In this case, a more elaborated plan is necessary [79]. Figure 4.13 shows the allocation of 802.11 channels for 12 transmission lines trying to minimize the interference between the channels.

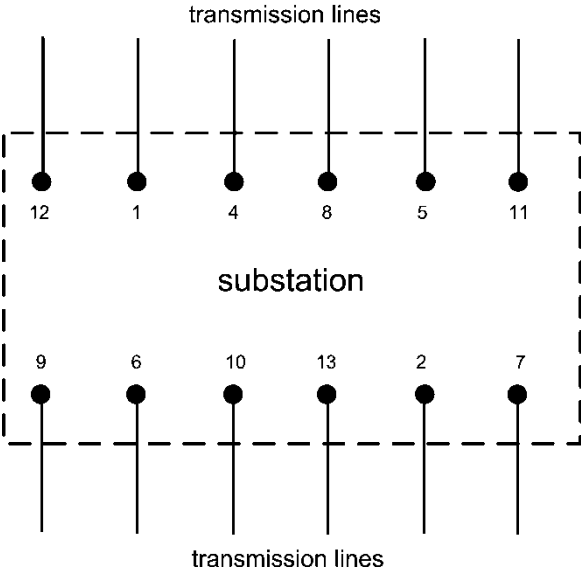


Figure 4.13 - Allocation of 802.11 channels for 12 transmission lines, the numbers indicate the channels.

4.10 Clock synchronization

Each sensor must send a timestamp with the measured values to correlate the values with every event in time. The sensors must therefore have a synchronized time. Because the events occur with low frequency, the synchronization does not need to have a great precision throughout the network. Since the neighboring sensors are synchronized with each other, with accuracy of the order of tenths of a second, the difference in timing of several seconds between distant sensors does not affect the system. The events in the transmission line are local, triggering data transmission of up to twenty sensors. If these sensors are synchronized, the data sent will have timestamps sufficiently close to be considered as being for the same event

Synchronization can be performed through a special sync message sent by the location system computer to all sensors using the broadcast address. As seen previously, this process works well on the network with linear topology using the technique of flooding. The simulations showed that in a network with 802.11 sensors operating at 1 Mbps, with 3000

nodes, and each node with a transmission range of 5 neighbors, the transit time is 1.8 seconds. Therefore, the difference of time between the computer and the last node is 1.8 seconds. Considering that the synchronization message goes into the network at both ends, because of the backup communication link, the nodes with greater delay will be in the middle of the network with 0.9 seconds (Figure 4.14). In case of the 802.15.4 standard, the simulations showed that, in the same situation, the transit time is 4.2 seconds and the maximum delay is 2.1 seconds in the middle of the network.

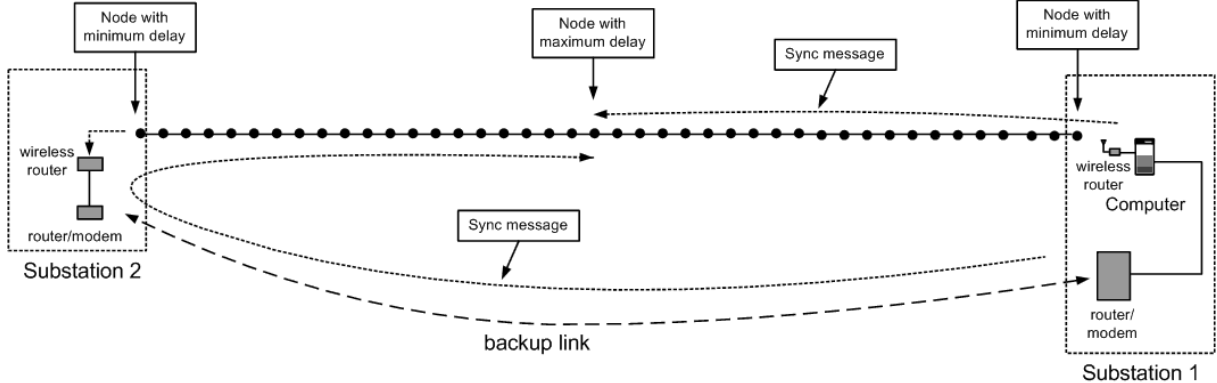


Figure 4.14 - The path of the sync messages.

According to the simulations presented in Chapter 5, the difference in timing between twenty neighboring sensors will be less than 20 ms for 802.15.4 sensors and less than 5.5 ms for 802.11 sensors (transmission range of 5 neighbors). The global synchronization can be enhanced if each sensor increases the time in the sync message with the transmission time of the packet, before relaying the message.

4.11 Selection of the transceiver technology

The options of wireless standards were analyzed to select the technologies that are most suitable to operate on OPTLs. The Standard 802.16, known as WiMax, is neither widely available nor cost effective as other wireless standards. The 802.15.1 and 802.15.3 standards have low transmission range.

The 802.15.4 is the standard of choice for most Wireless Sensor Networks. The transmission range is high, especially in the 915 MHz band. There is a large number of manufactures of equipments, modules and transceivers compliant with this standard what makes the hardware cost effective. The Zigbee alliance has defined a protocol stack to be used

with 802.15.4 MAC layer which includes the network layer, the routing protocol and the infrastructure of the application layer, simplifying the software development.

The 802.11 is used practically on all WLANs inside infrastructured networks. There are commercial wireless routers that include both AODV and OLSR to operate in Ad Hoc mode. Besides, the open source firmware OpenWrt includes Ad Hoc routing protocols [80] and is available for the transceivers of several manufacturers. The 802.11b/g standard has good transmission range, as detailed in Chapter 5, and wide availability of equipments, modules and transceiver chips.

The wireless network standards that are more suitable to the operate over power transmission line are the IEEE 802.15.4 and IEEE 802.11 because of the proven technology, good cost effectiveness, wide availability of products, and good transmission range. These two standards are the basis for the wireless hardware of the proposed system.

Several manufacturers produce single or dual chip 802.11 or 802.15.4 transceivers that implement the specifications of these standards [81][82]. There are manufacturers that produce transceiver modules that implement the specification of these standards and the interface to the microcontroller/microprocessor system. Table 4.1 lists some transceivers and their characteristics.

Table 4.1 - 802.15.4 and 802.11 transceivers.

Transceiver	Manufact.	Freq. (MHz)	P _{Tx} (dBm)	Sensit. (dBm)	Type of transceiver	Standard	Data rate
AT86RF212	Atmel	915	10	-100	chip	IEEE 802.15.4	250 Kbps
ZigBit 900	MeshNetics	915	10	-100	module	IEEE 802.15.4/ ZigBee	250 Kbps
LPR2400ER	RFM	2400	17	-95	module	IEEE 802.15.4	250 Kbps
ZFSM101	CEL	2400	20	-92	module	IEEE 802.15.4/ ZigBee	250 Kbps
AL2230S	Airoha	2400	20	-92	chip	IEEE 802.11b/g	1 Mbps
MAX2820-MAX2242	Maxim	2400	22.5	-97	chip	IEEE 802.11b/g	1 Mbps
Q802XKG	Qcom	2400	18	-94	module	IEEE 802.11b/g	1 Mbps
R52H	Mikrotik	2400	24	-92	module	IEEE 802.11b/g	1 Mbps

Most transceivers components implement only the physical and the MAC layers. The software design of sensors using these transceivers must include the development of link and network protocols, including the routing protocol, besides the application program. There are transceivers modules that implement the Zigbee specification like the ZigBit900 from

Meshnetics [73]. The software design of sensors using these transceivers must include only the development of the application program. Besides, the module has low power consumption, and includes the microcontroller and four 10-bit A/D converters.

The 802.11 modules from Mikrotik [83] are supported by the OpenWrt Linux-based firmware [80]. OpenWrt firmware is the framework to build an application without having to build a complete firmware around it. The application can be developed as a Linux application, the TCP/IP stack is ready to be used and the protocols AODV and OLSR are available to be installed. The OpenWrt is compiled for several platforms of several manufacturers. There are versions available for the chips from well known 802.11 transceiver manufacturers like Broadcom [81], Ralink [84] and Atheros [85]. DD-Wrt is another open source firmware available for several platforms of several manufacturers and implements the OLSR protocol.

4.12 The transmission range of the wireless sensors

The transmission range of the sensors is fundamental for the reliable operation of the WSN. The sensors installed on the top of the towers have a Line-of-Sight (LOS) to the closest neighbors at each side on every tower. In flat terrains, it is possible to have LOS to several neighbors at each side of a tower. In this case, the path loss can be calculated using the free space models. In Chapter 5 we present the calculation and field measurements of transmission range showing the feasibility of using IEEE 802.11b and IEEE 802.15.4 standards in sensors transceivers of Wireless Sensor Network to operate reliably on power transmission lines.

4.13 Power harvesting from shield wires to the wireless sensors

The wireless sensors and other instruments are usually powered by photovoltaic (PV) cells and batteries. However, the efficiency of PV cells is either reduced by dust collection or blocked by snow and must be periodically cleaned. Besides, the batteries must be dimensioned to operate for several hours during the night or during rainstorms or snowstorms. We investigated a reliable and low maintenance alternative to PV cells. The transmission line itself can supply the power to the sensors using the induced currents by means of current transformers installed on the shield wire [86].

4.13.1 Currents induced in shield wires

Currents in the phase cables of overhead power transmission lines induce a voltage on

any conductor running parallel to the cables, like the shield wires (detailed in Chapter 3).

The steady state current flowing in the shield wire (I_m) (Amperes) between the two towers due to the voltage induced on the wire (Volts per kilometer) can be calculated by the equation below:

$$I_m = \frac{V_m}{Z_W + Z_{T1} + Z_{T2}} l_w \quad (4.1)$$

where V_m is the voltage induced calculated by (3.4), Z_W is the wire impedance (Ohms), Z_{T1} and Z_{T2} are the sum of the tower structure impedance and grounding resistance (Ohms) of each tower, and l_w is the length (kilometers) of the shield wire between the towers. The tower impedance is usually negligible at 60 Hz and Z_T is basically the resistance of the tower grounding. The grounding resistance values are usually in the range from 5 Ω to 30 Ω [9]. On an overhead power transmission line, the current induced in each segment of shield wire (between two towers) flows to ground through the towers. However, the current flows most to the wire on the adjacent spans because at low frequencies the tower impedance is usually higher than the wire impedance. The resulting current flowing in the shield wire in any span is the sum of the individual contribution of each current induced in every span. Therefore, the resulting current depends on the impedances and on the voltage induced on every span.

The equivalent circuit to evaluate the distribution of currents along a power line is shown in Figure 4.15. V_{mn} is the voltage induced on span n by phase currents, Z_{Wn} is shield wire impedance of span n and Z_{Tn} is the sum of the tower structure impedance and grounding resistance. The current in span n (I_{m_n}) due only to the voltage induced on the span (V_{mn}), is calculated by the equation:

$$I_{m_n} = \frac{V_{mn}}{Z_{W_n} + Z_{EL_n} + Z_{ER_n}} l_{W_n} \quad (4.2)$$

where l_{W_n} is the length of the span, Z_{EL_n} and Z_{ER_n} are the equivalent impedances of wire and tower impedances of all spans to the “left” and to the “right” of the span n , respectively, and are calculated by the relations below:

$$Z_{EL_n} = \frac{1}{\frac{1}{Z_{T_n}} + \frac{1}{Z_{W_{n-1}} + Z_{EL_{n-1}}}} \quad (4.3)$$

$$Z_{ER_n} = \frac{1}{\frac{1}{Z_{T_{n+1}}} + \frac{1}{Z_{W_{n+1}} + Z_{ER_{n+1}}}} \quad (4.4)$$

V_{mn} depends on the mutual impedance between each phase cable and shield wire (Z_{mA_n} , Z_{mB_n} , Z_{mC_n}), depends on the length of the span l_{W_n} and depends on the current of each phase (I_A , I_B , I_C):

$$V_{m_n} = Z_{mA_n} I_A + Z_{mB_n} I_B + Z_{mC_n} I_C \quad (4.5)$$

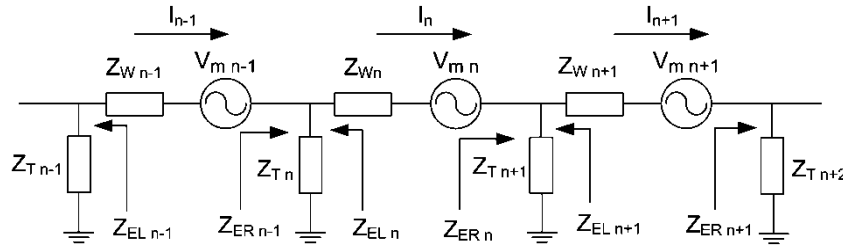


Figure 4.15 - The equivalent circuit of the shield wire and towers to evaluate the distribution of currents: Z_T is the tower and grounding impedance, Z_{ER} and Z_{EL} are the equivalent resistances to the right and to the left of the span, respectively, V_m and I_n are the voltage and current induced.

In case of an overhead transmission line, the current calculated by (4.2) is much higher than the current for a single span, calculated by (4.1), because Z_{EL_n} and Z_{ER_n} are smaller than Z_{T1} and Z_{T2} . Nevertheless, the resulting current is even higher because each span is a source of voltage and contributes with a fraction of its current to all spans. The resulting current I_n in the shield wire in span n , including I_{m_n} and the contributions of the other spans, is calculated by the equation below for a line with k spans and one shield wire:

$$I_n = \left[\sum_{i=1}^{n-1} \left(\prod_{j=i+1}^n \frac{Z_{ER_{j-1}}}{Z_{W_j} + Z_{ER_j}} I_{m_i} \right) \right] + \left[\sum_{i=n+1}^k \left(\prod_{j=n+1}^i \frac{Z_{EL_{j+1}}}{Z_{W_j} + Z_{EL_j}} I_{m_i} \right) \right] + I_{m_n} \quad (4.6)$$

The current calculated by (4.6) is higher than the current calculated by (4.2), and changes along the power transmission line with the lower values at the edges. For power lines with two shield wires equation (4.6) does not apply. In this case, the distribution of currents is different because the voltages induced in each shield wire are out of phase. The resulting currents flow to both wires with a more complex distribution.

We have simulated the power line using a power systems simulation program, to evaluate the induced currents to show the feasibility of this powering method. Field

measurements confirmed the simulations. The results are shown in Chapter 5.

4.13.2 Power supplied by current transformers

The power available in the shield wires can be supplied to the apparatus using a window type Current Transformer (CT) installed around the wire, close to the tower (Figure 4.16).

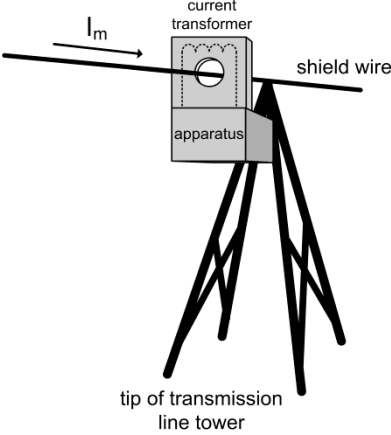


Figure 4.16 - The current transformer and apparatus installed on shield wire, I_m is the current induced in the shield wire.

Like PV cells, the CT is a current source but the current is alternate. The output current is proportional to the current induced in the shield wire (I_m/N). Figure 4.17 shows the equivalent circuit of the CT.

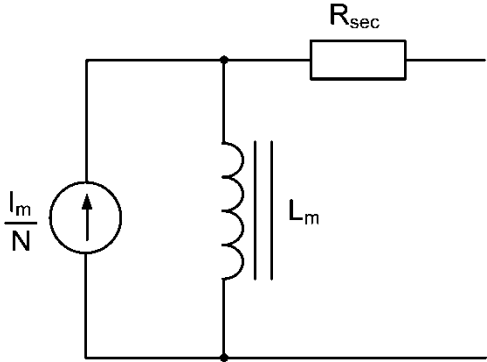


Figure 4.17 - The CT equivalent circuit, R_{sec} and L_m are the secondary resistance and inductance of the CT, respectively, I_m is the induced current and N is the number of turns of the secondary of a window type CT.

The maximum power available to the apparatus using a CT (P_{CTmax}), depends on the induced current and on the characteristics of the CT (for values well below the maximum available at the span). P_{CTmax} can be calculated by the equation below:

$$P_{CTmax} = V_{max} \left(\frac{I_m}{N} - I_e \right) \quad (4.7)$$

where V_{max} is the knee-point voltage of the excitation curve, I_m is the shield wire current (primary current), N is the secondary to primary turns ratio, and I_e is the secondary excitation current, out of phase with I_m .

To supply power to the sensors or other devices, the CT output feeds a current source voltage regulator, like the switching shunt voltage regulator used on PV cells [87]. Figure 4.18 shows a voltage regulator dimensioned to supply an output of 9 V_{dc}. The PWM of the switching shunt is a comparator with hysteresis. Using a 20 VA commercial transformer (60RBT) with a 1:30 ratio [88], the CT supplies 0.26 A_{rms} from a shield wire carrying a current of 8 A_{rms} (value measured in a real power line [86]) and can supply up to 1.8 W.

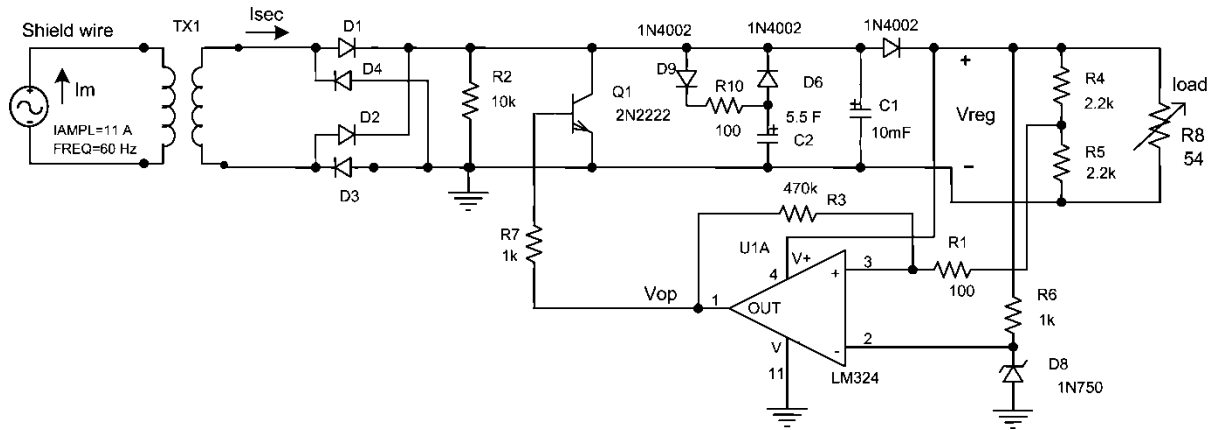


Figure 4.18 - Power supply circuit.

The super capacitor takes a long time to charge up to full voltage. The power supply allows the rapid start up of the power supply independent of the charging time of the supercap.

Figure 4.19 shows the current at the secondary of the CT (I_{sec}), the output of the operational amplifier (V_{op}) and the regulated output voltage (V_{reg}) for a load consuming 1.5 W of power. From 100 mW to 1.5 W, the voltage regulation of this power supply is 0.1%. The resistors R1 and R3 and the capacitor C1 control the ripple voltage, which is 0.1 V_{pp} at 1.5 W for the circuit shown (Figure 4.18). The capacitor C2 in the power supply is a super capacitor to keep the voltage for several seconds, and substitute a battery when the apparatus do not have to operate continuously after a power line outage. This is the case of the wireless sensors

monitoring the power line for location of faults and direct strokes. After the information about the transient disturbance is sent, the sensor can be powered off while the power transmission line is in outage state. Three super capacitors of 22 F connected in series can supply 100 mA for 72 seconds with a voltage drop less than one Volt.

If we consider the voltages and the duty cycle of transmission in case of wireless sensors, the super capacitor (supercap) can supply power for much longer time, even with lower values of capacitance. The sensors in the location system have very low transmission duty cycle, less than 1%. Therefore, we can consider only the power in the receiver state. In case of the Zigbit900 module [73], the voltage is 3.6 V and supply current of 15 mA in the receiver mode. With the power supply of Figure 4.18 (supercap of 5.5 F), and considering a voltage drop of 4 V, it is possible to supply power to the module using a 3.6 low dropout linear voltage regulator at the output of the power supply for 1460 seconds (24.3 minutes). In case of a sensor with 802.11 transceiver using the transceiver/amplifier Maxim MAX2820/MAX2242 [89] and Microchip PIC18F2685 [90] microcontroller, the combination of these chips operates at 3.6 V with supply current of 84 mA in the receiver mode. With the power supply of Figure 4.19 (supercap of 5.5 F) it is possible to supply power for 260 seconds (4.4 minutes) using a 3.6 V low dropout linear voltage regulator at the output of the power supply.

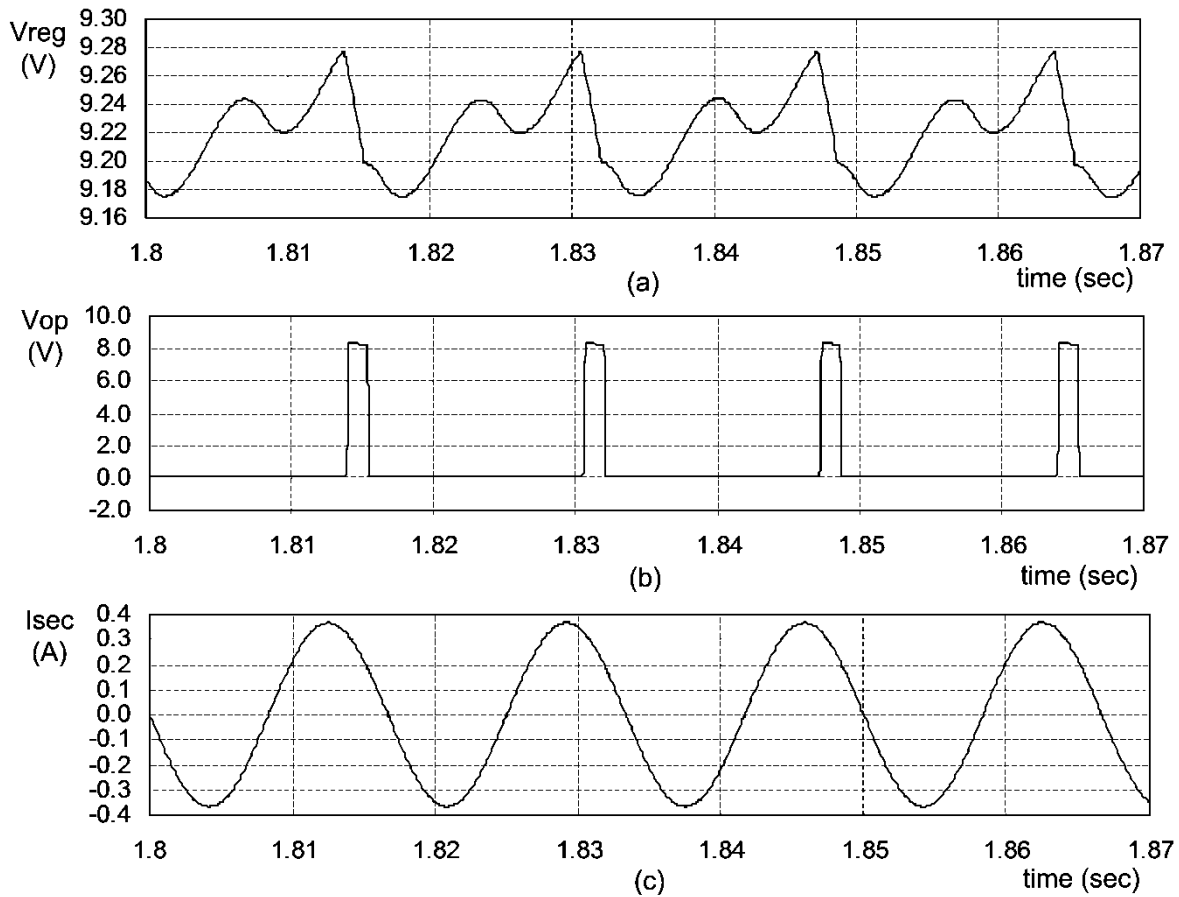


Figure 4.19 - The output voltage of the power supply (a), the output of the PWM (b), and the current at the secondary of the current transformer (c). V_{reg} , V_{op} , and I_{sec} refer to the labels in Figure 4.18.

If a lightning stroke hits the shield wire, close to the current transformer, a current of several kiloamperes flows through the primary of the CT. The core saturation and the poor high frequency response of the CT limit the voltage in the secondary winding. A surge protector installed on the output of the transformer, or in the apparatus power supply input, can provide additional protection lowering the surge voltage to a safe value. In general, the electromagnetic compatibility techniques used to protect the electronics of tower light controllers from lightning strokes can be used to protect the apparatus.

Chapter 5

Results

5.1 Simulations of direct lightning strokes to overhead power transmission lines

To evaluate the feasibility of the method we had analyzed the behavior of the direct stroke currents flowing through the shield wires and towers of power lines in different situations. To perform this analysis we have done several simulations using the ATP/EMTP program [27]. In the simulations, we have tested different combinations of power line characteristics like height of towers, tower grounding resistances, span lengths and soil resistivities, and different lightning stroke currents and hit positions along the line. We have also simulated the lightning that bypass the shield wire and strikes a phase cable (shielding failure). The simulations were exhaustive trying to cover all possible situations. The influence of every parameter on the currents was evaluated keeping all but one parameter constant and verifying the behavior of the currents in the towers with the variation of this parameter over a wide range of possible values. The range and the number of steps have taken into consideration the limitations of processing time for every simulation. Next, using the homogenous power line as a reference, the parameters were changed in steps to the values that lead to the worst precision of location. The limits of values for the parameters were the feasible values of a real line, like lowest and highest height of towers, or smallest and greatest length of spans. This simulation procedure works well because the parameters of the OPTL have a linear behavior.

Each span of the power line was programmed using the built-in line/cable module (LCC) (JMarti model) of the ATPDraw graphical preprocessor of ATP program [91]. The towers were represented by their surge impedance. For the simulated lightning stroke, it was chosen the concave current shape recommended by CIGRE guidelines [92]. The simulations have been done for homogeneous power lines (the same characteristics of towers, span

lengths, soil resistivity and grounding resistances along the line) and for non-homogeneous power lines.

We have simulated overhead power transmission lines with one and with two shield wires. We show below the results of these simulations. With these results it was possible to evaluate the precision of the method in different situations.

5.1.1 Simulations of lines with one shield wire

From several simulations of OPTLs with two shield wire, we have chosen one set of results for a 5 km non-homogeneous power line, with great variations in the span lengths and grounding resistances (worst-case situation), presented below to illustrate the method. The simulations results show the values of the currents flowing through the tower (measured on the top of the structure). Figure 5.1 shows the stroke positions, the span lengths and the tower grounding resistances used in the set of simulations presented. The towers where the currents were measured are numbered from 1 to 8 (abbreviated T1 to T8). The simulations include nine stroke positions on shield wire between towers 3 to 7. These positions are numbered 1 to 9 in the figure. The position 10 is the stroke to the tower structure below the coil. The lengths and resistances vary significantly around the stroke position. The characteristics of the simulated power line and other parameters are detailed in Appendix B.

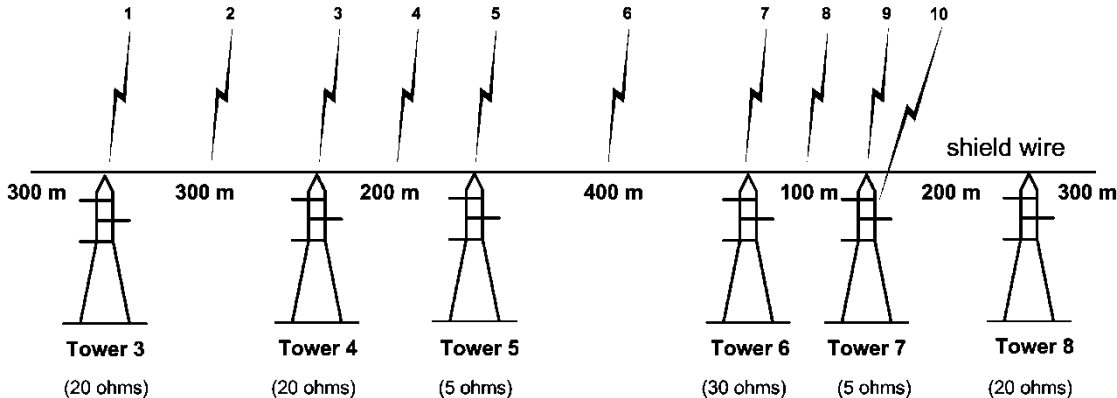


Figure 5.1 - The stroke positions, span lengths and footing resistances used in the simulations.

Figure 5.2 and Figure 5.3 show the wave shape of the currents flowing through the five towers closer to the stroke point for a 30 kA simulated lightning stroke. Figure 5.2 shows the currents generated by a lightning that strikes the top of tower 8. Figure 5.3 shows the currents generated by a lightning that strikes the middle of the span between tower 8 and tower 9.

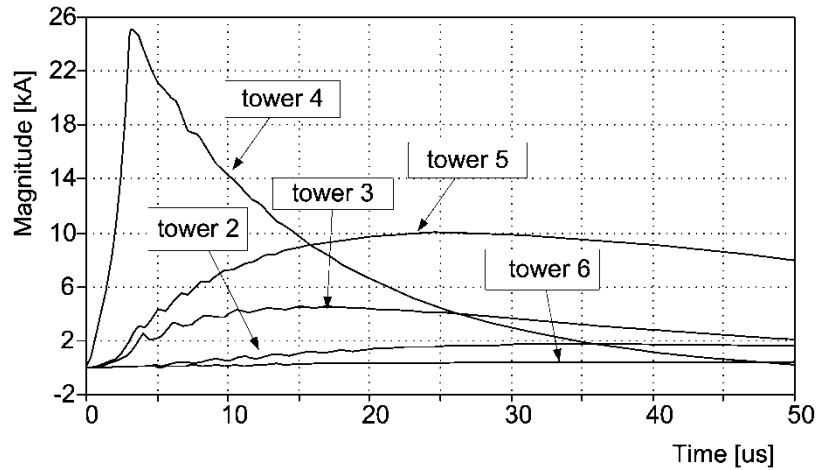


Figure 5.2 - Simulated currents of a direct lightning stroke to the top of tower 4.

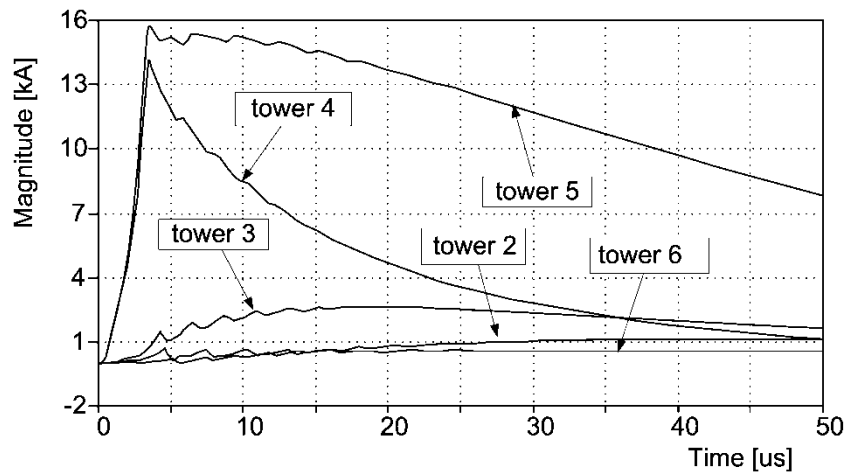


Figure 5.3 - Simulated currents of a direct lightning stroke to the middle of the span, between towers 4 and 5.

In Figure 5.3, the currents of towers 4 and 5 have different shapes because of the difference in the tower grounding resistances and span lengths (non-homogeneous power line). In a homogeneous power line, the currents are equal in the towers with the same distance from the stroke point. Table 5.1 below lists the values of the peak currents in the towers closer to the lightning stroke.

Table 5.1 - Results for one set of simulations of a non-homogeneous power transmission line (“Tn” is the abbreviation for “tower n”, “Tn-Tn+1” means between “tower n” and “tower n+1”).

Position in Figure 5.1	Lightning stroke position	Measured peak current (Amperes)							
		T1	T2	T3	T4	T5	T6	T7	T8
1	T3	2153	5112	25606	4487	4760	266	1132	222
2	mid-span T3-T4	1484	3265	14783	14414	6890	347	1402	269
3	T4	903	1790	4504	24962	9890	461	1744	329
4	mid-span T4-T5	620	1150	2641	14140	15737	871	2052	380
5	T5	436	715	1267	2668	27865	1491	2444	442
6	mid-span T5-T6	296	472	810	1632	15796	12529	7872	1040
7	T6	177	260	400	691	4613	21671	14479	1825
8	mid-span T6-T7	159	228	337	540	3113	12605	17491	2060
9	T7	147	207	300	461	2449	2923	26319	2341
10	T7 (below the coil)	147	207	300	461	2449	2923	-7948	2341

The analysis of the values in Table 5.1 and the analysis of the values of other sets of simulations, show that the behavior of the currents was as expected, even with great variations in the span length and tower grounding resistance. If the lightning strikes the shield wire in the middle of the span between two towers, the sensors on the top of these two towers measure the highest peak currents. If the lightning strikes the shield wire on the top of the tower or close to it, the sensor of this tower measures the highest peak current. The nearer the stroke position is to the tower, the higher is the measured peak current in this tower compared to the next towers.

In a homogenous power line, the peak currents decrease evenly moving away from the hit position. Besides, the peak currents are equal in the towers with the same distance from the stroke point.

If the lightning strikes the structure of the tower below the Rogowski coil, the sensor of this tower still measures the highest peak current but it flows in the opposite direction as indicated by the minus sign on the last row of Table 5.1.

In case of a shielding failure, the stroke current flows in the phase cable and it induces a current in the shield wires that flows mostly to the ground through the towers. The stroke current itself does not flow to ground through the towers. As a consequence, the behavior of the shield currents is different and they are less attenuated at each tower moving away from the stroke position as can be seen below.

The ATP program simulates the induction from phase cables to shield wires. Figure 5.4 shows the induced currents for a simulation of a 30 kA lightning stroke to phase cable (phase B), close to tower 4, flowing from shield wires to ground in the five towers closer to the stroke point.

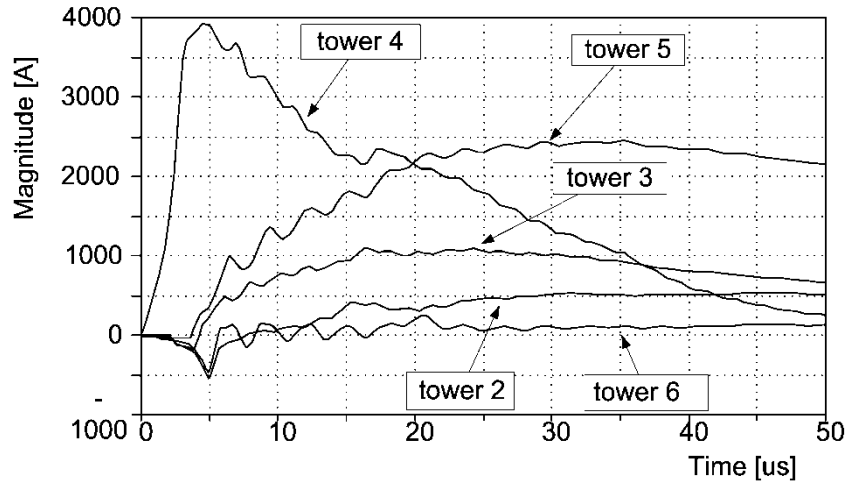


Figure 5.4 - Simulated currents for a lightning stroke to phase cable, close to tower 4.

In Table 5.2, we show the results of the simulations of shielding failure. The values show that the currents induced in the shield wires are higher in the two towers close to the stroke point. The peak values are much lower than the values shown in Table 5.1 but still high enough to be reliably detected.

Table 5.2 - Results for the simulations of a direct stroke to phase cable (shielding failure) (“Tn” is the abbreviation for “tower n”).

Lightning stroke position	Measured peak current (Amperes)							
	T1	T2	T3	T4	T5	T6	T7	T8
T3	549	1329	4233	1093	1231	451	374	365
Mid-spam T3-T4	522	912	2550	2540	1725	448	383	375
T4	544	548	1098	3922	2445	475	468	392
Mid-spam T4-T5	530	547	725	2265	3395	367	547	399

5.1.2 Simulations of lines with two shield wires

From several simulations of OPTLs with two shield wire, we have chosen one set of results for a 52 km non-homogeneous power line, with great variations in the span lengths and grounding resistances (worst-case situation), presented below to illustrate the method. The results show the absolute peak values of the currents flowing from both shield wires to ground

through the towers (measured on the top of the structure) for a 40 kA lightning stroke. Figure 5.5 shows the stroke points used in the simulations. The towers where the simulated currents were measured are numbered from 1 to 8 (identified as T1 to T8). The simulations include eight stroke points on shield wire 1 between towers 3 to 5. These points are numbered 1 to 7 in Figure 5.5. The point 8 is the stroke to the tower structure, below the coil. The lengths and resistances vary significantly around the stroke points to simulate a worst case. The characteristics of the simulated power line and other parameters are detailed in Appendix C.

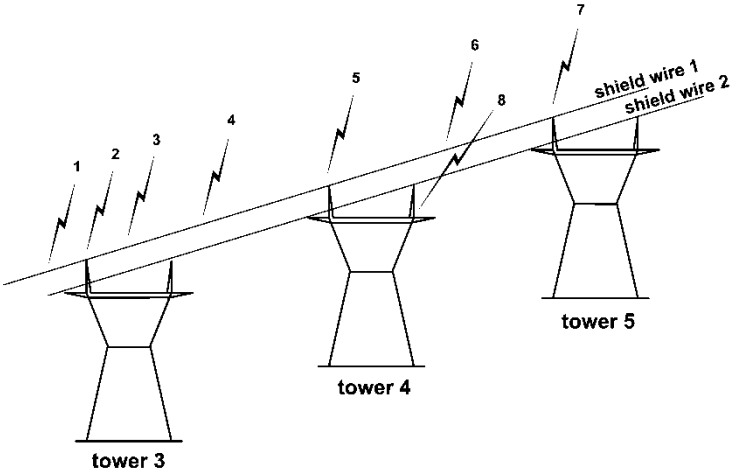


Figure 5.5 - The stroke points used in the simulations.

Figure 5.6 shows the wave shape of the currents flowing from shield wires to ground in the four towers closest to the stroke point. The 40 kA simulated lightning stroke hit the middle of the span between towers 3 and 4 (point 4 in Figure 5.5).

In Figure 5.7, the currents in towers 3 and 4 (and also 2 and 5) have different shapes because of the difference in the tower grounding resistances and span lengths (non-homogeneous power line). In a homogeneous power line, the currents are equal in the towers with the same distance from the stroke point.

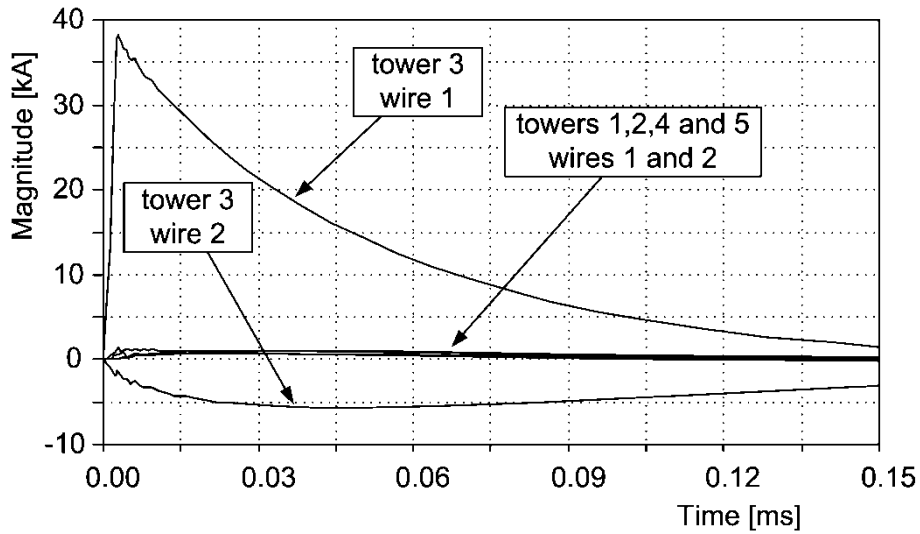


Figure 5.6 - Currents of a direct stroke to shield wire 1 in tower 3.

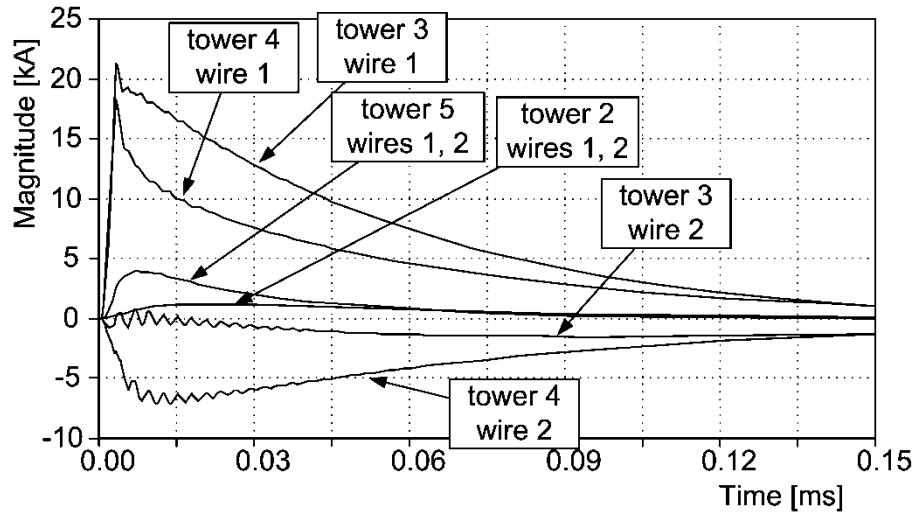


Figure 5.7 - Currents of a direct stroke to shield wire 1 at the middle of the span, between towers 3 and 4.

Table 5.3 lists the values of the peak currents flowing from shield wire 1 and from shield wire 2 to ground on the towers closest to the lightning stroke. The analysis of the values in Table 5.3 and the analysis of the values of other sets of simulations show that the behavior of the currents was as expected, even with great variations in the span length and tower grounding resistance. If the lightning strikes the shield wire in the middle of the span between two towers, the sensors on the top of these two towers measure the highest peak currents from shield wire 1 or 2 to ground. If the lightning strikes the shield wire on the top of the tower or close to it, the sensor of this tower measures the highest peak current from shield wires 1 or 2 to ground. The nearer the stroke point is to the tower, the higher is the measured

peak current in this tower compared to the next towers. The negative values of currents in Figure 5.6 and Figure 5.7 are caused by the current flowing from the shield wire 1, where the stroke has hit, to the shield wire 2 (opposite direction in the coil), in the towers closest to the stroke position.

Table 5.3 - Results for one set of simulations of a non-homogeneous power transmission line (“Tn” is the abbreviation for “tower n”, “Tn-Tn+1” means between “tower n” and “tower n+1”).

Position in Figure 5.5	Lightning striking point	Path of current	Absolute values of the peak currents (A)							
			T1	T2	T3	T4	T5	T6	T7	T8
1	T2-T3, 20 m from T3	wire 1	1215	5234	35100	854	1018	483	409	283
		wire 2	1215	852	4671	854	1018	483	409	283
2	T3	wire 1	1102	1383	38149	925	1050	496	420	290
		wire 2	1102	1383	5687	925	1050	496	420	290
3	T3-T4, 20 m from T3	wire 1	1067	1325	37017	3451	1131	520	438	293
		wire 2	1067	1325	5420	780	1131	520	438	293
4	mid-span T3-T4	wire 1	744	818	21191	18268	3981	1184	899	534
		wire 2	744	818	1522	7107	3981	1184	899	534
5	T4	wire 1	447	359	4122	32124	7287	2083	1542	875
		wire 2	447	359	4122	14053	7287	2083	1542	875
6	mid-span T4-T5	wire 1	401	314	3488	17860	19529	2374	1731	970
		wire 2	401	314	3488	5714	4082	2374	1731	970
7	T5	wire 1	363	278	3031	3752	39056	2730	1944	1070
		wire 2	363	278	3031	3752	10871	2730	1944	1070
8	T4 (below the coil)	wire 1	447	359	4122	14054	7287	2083	1542	875
		wire 2	447	359	4122	14054	7287	2083	1542	875

In a homogenous power line, the peak currents decrease evenly moving away from the hit position. Besides, the peak currents are equal in the towers with the same distance from the stroke point.

If the lightning strikes the structure of the tower below the Rogowski coil, the sensor of this tower still measures the highest peak currents but it flows in the opposite direction on both wires.

In case of a shielding failure, the stroke current flows in the phase cable and it induces a current in the shield wires that flows mostly to the ground through the towers. The stroke current itself does not flow to ground through the towers. Consequently, the behavior of the shield currents is different and they are less attenuated at each tower moving away from the stroke point as can be seen below.

With the ATP program we have simulated the induction from phase cables to shield wires. Figure 5.8 shows the induced currents flowing from shield wires to ground in the five

towers closest to the stroke point for a simulation of a 40 kA lightning stroke to phase cable (phase A), near tower 4.

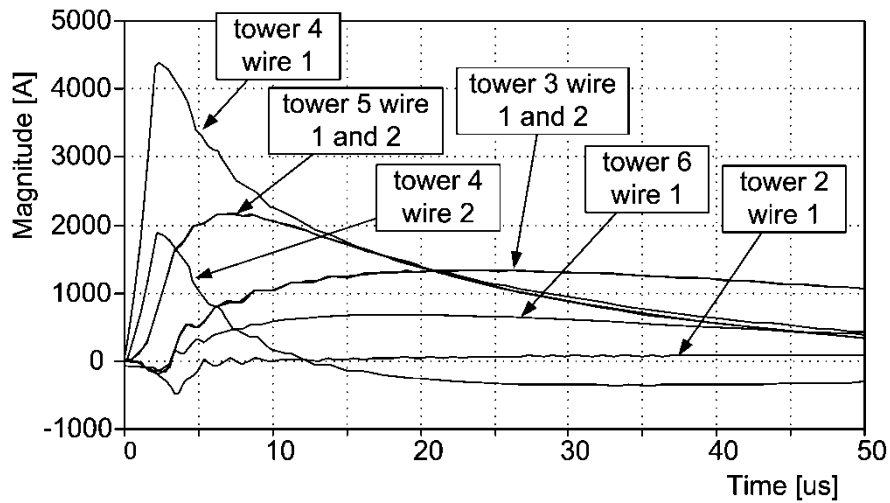


Figure 5.8 - Simulated currents for a direct stroke to phase cable, near tower 4.

In Table 5.4, we show the results of the simulations of shielding failure. The values show that the currents induced in the shield wires have a behavior similar to the currents of the stroke to shield wire in the towers closest to the stroke point. However, the peak values are much lower than the values shown in Table 5.3 but still high enough to be reliably detected. Besides, we verified that in the towers before T1 and after T8 the peak currents oscillate around the values of T1 and T8, respectively, without significant attenuation.

Table 5.4 - Results for the simulations of a direct stroke to phase cable (shielding failure) (“Tn” is the abbreviation for “tower n”, “Tn-Tn+1” means between “tower n” and “tower n+1”).

Lightning striking point	Path of current	Absolute values of the peak currents (A)							
		T1	T2	T3	T4	T5	T6	T7	T8
T3	wire 1	557	331	5936	252	363	316	343	529
	wire 2	500	580	3564	252	364	303	349	483
mid-span T3-T4	wire 1	551	315	3646	2878	1183	384	417	539
	wire 2	500	442	2464	1365	1184	382	329	492
T4	wire 1	582	506	1323	4364	2156	665	623	562
	wire 2	532	277	1318	1874	2161	662	487	509
mid-span T4-T5	wire 1	582	522	1154	2512	3222	747	678	568
	wire 2	533	260	1155	1284	2069	745	553	509

5.1.3 Stroke location processing

When there is a transient current in the tower, if the output of the integrator exceeds a preset threshold (to avoid reading very small transients from other sources), the sensor reads this output voltage of the Rogowski coil and its value integrated, and sends the peak values

and the sensor identification to the computer, through the communication subsystem. The computer processes the information received from the sensors and locates the stroke position.

After receiving the measurements from the sensors, and the corresponding sensor identification and time stamp, the computer locates the highest measured value and the corresponding tower number associated with the sensor identification. The values analyzed must be within a time interval of 10 ms to separate currents of subsequent strokes. The stroke point is located between the tower with the highest peak current and its adjacent towers.

There are two possibilities for measurements on each tower. The sensors can measure the currents from only one shield wire (one Rogowski coil) or from two shield wires (two Rogowski coils). After the analysis of several simulations results, we verified that the precision (of the algorithm) is two spans when measuring from a single shield wire, while the precision is one span when measuring from two shield wires. Measuring from two wires, there is a high probability that the stroke point is located between the tower with the highest peak current and the adjacent tower with the highest peak value (precision of one span). When the highest value is much higher than the peak current on the adjacent towers (four times or more), there is a high probability that the position is very close to the tower with the highest peak value.

It is possible to install one sensor at every other tower reducing the precision of the location system to four spans, measuring only one shield wire, or to two spans, measuring both shield wires, which is acceptable in most cases.

Table 5.5 shows the stroke position estimation based on the relative amplitude of the highest peak currents of Table 5.3 and Table 5.4, using the measurements of the current from one shield wire and from two shield wires.

Table 5.5 - Lightning stroke position estimation using the values of Table 5.3 and Table 5.4 (“Tn” is the abbreviation for “tower n”).

Stroke point	Estimated stroke position	
	Measuring from one wire	Measuring from two wires
T2-T3, 20 m from T3	Between T2 and T4	Between T2 and T3, close to T3
T3	Between T2 and T4	Between T2 and T3, close to T3
T3-T4, 20 m from T3	Between T2 and T4	Between T3 and T4, close to T3
mid-span T3-T4	Between T3 and T5	Between T3 and T4
T4	Between T3 and T5	Between T4 and T5, close to T4
mid-span T4-T5	Between T3 and T5	Between T4 and T5
T5	Between T4 and T6	Between T4 and T5, close to T5
T4 (below the coil)	Between T4 and T6	Between T4 and T5, close to T5
T3 (shielding failure)	Between T2 and T4	Between T2 and T3, close to T3
Mid-span T3-T4 (shielding failure)	Between T2 and T4	Between T3 and T4
T4 (shielding failure)	Between T4 and T6	Between T4 and T5
Mid-span T4-T5 (shielding failure)	Between T4 and T6	Between T4 and T5

5.1.4 Evaluation of the results of stroke simulations

The simulations and the analysis presented in Table 5.1 to Table 5.5 show that it is feasible to detect and locate the stroke position with the precision of one span in most cases, installing the wireless sensors at every tower.

Despite the high number of sensors to be placed in a typical power transmission line with length of hundreds of kilometers (hundreds of sensors), the cost of a system implementing the proposed method is very low compared to the line itself and the benefits of prevention and minimization of outage time.

One such system is simple and accurate and can be made reliable with proper product engineering. Besides, the system can store the data received for long periods and use this information to provide statistical analysis and evaluation of the lightning performance of overhead power transmission lines.

The method is fully applicable to branched transmission lines or parallel transmission lines. The installation is easy and the sensors can be installed with the line in operation because the phase cables are not used for measurement.

5.2 Simulations of short-circuits faults

To evaluate the feasibility of the method we have analyzed the behavior of the transient currents induced by the fault flowing through the shield wires and towers of power lines in different situations. To perform this analysis we have done several simulations using the

ATP/EMTP program [27]. We simulated different types of short-circuits in homogeneous and non-homogeneous, transposed and untransposed overhead power lines. We tested short-circuit faults in different positions, changing characteristics like the length of the line, span lengths, tower height, tower impedance, tower grounding resistances and soil resistivity. We simulated short-circuits of one, two and three phases to ground, short-circuits between phases, and both low impedance and high impedance faults. The value of the currents and the instant of the faults (related to the waveform cycle) were also changed. The simulations were exhaustive trying to cover all possible situations. The influence of every parameter on the currents was evaluated keeping all but one parameter constant and verifying the behavior of the currents in the towers with the variation of this parameter over a wide range of possible values. The range and the number of steps have taken into consideration the limitations of processing time for every simulation. Next, using the homogenous power line as a reference, the parameters were changed in steps to the values that lead to the worst precision of location. The limits of values for the parameters were the feasible values of a real line, like lowest and highest height of towers, or smallest and greatest length of spans. This simulation procedure works well because the parameters of the OPTL have a linear behavior.

Table 5.6 and Table 5.7 show the results for two sets of these simulations for a non-homogeneous transmission line. It is important to observe that, unlike the tables of the stroke simulations shown before, the values in these tables are the values of integrator output, not the values of the currents in the towers. In Appendix C, we detail the characteristics of the line and the simulation. The measurement of the currents included 19 towers but only the eight towers closest to the fault are shown to reduce the tables. In the tables, the towers are identified as T1 to T8. In Table 5.6 the faults occur in T4 (or very close to it). In Table 5.7 the faults occur in the middle of the span between T4 and T5. Table 5.6 and Table 5.7 include line-to-ground faults and line-to-line faults. Table 5.6 also includes short-circuits from phase to the tower structure at 21 m from the bottom of the tower (position of the lower cables). The results show the absolute peak values (Volts) measured by the Rogowski coil and integrated by a low-pass first-order active filter with corner frequency of 1500 Hz (details in Appendix D).

Table 5.6 - Results of the fault simulations in T4.

Fault type	Fault resist.	Integrator output (Volts)							
		T1	T2	T3	T4	T5	T6	T7	T8
phase A to ground	5 Ω	5.3	10.4	14.3	44.5	17.1	5.8	6	2.9
phase A to ground	50 Ω	4.6	8.6	11.0	36.5	12.2	4	5.3	2.4
phase A to ground	1 kΩ	1.3	1.8	2.5	8.3	2.5	1.0	1.5	0.7
phases A and B to ground	50 Ω	5.4	9.8	12.9	42.9	14.1	4.6	6.3	2.8
phase B to tower	1.5 Ω	2.8	5.3	6.6	32.9	7.4	3.6	2.9	1.3
between phases A-B	2 Ω	1.8	2.4	3.4	11.3	4.2	2.2	1.8	0.9

Table 5.6 shows that the peak value of the transient current is much higher in the tower closest to the fault (T4) than in the other towers (bold values). Table 5.7 shows that the peak values in T4 and T5 have close values, which are much higher (bold values) than in the other towers. Despite the variation of the tower grounding resistances and the variation of the length of the spans, the towers closest to the fault have the highest transient currents.

Table 5.7 - Results of the fault simulations in the middle of the span (between T4 and T5).

Fault type	Fault resist.	Integrator output (Volts)							
		T1	T2	T3	T4	T5	T6	T7	T8
phase A to ground	5 Ω	4.6	7.8	8.1	34.7	39.6	8.5	5.6	3.1
phase A to ground	50 Ω	4.2	5.7	6.7	30.1	33.7	6.5	5.1	2.6
phase A to ground	1 kΩ	1.1	1.2	1.9	7.7	8.3	1.5	1.6	0.7
phases A and B to ground	50 Ω	4.8	6.8	7.7	34.7	39.0	7.4	5.9	3.0
Between phases A-B	2 Ω	1.7	2.3	3.5	11.4	12.2	3.8	2.7	1.2

Analyzing the several simulation results, there are some situations that generate a small value of transient current and consequently a small value of di/dt: high impedance short-circuits; one-phase-to-ground faults at voltage zero crossing; and phase-to-phase faults when the voltage of the two shorted phases are close. Despite the measurement flexibility of the Rogowski coil, the wide range of values can be a problem to the integrator circuit. To get around this problem, each sensor may have two or more coils placed around the wire to work with a lower range of values: one for detection of high values and another one for detection of lower values.

The simulated power lines have one shield wire but the results are fully applicable to lines with two shield wires, measuring the currents from only one in each tower. The second shield wire has the effect of reducing the attenuation of the transient currents in the adjacent towers but the simulations showed the same behavior of the currents with the highest peak values on the towers closest to the fault.

5.2.1 Fault location processing

When there is a transient current in the tower, if the output of the integrator exceeds a preset threshold (to avoid reading very small transients from other sources), the sensor reads this output voltage and sends the peak value and the sensor identification to the computer, through the communication subsystem. The computer processes the information received from the sensors and locates the fault.

After receiving the values sent by the sensors, together with the sensor identification and the time stamp, the computer locates the two highest peak values of current (with close time stamps to discriminate events in time) and the corresponding sensor identifications. The fault position is located between the two towers associated with the sensor identifications. If one of the two sensors measured a peak value much higher than the other one, 100% or more, there is a high probability of a short-circuit fault in the tower (or very close to it) with the highest transient current.

5.2.2 Evaluation of the results of fault simulations

The proposed method allows a great precision in the location of faults. It is possible to determine the tower or the span where the fault has occurred. It allows the location of faults in a wide range of impedances. Besides, it is possible to apply the method on both AC and DC transmission lines. The method is fully applicable to branched transmission lines or parallel transmission lines. Besides, the installation is easy and the sensors could even be installed with the line in operation because the phase cables are not used for measurement. The method uses the same hardware of the system for direct stroke location with very few modifications, adding a great functionality with a minimum additional cost.

5.3 Identification of the type of transient disturbance

There is a great difference between the peak value of di/dt of a direct stroke to shield cable, the peak value of di/dt of a direct stroke to phase cable, and the peak value of di/dt of a short-circuit fault. Table 5.8 shows typical values of di/dt for different transient disturbances in a simulated power line.

Table 5.8 - di/dt values for different types of transient disturbances.

Type of event	Measured peak di/dt (A/us)
low impedance short circuit (5 Ω)	361
3 kA stroke on phase	966
30 kA stroke on phase	3028
3 kA stroke on shield cable	5285
30 kA stroke on shield cable	17865

The di/dt measured for direct strokes to the shield cable are much higher than the values measured for the other transients. The di/dt measured for direct stroke in phase cable, in turn, is higher than for the direct stroke to phase cable. These values can be used to discriminate between different types of transient disturbances.

The energizing of a capacitor bank also generates transients that could be identified by the system as being a short-circuit. Nevertheless, the operation of a capacitor bank is manual and planned. The operators of the direct stroke and fault location system can be notified about these operations by the technical staff of the substation.

5.4 Simulations and measurements of steady state currents induced in the shield wires

To evaluate the feasibility of the use of the steady state current induced in the shield wires to power the sensors, we have done several simulations using the Alternative Transient Program (ATP) and also field measurements.

5.4.1 Simulation of the steady state induced currents

To evaluate the voltage induced on a single span we have simulated 500 m of phase cables and shield wire between two towers carrying current of 300 A_{rms} (60 Hz) in each phase ($\rho=500 \Omega.m$). Figure 5.9 shows the cable positions on the tower used in the simulations (in the data section of the LCC objects). The voltage induced between the edges of the shield wire was 7.6 V_{rms} (15.2 V/km), using the LCC routine.

To evaluate the currents induced in the shield wire by the phase currents, we have simulated a small overhead power transmission line with 18 km. The line has 61 towers, the cable positions of Figure 5.9, and span lengths of 300 m. The soil resistivity, wire resistance and tower grounding resistances were considered to be 500 Ω.m, 4 Ω/km, and 20 Ω, respectively.

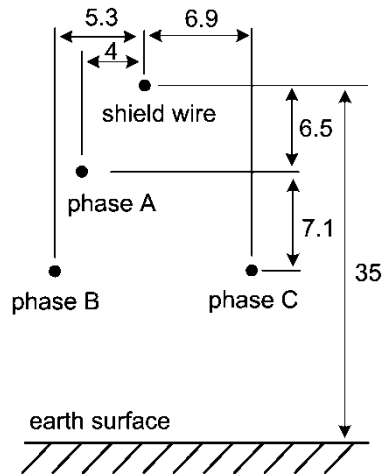


Figure 5.9 - Positions of the phase cables and shield wire (dimensions in meters).

For balanced phase currents of $300 A_{\text{rms}}$, the 60 Hz induced current in the shield wire is $3.6 A_{\text{rms}}$ at 21th span (between towers 21 and 22). From tower 10 to tower 50 the induced currents vary between $3.3 A_{\text{rms}}$ and $3.6 A_{\text{rms}}$.

Keeping the same geometry of the cables, the simulations showed that the length of the spans, the phase currents and the wire resistance are the parameters that affect most the induced current. The currents vary slightly along the power line even if the spans lengths and ground resistances change significantly. There is no sudden variation of current from one span to an adjacent span.

The simulations with the 18 km power line showed that the maximum power available to a resistive load in the 21th span is 33 W (no load on the other spans) using an ideal current transformer to supply current from the shield wire to a burden resistor. Getting power simultaneously from two or more spans affects the distribution of currents and the maximum power per span decreases. Table 5.9 shows the maximum power that eight spans can supply simultaneously. The apparatus for monitoring purposes need only a fraction of the power available at each span. It is possible to install low power equipments (e.g. up to 2 W) on every tower.

Table 5.9 - Maximum power available simultaneously from eight spans.

Span	Power (W)
3	9,7
10	24,1
21	28,1
31	24,1
37	23,3
46	20,9
51	15,4
55	13,2

Neglecting the excitation current, for a 20 VA commercial window-type current transformer (60RBT) [88], with 1:30 transformer ratio and the excitation curve of Figure 5.10, the maximum power available for the apparatus in the 21th span ($I_P=3.5 A_{rms}$) of the 18 km simulated power line is 1.2 W (resistive load and $V_{max}= 10 V_{rms}$) calculated using equation (4.7).

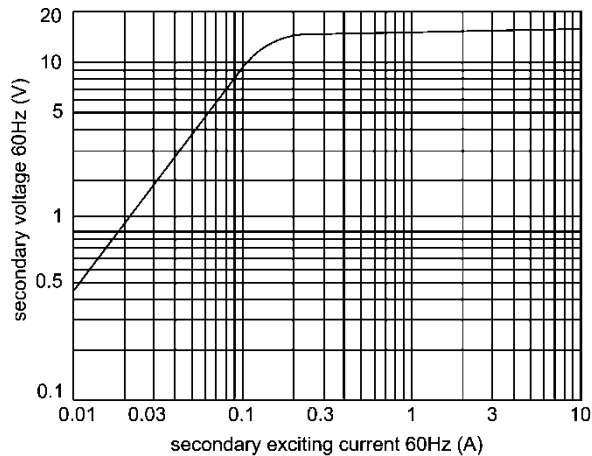


Figure 5.10 - Current transformer excitation curve.

In the simulated power transmission line, we have included a one-turn primary current transformer on the shield wire, between towers 21 and 22, to simulate the CT operation. The transformer was simulated by the saturable transformer component of the ATP program [93] (shown in Figure 5.11) with the parameters available in [88], including 1:30 ratio and the curve of the secondary excitation current of Figure 5.10.

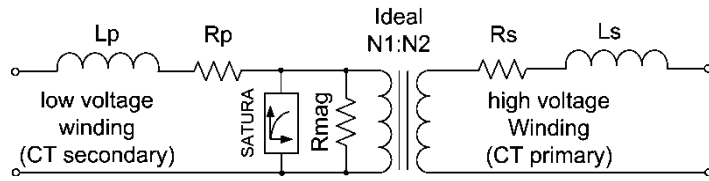


Figure 5.11 - ATP saturable component: L_p , R_p , L_s and R_s are the primary inductance and resistance, and secondary inductance and resistance, respectively, R_{mag} is the magnetizing resistance, SATURA is the ATP support routine.

In the simulations, with balanced phase currents of $300 A_{rms}$, the current transformer operating below the knee-point voltage supply $0.85 W$ at the 21th span to a 120Ω burden resistor. With an ideal CT it would be possible to supply up to $33 W$. The CT can supply enough power to electronics sensors, since these devices consume typically less than one Watt. Figure 5.12 shows the current in the shield wire and the corresponding CT secondary current and voltage.

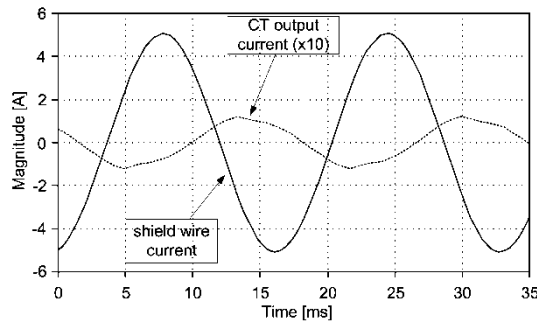


Figure 5.12 - The current induced in the 21th span and the CT output current.

Figure 5.13 shows a piece of the diagram of the simulated 18 km overhead power line, drawn in the ATPDraw graphical pre-processor of ATP program.

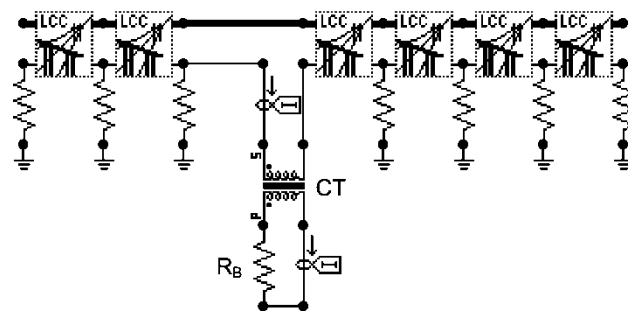


Figure 5.13 - A piece of the diagram of the simulated overhead power line showing six spans and the CT: the cables are modelled by the LCC objects, the grounded resistors represent the tower grounding resistances, R_B is the burden resistor.

5.4.2 Measurements in a power transmission line

The electricians from CEMIG have measured the shield wire currents in a 500 kV overhead power transmission line operated by that company with length of 24 km, and 60 towers. The average span length is 400 m, varying from 102 m to 858 m, the shield wire resistivity is $3.5 \Omega/\text{km}$ and the geometry of cables is as shown in Figure 5.14. The current measured between towers 12 and 13 was $8.5 \text{ A}_{\text{rms}}$ in shield wire 2 with phase currents of $596 \text{ A}_{\text{rms}}$ (phase A), $601 \text{ A}_{\text{rms}}$ (phase B), and $596 \text{ A}_{\text{rms}}$ (phase C).

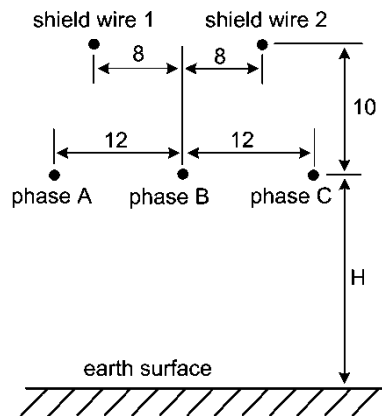


Figure 5.14 - Positions of the phase cables and shield wires, H varies for every tower (dimensions in meters).

Using the value of $1000 \Omega \cdot \text{m}$ for the soil resistivity, towers with an average value of 33 m of height and grounding resistances of 20Ω for all towers, we have simulated this 500 kV power line using the actual length of each span to evaluate the current distribution. The results of the simulation showed currents varying from $8.1 \text{ A}_{\text{rms}}$ to $8.8 \text{ A}_{\text{rms}}$ in shield wire 2, along the power line, using the same phase currents measured in the real power line ($596 \text{ A}_{\text{rms}}$, $601 \text{ A}_{\text{rms}}$, and $596 \text{ A}_{\text{rms}}$). Between towers 12 and 13, the value was $8.8 \text{ A}_{\text{rms}}$ in shield wire 2, which is very close to the measured value.

The simulations showed that the maximum power available in the shield wire 2 at tower 13 is 60 W (no load on the other spans) using an ideal current transformer to supply current from the shield wire to a burden resistor. Table 5.10 shows the maximum power that ten spans can supply simultaneously, and the length of each span. There is a direct correlation of the power available and the length of the span.

Table 5.10 - Simulation results for the maximum power available simultaneously from ten spans of the 24 km power line.

Span	Length (m)	Power (W)	Power/length (W/m)
6	253	28	9.0
11	226	26	8.7
13	492	56	8.8
15	280	32	8.8
21	257	32	8.0
31	386	45	8.6
35	641	72	8.9
41	396	46	8.6
51	310	33	9.4
57	282	31	9.1

5.4.3 Evaluation of the results of simulations and field measurements

The simulations and the field measurements showed that the shield wires carry several Amperes of current useful to supply power to apparatus on the top of the towers. The power consumption of wireless sensors is typically below 500 mW with low duty cycle. The results show that a small current transformer can supply enough power from the shield wire to electronic sensors. The shield wire can supply several Watts of power allowing the use these apparatus distributed along the power line. The current transformers have much higher useful life than the PV cells, there is no need to do periodic maintenance and the installation is easy using a split-core transformer. The power is supplied by the power line 24 hours with no interruption, except in case of a transmission line fault or preventive maintenance. The power supply shown in Figure 4.18 can also be used to supply energy to other equipments like low power wireless cameras used for surveillance [94], with power consumption below one Watt.

5.5 Simulation of routing protocols in linear topology

We have evaluated the use of the routing protocols HTR, AODV, OLSR and Flooding in the WSN operating on power transmission lines with high number of sensors. The evaluation was performed via a prior analysis of the of the protocol parameters and through simulations using versions 2.34 of the network simulator NS2 [77]. AODV is a native protocol included in standard NS2. The HTR and OLSR protocols were installed from third party contributors [95] [96]. NS2 is one of the most widely used simulators for wired and wireless networks.

To perform the simulations, we had to choose the parameters that could affect most the behavior of the protocols. In the wireless networks, the sharing of radio channel is an important issue. The nodes transmitting at the same time (collision) degrades the signal. Both technologies have mechanisms to minimize the collision between the nodes, ordering the beginning and duration of transmissions of each node (CSMA/CA mechanism describe earlier). But the collisions still happen and increase with the number of nodes that are inside the range of each other. Besides, the nodes have to contend for the channel and more nodes mean more delay to begin transmission. Increasing the range increases the delay and the probability of data packet loss. Therefore, the transmission range is very important to the routing protocol. To guarantee the reliability of network the transmission range must be at least two nodes, as already stated.

The number of sensors transmitting simultaneously is a parameter that, together with the transmission range, is very important because it worsens the problem of the collisions and transmission delay when the transmission range of nodes is high.

Other important issue is the total number of nodes. Considering the average span of 400 m, a relatively short 100 km OPTL will have 250 nodes and a long 1 000 km OPTL will have 2500 nodes. The default values of timeouts and other parameters of the routing protocols can limit the number of nodes, especially in the linear topology.

5.5.1 Network simulator configuration

The simulations were done for the linear topology with up to 3000 nodes, changing the range from one to eight nodes, and the number of transmitting sensors up to 20. The distance between two neighbor nodes is equal for every pair of neighbor nodes. The source nodes are at one end of the line and the destination node is at the other end. Figure 5.15 shows the simulation scenario.

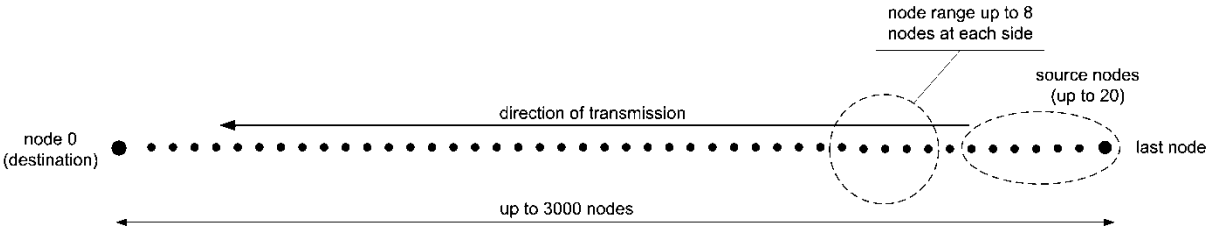


Figure 5.15 - Simulation scenario.

The first simulations showed a limitation in the NS2 default configuration for simulations of a high number of sensors. The parameter TTL (Time to Live) used for all protocols is very small. This parameter determines the number of times the packet will be forwarded (hops) before being discarded by a node. The original value of TTL was 32 hops and it was changed to 2000 (ns-default.tcl file). With this value it is possible to simulate a network with up to 2000 nodes in the worst case, with a transmission range of only one node, and larger networks with higher transmission ranges.

5.5.1.1 HTR protocol

A preliminary analysis of the protocol HTR shows an important limitation that precludes its use in networks with linear topology. This routing protocol organizes the network as tree. Because of physical linear topology of the network on the OPTL, the number of leafs is limited by the transmission range at each level of the tree. The maximum depth of the tree is represented in the HTR with 8 bits which limits the depth to 255 levels [42]. Assuming an average range of 5 nodes (leafs), which allows up to five sensors per level, the network cannot have more than 1275 nodes.

Besides, the HTR protocol implemented in the NS2 has a limitation of the maximum number of nodes. Because of the use of short address format, with 16 bits, the address formation algorithm of the hierarchical tree limits the addressing of nodes to approximately 250 addresses.

5.5.1.2 OLSR protocol

The OLSR protocol implemented in NS2 has a practical limitation of the maximum number of nodes in the simulation because of the processing time. With 250 nodes the simulation takes several hours in a desktop computer with a Intel E8400 3.0 GHz dual core CPU which is high performance desktop processor. Therefore, we had to limit the simulations with OLSR to 250 nodes to compare it to the other protocols.

It was necessary to change some parameters of the protocol in the simulator to enable the operation with 250 nodes. Table 5.11 shows the parameters changed with the original values and new ones.

Table 5.11 - OLSR NS2 parameters.

Parameter	Default value	New value	File
OLSR_REFRESH_INTERVAL	2	10	olsr.h
OLSR_NEIGHB_HOLD_TIME	3*OLSR_REFRESH_INTERVAL	20*OLSR_REFRESH_INTERVAL	olsr.h
OLSR_TOP_HOLD_TIME	3*OLSR_TC_INTERVAL	20*OLSR_TC_INTERVAL	olsr.h
OLSR_DUP_HOLD_TIME	30	150	olsr.h
OLSR_MAX_MSGS	4	8	olsr_pkt.h
OLSR_MAX_HELLOS	12	24	olsr_pkt.h
OLSR_MAX_ADDRS	64	128	olsr_pkt.h

5.5.1.3 AODV protocol

The AODV protocol with the original parameters does not work with more than a few tens of sensors in the linear topology. It was necessary to change many parameters of the protocol in the simulator to allow operation with thousands of nodes. Table 5.12 shows the parameters changed with the original values and the new ones.

Table 5.12 - AODV NS2 parameters.

Parameter	Default value (sec)	New value (sec)	File
MY_ROUTE_TIMEOUT	10	300	aodv.h
ACTIVE_ROUTE_TIMEOUT	10	300	aodv.h
NETWORK DIAMETER	30	2000	aodv.h
REV_ROUTE_LIFE	6	300	aodv.h
RREP_WAIT_TIME	1	20	aodv.h
TTL_START	5	2500	aodv.h
TTL_THRESHOLD	7	2200	aodv.h
TTL_INCREMENT	2	1000	aodv.h
RREQ_RETRIES	3	5	aodv.h
MAX_RREQ_TIMEOUT	10	30	aodv.h
INFINITY	0xFF	0xFFF	aodv_rtable.h
AODV_RTQ_TIMEOUT	30	200	aodv_rqueue.h

5.5.2 Simulations

The simulations parameters used for each protocol are summarized in Table 5.13 and Table 5.14.

Table 5.13 - NS2 parameters of 802.11 simulations.

IEEE 802.11			
parameters	AODV values	OLSR values	Flooding values
addressType	flat	flat	flat
wiredRouting	OFF	OFF	OFF
llType	LL	LL	LL
macType	Mac/802_11	Mac/802_11	Mac/802_11
ifqType	Queue/DropTail/ PriQueue	Queue/DropTail/ PriQueue	Queue/DropTail/ PriQueue
phyType	Phy/WirelessPhy	Phy/WirelessPhy	Phy/WirelessPhy
adhocRouting	AODV	OLSR	DumbAgent
propType	Propagation/ TwoRayGround	Propagation/ TwoRayGround	Propagation/ TwoRayGround
antType	Antenna/ OmniAntenna	Antenna/ OmniAntenna	Antenna/ OmniAntenna
channel	Channel/ WirelessChannel	Channel/ WirelessChannel	Channel/ WirelessChannel
ifqLen	400	400	400
bandwidth_	1 Mb	1 Mb	1 Mb
sending agent	Agent/UDP	Agent/UDP	Agent/MessagePassing/Flooding

Table 5.14 - NS2 parameters of 802.15.4 simulations.

IEEE 802.15.4		
parameters	AODV values	802.15.4/Flooding values
addressType	flat	flat
wiredRouting	OFF	OFF
llType	LL	LL
macType	Mac/802_15_4	Mac/802_15_4
ifqType	Queue/DropTail/ PriQueue	Queue/DropTail/ PriQueue
phyType	Phy/WirelessPhy/ 802_15_4	Phy/WirelessPhy/ 802_15_4
adhocRouting	AODV	DumbAgent
propType	Propagation/ TwoRayGround	Propagation/ TwoRayGround
antType	Antenna/ OmniAntenna	Antenna/ OmniAntenna
channel	Channel/ WirelessChannel	Channel/ WirelessChannel
ifqLen	100	100
bandwidth_	250 kb	250 kb
sending agent	Agent/UDP	Agent/MessagePassing/Flooding

The 802.11 was tested with RTS/CTS disabled because the RTS/CTS handshake is not effective on 802.11 network operating in Ad Hoc mode [97], confirmed with simulations. The 802.15.4 with AODV and flooding was tested without the association procedure because it is useless in these cases.

To analyze the protocols and compare their performances, we have performed the first simulations with only 250 nodes to allow the inclusion of the OLSR protocol in the comparison. For an average span of 400 m in the OPTLs, each sensor can reach up to six neighbors with the measured range of 2400 m for 2.4 GHz radio transceivers. Considering a power loss caused by intermediate towers in the Fresnel zone, we configured the range to five nodes, or 2000 m. The simulations were performed with all sensors transmitting almost simultaneously (interval of 1 ms), and with intervals of five seconds. Every simulation included two sequences of transmissions. Each node transmits only one message at each sequence. Therefore, only 20 messages are transmitted in each simulation, 10 messages in each sequence. The first sequence of messages aims at studying the behavior of routing protocols when the route has not been established yet. The second sequence of messages aims at studying the behavior of routing protocols when the route has already been established. All source nodes transmit to a single receiving node using UDP datagram which means that the transport service is unreliable. The transmitting nodes are close to one of the ends of the transmission line while the receiving node is at the opposite end. Table 5.15 shows the common parameters and Table 5.16 shows the results for each simulation.

Table 5.15 - Common parameters of the simulation.

Parameter	Value
Total number of nodes	250
number of nodes transmitting	10
range (nodes)	5
packet length (bytes)	100

Table 5.16 - Results for the simulations with 250 nodes.

Wireless standard	Protocol	Transmission interval between each sensor (sec)	Transmission rate (kbps)	Route setup (sec)	Delay time of 1st reception (sec)	Number of packets received in 1st sequence	Number of packets received in 2nd sequence
802.11	AODV	0.001	1000	0.4	0.2	10	10
802.11	AODV	5	1000	0.4	0.2	10	10
802.11	OLSR	0.001	1000	40	0.2	4	4
802.11	OLSR	5	1000	70	0.3	8	10
802.11	flooding	0.001	1000	n/a	0.2	8	10
802.11	flooding	5	1000	n/a	0.2	10	10
802.15.4	AODV	0.001	250	0.8	0.4	5	3
802.15.4	AODV	5	250	0.8	0.4	5	7
802.15.4	flooding	0.001	250	n/a	0.4	4	4
802.15.4	flooding	5	250	n/a	0.3	10	10

The simulation results show that the simultaneous transmission by the nodes causes loss of messages in most simulations. Only in case of the 802.11 nodes with AODV there is no message loss. As the transmission of data has no serious constraints of time, the transmission can be done with an interval of a few seconds to avoid losing packets. The sensor can use the tower identification which is sequential as a seed to select transmission delay after the event detection. The message losses are caused by the collisions because of large number of nodes contending for the channel and the use of the unreliable UDP datagrams. The broadcast messages used by the flooding protocol, and by the routing protocols in the initial phase of route discovery, are not acknowledged by ACK packets in the MAC layer. Therefore, if a flooding or a routing packet is lost because of the collisions or noise interference, the sending node does not retransmit the packet. In case of flooding, the data message is lost. In case of routing protocol, the route is not established and the data message does not have a route to the destination node. The UDP protocol neither has a retransmission mechanism and the message is not retransmitted by the transport layer. To resolve these problems, the error detection and recovery should be performed in the application.

In some simulations, with several nodes trying to send data messages simultaneously with a transmission range of 4 nodes or higher, the AODV protocol had problems with the “broadcast storm”. The destination node cannot send back the reply message and the route is not established because there are many nodes still receiving and forwarding the request messages.

The flooding technique has a good performance with a time interval between transmissions. The performance of the 802.11 transceiver was better than the performance of the 802.15.4 transceiver because the transmission rate is much higher in 802.11 (1 Mbps) than in 802.15.4 (250 kbps) [98] which means that the probability of collisions and interference is lower.

The analysis of the results has shown the best results for 802.11 transceivers with AODV, 802.11 transceivers with flooding, and 802.15.4 transceivers with flooding. To verify the behavior of these combinations of transceivers and protocols in the limits of the transmission range and length of the network, the next simulations were performed with up to 3000 nodes, up to 15 nodes transmitting, and transmission ranges of 1, 2, 5 and 8 nodes. The simulations were performed with all sensors transmitting almost simultaneously (interval of 1 ms), and with intervals of 5, 10, 15 and 20 seconds. Every simulation included two sequences of transmissions. Each node transmits only one message in each sequence. Therefore, only 20 messages are transmitted in each simulation, 10 messages in each sequence. Table 5.17 shows the results of these simulations.

Table 5.17 - The results of worst case simulations.

Wireless standard	Protocol	Number of nodes	Transmission interval between each sensor (sec)	Number of sensors transmitting	Range (number of nodes at each side)	Transmission rate (kbps)	Route setup (sec)	Transit time (sec)	Number of packets received in 1st sequence	Number of packets received in 2nd sequence
802.11	AODV	2000	20	10	1	1000	16.5	5	10	10
802.11	AODV	3000	20	10	2	1000	11.8	4	10	10
802.11	AODV	2000	0.001	10	5	1000	3.3	2	10	10
802.11	AODV	2000	20	10	5	1000	3.1	1.2	10	10
802.11	AODV	3000	20	10	5	1000	4.4	1.8	9	10
802.11	AODV	2000	0.001	15	8	1000	2	1.3	14	14
802.11	AODV	2000	20	15	8	1000	2	0.8	15	15
802.11	flooding	2000	0.001	10	1	1000	not applicable	5	2	1
802.11	flooding	2000	5	10	1	1000	not applicable	5	10	10
802.11	flooding	3000	5	10	1	1000	not applicable	7.5	10	10
802.11	flooding	2000	0.001	10	5	1000	not applicable	1.38	9	9
802.11	flooding	2000	5	10	5	1000	not applicable	1.43	10	10
802.11	flooding	3000	5	10	5	1000	not applicable	2.11	10	10
802.11	flooding	2000	10	15	8	1000	not applicable	0.9	15	15
802.15.4	flooding	2000	15	10	1	250	not applicable	11.5	10	10
802.15.4	flooding	3000	20	10	1	250	not applicable	17.2	10	10
802.15.4	flooding	2000	0.001	10	5	250	not applicable	2.8	4	5
802.15.4	flooding	2000	5	10	5	250	not applicable	2.9	10	10
802.15.4	flooding	3000	5	10	5	250	not applicable	4.2	10	10

5.5.3 Analysis of the results of network simulations

The results show that 802.11 with AODV is the most efficient protocol in all simulations, even when all the nodes transmit at the same time because there was a loss of only one message in all simulations. On the other hand, the flooding technique works well in almost all simulations, especially with the 802.11 transceiver and an interval of 5 seconds between transmissions. We have simulated the flooding process without the modifications of TTL parameter of NS2 and the results show, as expected, that the flooding process does not depend on this parameter. There is a paper comparing flooding with reactive protocols with up to 200 nodes that states that flooding can be a good alternative for some configurations [99]. The good performance of flooding is due to the absence of traffic routing and the linear topology. The data message is sent without the need to establish a route previously. Besides, the message is routed by the other routing protocols from one node to another node in each hop. On the other hand, the message is routed by the flooding by every node which means that several copies of the message flow through the network. When a message is lost, the copies continue flowing toward the destination node.

The flooding technique has an interesting side effect. A copy of each message flows to every edge of the transmission line. This behavior is very beneficial for the network reliability. The messages must have an alternate path to the computer in the event of failure of several consecutive sensors. The power lines always end in a substation that has a good infrastructure, including communication facilities. The substation may have a backup communication link to establish alternative paths to the computer. Upon arriving at the substation, the copy of the message is routed to the computer through a WAN communication link. In case of power line with branches (Figure 5.16), the flooding process sends a copy of each message to each edge of the line. Thus, at any point of the power line where the message is generated, the process of flooding will deliver a copy of the message to the computer and to the substations at the other ends of the line. In the case, the computer will receive duplicated messages (one of each edge) but it is not a problem because the messages have a sequence number and the duplicate ones will be discarded by the computer after the verification of the sequence number.

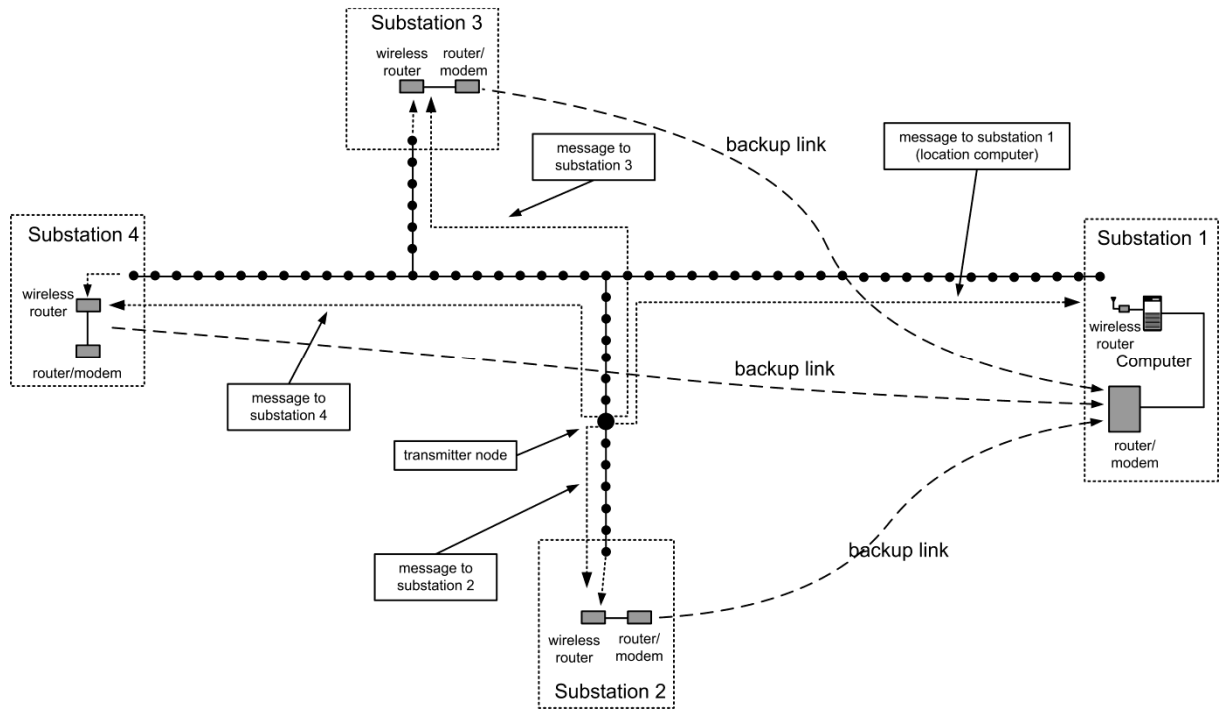


Figure 5.16 - The alternative paths of the network in a power line with branches.

5.5.4 Simulation of a WSN on branched power transmission lines

To evaluate the behavior of the 802.11 transceiver with the flooding mechanism in a WSN on a branched power line, we have simulated the network using parameters to force the operation of the protocol to the upper limits: 3000 nodes, being 2600 nodes in the main line and 200 in each branch; 20 nodes transmitting messages with 200 bytes at intervals of 0.001, 1 and 5 seconds; and ranges of 2, 5 and 10 nodes. The nodes 849, 1500, and 2990 send 20 messages to node 0. The topology is shown in Figure 5.17 and corresponds to a 1040 km line with two branches with 80 km each (considering the average span of 400 m).

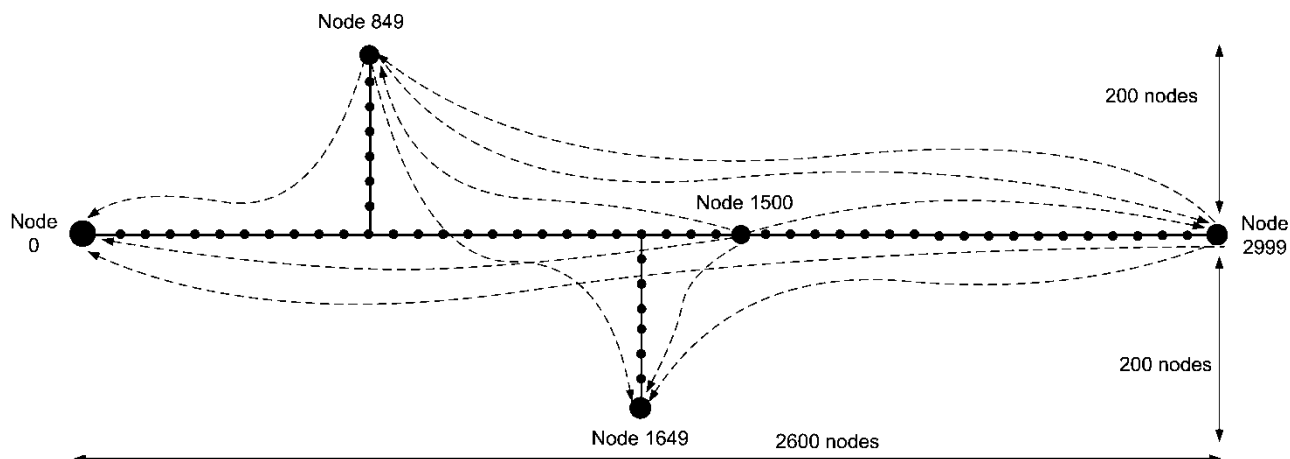


Figure 5.17 - The simulation of branches.

5.5.5 Evaluation of the results of simulations of a WSN on branched OPTLs

The results show that every message sent by node 1500 arrived at node 0 and also at nodes 849, 1649 and 2999. Every message sent by node 849 arrived at node 0 and also at nodes 1649 and 2999. Every message sent by node 2999 arrived at node 0 and also at nodes 849 and 1649. No message was lost and the delay is very small, between 0.2 and 2 seconds. We have simulated with other intervals and ranges to stress the flooding protocol to the limits of operation and the results are shown in Table 5.18.

Table 5.18 - Results of simulations of branches.

Transm. Range (number of nodes at each side)	Interval between transm. of each node (sec)	Delay from node 2999 to node 0 (ms)	Messages received by node 0			Messages received by node 1649			Messages received by node 849		Messages received by node 2999	
			From nodes 2990 to 2999	From node 1481 to 1500	From node 830 to 849	From nodes 2990 to 2999	From node 1481 to 1500	From node 830 to 849	From nodes 2990 to 2999	From node 1481 to 1500	From node 1481 to 1500	From node 830 to 849
2	5	4.1	20	20	20	20	20	20	20	20	20	20
5	0.001	1.8	18	15	16	18	17	16	18	15	15	15
5	1	1.8	20	20	20	20	20	20	20	20	20	20
10	0.001	0.9	18	20	19	18	20	19	18	20	20	19
10	1	0.9	20	20	20	20	20	20	20	20	20	20

The results confirmed the behavior of the flooding protocol even in the worst simulation conditions. Its simplicity, easy implementation, good performance, and facility to create alternative paths, turn this protocol the preferred choice for routing in the linear topology.

The transit time of messages is important to allow the use of super capacitors instead of batteries. We can observe in Table 5.18 that, using the technique of flooding across a branched network of 3000 sensors, the transit time of a message from end to end of the network is 1.8 seconds. Besides, with an interval of 1 second between transmissions, all messages get to the destination in less than 22 seconds. Therefore, transmitting at every second, 20 sensors can send the messages and receive the acknowledgements in 44 seconds. The smaller is this time the lower can be the value of the super capacitor. Super capacitors with lower capacitances are cheaper and the cost of super capacitors is significant in the total cost of the sensor. If all the sensors transmit in 44 seconds, the value of capacitance of 5.5 F in the circuit of power supply can be lowered to 1 F. This capacitance gives up to 47 seconds of operation to each sensor using the 802.11 transceivers. The flooding protocol has an advantage over AODV because the data message is sent immediately, while with the AODV the router must be established first.

The results show that the following combinations of transceivers and routing protocols provide the best performance for linear network topology of power transmission lines:

- Transceiver IEEE 802.11 (RTS/CTS disabled), with flooding protocol and transmission interval of 1 second.
- Transceiver IEEE 802.15.4 (association disabled) with flooding protocol and transmission interval of 5 seconds.
- Transceiver IEEE 802.11 (RTS/CTS disabled) with AODV and transmission interval of 5 seconds.

Any of these options will work well in long transmission lines with thousands of sensors and transmission ranges from 1 to 10 sensors.

5.6 Transmission range calculations and measurements

We have calculated the transmission range of for the most common frequencies used on wireless networks: 915 MHz, 2.4 GHz, and 5.8 GHz. Table 5.19 shows the calculated range for typical values of transmitter power and receiver sensibility for sensors installed on towers

with 20 meters of height. The value of antenna gain is 2.15 dBi which is the gain of a simple dipole antenna. It was included 10 dB of gain margin to account for cable and connector losses, and signal to noise ratio.

Table 5.19 - Transmission range calculation.

Freq. (MHz)	P_{Tx} (dBm)	G_{Tx} (dBi)	G_{Rx} (dBi)	Sensit. (dBm)	Tower height (m)	Gain Margin (dB)	d (m) Friis	d (m) two-ray	dc (m)
915	24	2.15	2.15	-92	20	10	8525	11443	15331
2400	24	2.15	2.15	-92	20	10	3250	11443	40212
5150	24	2.15	2.15	-92	20	10	1515	11443	86289

Table 5.20 shows the range for each frequency of Table 5.19 using a collinear antenna with gain of 5.8 dBi.

Table 5.20 - Transmission range calculation with 5.8 dBi antennas.

Freq. (MHz)	P_{Tx} (dBm)	G_{Tx} (dBi)	G_{Rx} (dBi)	Sensit. (dBm)	Tower height (m)	Gain Margin (dB)	d (m) Friis	d (m) two-ray	dc (m)
915	24	5.80	5.80	-92	20	10	19756	17419	15331
2400	24	5.80	5.80	-92	20	10	7532	17419	40212
5150	24	5.80	5.80	-92	20	10	3510	17419	86289

Because of the height of towers, in all frequencies the critical distance is much greater than the range calculated using the Friis model. Therefore, the range is calculated by the Friis model.

In the CEMIG power transmission system, the largest span has a length of 1250 m. To have redundancy in case of a failure in one sensor, each sensor should be able to communicate with two neighbors at each side of the tower (Figure 5.18). Therefore, the radio transceiver must have a range of 2500m or more. Considering the values of Table 5.19, the radio transceiver must operate at 915 MHz or 2.4 GHz. With 5.8 dBi antennas it is possible to use the 5.15 GHz band (Table 5.20).

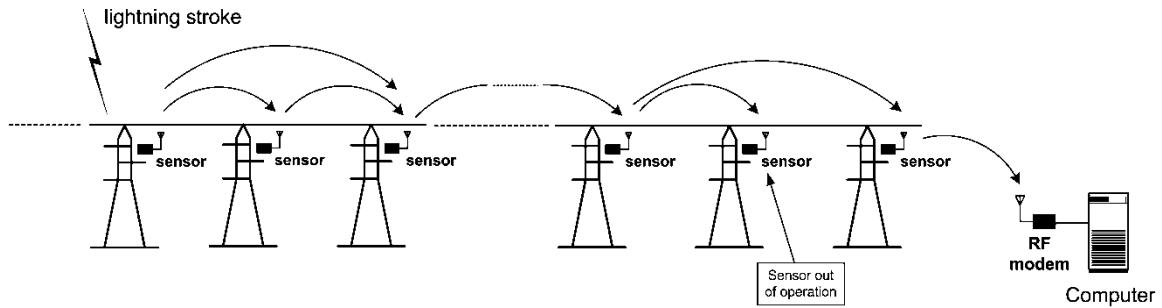


Figure 5.18 - Communication in case of a failure in one sensor.

Table 5.21 shows the range calculation for the components listed in Table 4.1.

Table 5.21 - Range calculation for the components of Table 4.1.

Component	Freq. (MHz)	P_{Tx} (dBm)	G_{Tx} (dBi)	G_{Rx} (dBi)	Sensit. (dBm)	Tower height (m)	Gain Margin (dB)	d (m) Friis
AT86RF212	915	10	2.15	2.15	-100	20	10	4273
ZigBit 900	915	10	2.15	2.15	-100	20	10	4273
LPR2400ER	2400	17	2.15	2.15	-95	20	10	2051
ZFSM101	2400	20	2.15	2.15	-92	20	10	2051
AL2230S	2400	20	2.15	2.15	-92	20	10	2051
MAX2820-MAX2242	2400	22.5	2.15	2.15	-97	20	10	4863
Q802XKG	2400	18	2.15	2.15	-94	20	10	2051
R52H	2400	24	2.15	2.15	-92	20	10	3250

Meshnetics specification [73] reports that the ZigBit900 transceivers with 10 dBm power output, operating at 20 kbps with -110 dBm sensitivity, have an outdoor line-of-sight range of up to 6 km with a 3 dBi antenna. The reported range is compatible with the range calculated in Table 5.21 for the ZigBit900 with (sensitivity of -100 dBm for the data rate of 250 kbps).

The Brazilian legislation, through the resolution number 365/2004 of National Telecommunications Agency (ANATEL), limits to 400 mw the transmit power of equipments operating in the 2.4 GHz band and limits to 250 mw the transmit power of equipments operating in the 915 MHz band in cities with a population above 500,000 [100].

5.6.1 Field measurements and path loss budget

To evaluate the range of a real transceiver we have done field measurements of the transmission range between two 802.11b/g wireless routers. The equipments used were two Linksys/Cisco WRT54GL 802.11b/g router with the original firmware replaced by the DD-

WRT firmware to allow full control over the power transmitted and information about the received signal. The measurements were done over a lagoon surface with LOS path between the two equipments. The longest LOS path over the lagoon was 2420 m. The two antennas were placed at 4 m and 6 m above the surface (5 m at the middle of the path). Figure 5.19 shows the positions of antennas in the field measurements.

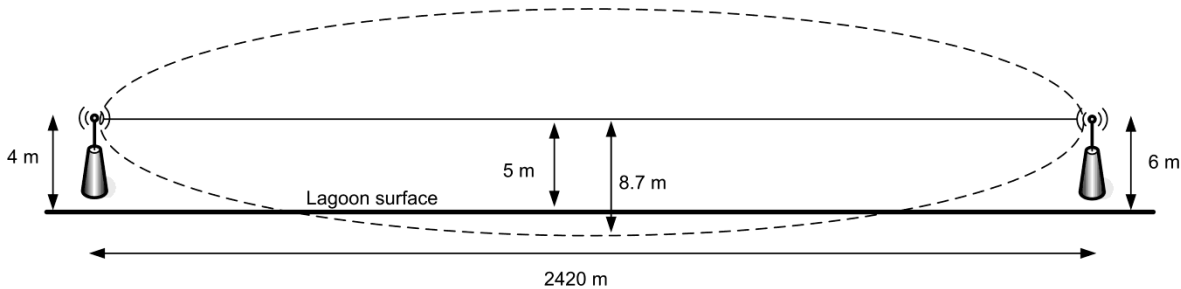


Figure 5.19 - The position of antennas in the field measurements.

The transmitting power was programmed to 250 mW (24 dBm), the receiver sensitivity is -94 dBm for 1 Mbps of data rate (802.11b), and the antennas used were the 2.15 dBi dipole. The routers established a communication link over a 2420 m LOS path and the tools of the router firmware were used to retrieve information about the received signal. The power at the receiver was -84 dBm with a Signal-to-Noise Ratio (SNR) of 8 dB. Using a computer to send IP echo request packets and receive the corresponding echo reply packets, 600 requests were sent and 600 replies were received in a 10 minutes test (no packet lost). To compare the value of power received in the measurements and the value calculated, we have to compute the Fresnel zone to calculate if there was any obstruction. Despite the surface of the lagoon do not have any obstacle in the path, the surface itself can be an obstacle because of the low height of the antennas relative to the surface. The Radius of first Fresnel zone in the middle of the path and the ratio h/F_1 are:

$$F_1 = [(300 \cdot 2420) / (4 \cdot 2400)]^{1/2} = 8.7 \text{ m} \tag{5.1}$$

$$h/F_1 = (8.7 - 5) / 8.7 = 0.3 \tag{5.2}$$

For the h/F_1 ratio equal to 0.3, the attenuation caused by the obstruction is 2 dB [55]. Table 5.22 shows the calculated received power including the Fresnel obstruction loss and 1 dB for the connector losses:

Table 5.22 - Calculation of received power with the parameters of the field measurements.

Freq. (MHz)	P _{Tx} (dBm)	G _{Tx} (dBi)	G _{Rx} (dBi)	Freq. (MHz)	obstruction loss (dB)	connector losses (dB)	P _{Rx} (Friis) (dBm)	h _{Tx} (m)	h _{Rx} (m)	P _{Rx} (2-ray) (dBm)	dc (m)
2412	2420	2.15	2.15	24	2	1	-82.5	4.0	6.0	-82.2	2425

The value calculated for the power received (-82.5 dBm) is very close to the measured value (-84 dBm). The distance of 2420 m is very close to the critical distance dc (2425 m) and the values calculated by Friis model and 2-ray ground model are nearly equal.

With the hardware of these routers, even in case of large consecutive spans with more than 1000 m, the sensors can reach two neighbors at each side. To reach two sensors at each side, the next towers are obstacles in the first Fresnel zone (Figure 5.20) to the propagation signal of the transmit sensor.

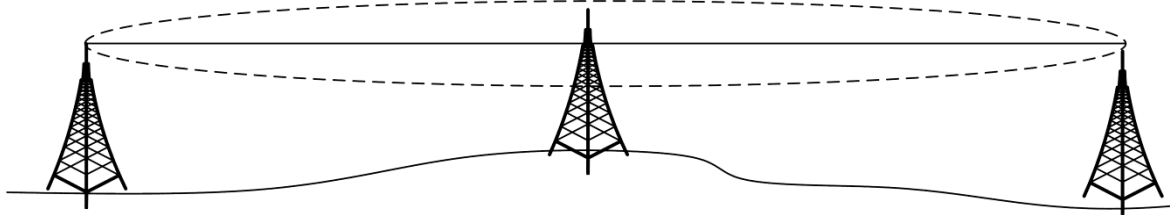


Figure 5.20 - The tower as an obstacle inside the Fresnel zone.

If the towers are at same surface level, the h/F_1 ratio is one. In the worst case, the tower in the middle of the path is at a higher surface level and obstructs completely the Fresnel zone ($h/F_1 \leq -1$). In case of a solid obstacle like a hill, the attenuation is 16 dB for $h/F_1 = -1$. Nevertheless, the tower is not a solid obstacle and the tower lattice is much larger than the wavelength of the signal. Therefore, the attenuation is much smaller. The antennas used in the test were the low gain dipoles. With collinear antennas of 5.8 dBi it is possible to add 7.3 dB to the path loss budget and increase the range of the radio transceivers or compensate for the loss added by the towers in the Fresnel zone. Using antennas with 5.8 dBi, Table 5.23 shows that it is possible to add 4 dB of obstruction loss and still have a range of 3500 m with the same received power level of the Table 5.22.

Table 5.23 - Path loss budget with 5.8 dBi antennas.

Freq. (MHz)	P _{Tx} (dBm)	G _{Tx} (dBi)	G _{Rx} (dBi)	Freq. (MHz)	obstruction loss (dB)	connector losses (dB)	P _{Rx} (Friis) (dBm)
2412	3500	5.8	5.8	24	6	1	-82.4

5.6.2 Evaluation of the results of calculations and measurements

The calculations and field measurements show that it is feasible to use both 802.11 and 802.15.4 IEEE wireless standard in the sensor transceiver and have a good transmission range to guarantee a reliable operation of the network even in case of failure of sensors. Even in case of adjacent spans with lengths of 1200 m, the transmission range is enough to reach at least two sensors at each side of the transmission line.

Chapter 6

Conclusions and future work

6.1 Conclusions

The principles of the system have been demonstrated and verified using simulations. The technical feasibility for the use of wireless sensors for detection and location of direct strokes and short circuits in overhead power transmission lines will be verified by a research project to be submitted to the research funding agencies. Simulations of the transmission lines showed that the measurements of transient currents in the towers allow the detection of the impulsive transients generated by direct lightning strikes or short-circuits. The simulations also show that these transients are higher in the towers closer to the location of the event which allows the location of direct strokes and faults with good accuracy. The measurement of these transients can be made using devices with proven efficiency for this type of measurement, the Rogowski coils. The network simulations, the theoretical calculations and the field measurements of the transmission range, show that the sensors can send the data reliably using a wireless network to be processed at one end of a transmission line.

The work presented a solution to the problem of power supplying to the sensors and its periodic maintenance, which has great impact on the economic feasibility of the system. The energy extraction from shield wires and the use of super capacitors eliminate the need for periodic maintenance. The work demonstrate through simulations, field measurements and the design of a power supply for the sensors, the feasibility of this solution that can also be used in other types of equipments installed in transmission lines, as well as wireless sensors.

The work is an important contribution to the management of energy systems because there is not a system for detection and location of direct strokes in power transmission lines with the features of the proposed system. Besides, the use of the same system for locating short-circuits with good accuracy, in a large range of fault resistances, increases the importance of the work for power transmission systems. Another important feature is the easy

installation of the sensors, which can be done with the lines in operation and no need for special procedures for protection, in addition to the normal security procedures.

Despite the great number of sensors necessary to a long transmission line, the cost of the proposed system is not high compared to benefits to the management of the energy transmission system. The use of components of high availability and the wide variety of manufacturers allow the design of low-cost sensors. The solution of extracting power from shield wires eliminates periodic maintenance that would represent high costs to maintain photovoltaic cells clean and to replace thousands of rechargeable batteries at their end of life, most often in places difficult to access. The facility to warn for the need of preventive maintenance in cases of direct strokes, and the streamlining of corrective maintenance of transmission lines, represent an important reduction in revenue losses by reducing the time of outage of the lines. The cost of the system can be quickly amortized with the reduction of revenue losses. Furthermore, the existence of a system using wireless sensors to monitor power transmission lines under research in an institution of great relevance (EPRI), demonstrates that these institution believes that the system can be economically viable.

6.2 Future work

From the results presented in this thesis, there are some work that can be carried out:

- a) Construction of a prototype of the power supply to extract energy from the shield wire.
- b) Construction of low cost prototypes of the sensors using 802.11 hardware modules;
- c) Development of the sensor firmware using the open source firmware or commercial development tools;
- d) Development of the location processing software;
- e) Product engineering design of the sensor using techniques of electromagnetic compatibility and of resistance to extreme environmental conditions.

With these future developments it is possible to perform tests in a real transmission line which would be the first step in the construction of an operational location system.

Bibliography

- [1] A. M. Carvalho, M. S. Abreu, A. Cazetta Filho, A. C. Carvalho, L. C. L. Cherchiglia, J. H. Diniz, Tecnologias para Análise e Melhoria do Desempenho de Instalações de Transmissão Frente a Descargas Atmosféricas, XV SNPTEE - Seminário Nacional de Produção e Transmissão de Energia Elétrica (1999), Foz do Iguaçu, Paraná, Brazil, 1999.
- [2] Zhaoyu Qin, Zhaogu Cheng, Zhiping Zhang, Jianqiang Zhu, and Feng Li, New method for lightning location using optical ground wire, Chinese Optics Letters Vol. 4, No. 12, December 10, 2006.
- [3] Noraliza Hamzah, Azah Mohamed, A New Method For Locating The Source Of Lightning Transients, First International Power and Energy Conference PECon 2006, Putrajaya, Malaysia, November 28-29, 2006.
- [4] M. Bernardi, A. Borghetti, C. A. Nucci, F. Napolitano, M. Paolone, F. Rachidi, R. Vitale, K. Yamabuki, Lightning-Related Faults in Power Distribution Networks, PowerTech 2007.
- [5] J. G. Kappenman, T. W. Guttormson, High-Precision Location of Lightning-Caused Distribution Faults, Transmission and Distribution Conference and Exposition, 2001 IEEE/PES Transmission and Distribution Conference, pp. 1036-1040, 2001.
- [6] S. D. Kim, M. M. Morcos, An improved method for classifying power quality disturbances, Electric Power Components and Systems, 32(4), 407–420, 2004.
- [7] S. Visacro, Direct Strokes to Transmission Lines: Considerations on the Mechanisms of Overvoltage Formation and their Influence on the Lightning Performance of Lines, Journal of Lightning Research, volume 1, pages 60-68, 2007.
- [8] Weber Melo de Sousa, Carlos Alberto B. Costa, Izonel H. Pereira Junior, Clever Sebastião P. Filho, Sistema de Localização Automática de Faltas em Linhas de Transmissão Utilizando Dados de Dois Terminais - Experiência da CEMIG, XVIII SNPTEE - Seminário Nacional de Produção e Transmissão de Energia Elétrica, Curitiba, Brasil, Outubro de 2005.
- [9] S. Visacro, Descargas Atmosféricas - Uma Abordagem de Engenharia, Artliber, 2005.
- [10] O. Pinto Jr., I. R. A. C. Pinto, Tempestades e relâmpagos no Brasil, São José dos Campos: INPE, 2000.

- [11] R. B. Anderson, A. J. Eriksson, A summary of lightning parameters for engineering application, Proceedings of International Conference on Large High Voltage Electric Systems, 1980.
- [12] M. A. O. Schroeder, Modelo eletromagnético para descontaminação de ondas de corrente de descargas atmosféricas: aplicação às medições da estação do Morro do Cachimbo, Tese (Doutorado) - Programa de Pós-Graduação em Engenharia Elétrica, Universidade Federal de Minas Gerais, Belo Horizonte, 2001.
- [13] Antônia Navarro Gómez, Uma Contribuição Para A Medição das Componentes De Correntes de Descargas Atmosféricas Através De Transdutores Resistivos, Programa de Pós-Graduação em Engenharia Elétrica, Universidade Federal de Minas Gerais, Belo Horizonte, 2007.
- [14] Electric Power Research Institute (EPRI), Handbook for Improving Overhead Transmission Line Lightning Performance, Palo Alto, CA, 2004.
- [15] G. Diendorfer, Lightning location systems (LLS), IX International Symposium on Lightning Protection, Foz do Iguaçu, Brasil, November 2007.
- [16] IEEE Power Engineering Society, IEEE Guide for Determining Fault Location on AC Transmission and Distribution Lines, June 2005.
- [17] Arlan Luiz Bettiol, Ricardo Lira, Ildemar Cassana, Decker Sérgio, Luiz Zimath, Localização de Falhas em Linhas de Transmissão Usando Medição Fasorial Sincronizada, X STPC Seminário Técnico de Proteção e Controle, Recife, Brasil, Outubro de 2010.
- [18] Sergio Luiz Zimath, Marco Antonio Ramos, Jayme Silva Filho, Joaquim Moutinho Beck, Nei Mueller, Traveling Wave-Based Fault Location Experiences, 2010 63rd Annual Conference for Protective Relay Engineers, College Station, Texas, 2010.
- [19] ISA - Istrumentazioni Sistemi Automatici, TDU 100 Traveling Wave Data Acquisition Unit User Manual, available on-line (www.isatest.com), Italy.
- [20] N.P. Subramaniam¹, K. Bhoopathy Baga, Analysis of High Impedance Transients and Improved Data Compression Using Wavelet Transform, Serbian Journal of Electrical Engineering, Vol. 3, No. 1, 19 - 31, June 2006.

- [21] T. Yamada, A. Mochizuki, J. Sawada, E. Zaima, T.Kawamura, A. Ametani, M. Ishii and S. Kato, Experimental Evaluation of a UHV Tower Model for Lightning Surge Analysis, IEEE Trans. on Power Delivery, Vol.10, No.1, pp. 393-402, 1995.
- [22] W.A. Chisholm and Y.L. Chow and K.D. Srivastava, Lightning Surge Response of Transmission Towers, IEEE Trans. on Power Apparatus and Systems, Vol. PAS-102, No.9, pp. 3232-3242, 1983.
- [23] H. Motoyama and H. Matsubara, Analytical and Experimental Study on Surge Response of Transmission Tower, IEEE Trans. on Power Delivery, Vol.15, No.2, pp. 812- 4819, 2000.
- [24] M. A. Sargent, Tower surge impedance, IEEE Transactions on power apparatus and system, vol. 88, No. 5, pp. 680-687, 1969.
- [25] W. A. Chisholm, Y. L. Chow and K. D. Srivastava, Travel Time of Transmission Towers, IEEE Transactions on Power Apparatus and Systems, PAS-104, (10), pp. 2292-2928, 1985.
- [26] IEEE Working Group Report, Estimating Lightning Performance of Transmission Lines II Updates to Analytical Models, IEEE Transactions on Power Delivery, Vol. 8, No. 3, July 1993.
- [27] Canadian/ American EMTP User Group, Alternative Transients Program (ATP) Rule Book, 1987-1998.
- [28] H. W. Dommel, Electromagnetic Transients Program reference manual (EMTP Theory Book), Bonneville Power Administration, Oregon, USA, August 1986.
- [29] C. Chunkull, K. Tunlasakun, S. Nomnamsapl and N. Chayawattol, A study of the mutual coupling between a three-phase power line 115 kV and a parallel telephone line by using ATP/EMTP: case study distribution line in thailand alarm, SICE-ICASE International Joint Conference 2006 in Bexco, Busan, Korea, Oct. 18-21, 2006.
- [30] B. Chuco Paucar, J.L. Roel Ortiz, J. O. Pereira Pinto, P. I. Koltermann, Induced voltage on gas pipeline with angle between a transmission line, Power Tech, IEEE Lausanne, Swiss, 2007.

- [31] J. F. Arcega, J. A. Artero, Current sensor based on Rogowski coil, ICREPQ 2004 - International Conference on Renewable Energies and Power Quality, Barcelona, Spain, March 2004.
- [32] Andrew S. Tanenbaum, David J. Wetherall, Computer Networks (5th Edition), Prentice Hall, 2010.
- [33] ISO/IEC JTC1, Information Technology - Open System Interconnection - OSI Reference Model: Part 1 - Basic Reference Model, ISO/IEC 7498-1, 1994.
- [34] Netbios documentation available on-line (<http://msdn.microsoft.com/en-us/library/>).
- [35] IEEE Standard for Information technology, IEEE Std 802.2: Logical Link Control, IEEE Computer Society; 1998.
- [36] IEEE Standard for Information technology, IEEE Std 802.3: Carrier Sense Multiple Access with Collision Detection (CSMA/CD) Access Method and Physical Layer Specifications, IEEE Computer Society; 2008.
- [37] IEEE Standard for Information technology, IEEE Std 802.11: Wireless LAN Medium Access Control (MAC) and Physical Layer (PHY) Specifications, IEEE Computer Society, 2001.
- [38] IEEE Standard for Information technology; IEEE Std 802.15.4 Wireless Medium Access Control (MAC) and Physical Layer (PHY) Specifications for Low-Rate Wireless Personal Area Networks (WPANs), IEEE Computer Society, 2006.
- [39] IEEE Standard for Information technology, IEEE Std 802.16: Air Interface for Broadband Wireless Access Systems, IEEE Computer Society, 2009.
- [40] IEEE Standard for Information technology, IEEE Std 802.15.1: Wireless medium access control (MAC) and physical layer (PHY) specifications for wireless personal area networks (WPANs), IEEE Computer Society, 2005.
- [41] IEEE Standard for Information technology, IEEE Std 802.15.3: Wireless Medium Access Control (MAC) and Physical Layer (PHY) Specifications for High Rate Wireless Personal Area Networks (WPANs), IEEE Computer Society, 2003.
- [42] ZigBee Standards Organization, ZIGBEE Specification, January 17, 2008.

- [43] Mustafa Ergen, IEEE 802.11 Tutorial, Department of Electrical Engineering and Computer Science University of California Berkeley, June 2002 (www.eecs.berkeley.edu/ergen/docs/ieee.pdf).
- [44] IEEE Standard for Information technology, IEEE Std 802.11: Wireless LAN Medium Access Control (MAC) and Physical Layer (PHY) Specifications - High-speed Physical Layer in the 5 GHz Band, IEEE Computer Society, 2003.
- [45] IEEE Standard for Information technology, IEEE Std 802.11: Wireless LAN Medium Access Control (MAC) and Physical Layer (PHY) Specifications - Amendment 2: Higher-speed Physical Layer (PHY) extension in the 2.4 GHz band, IEEE Computer Society, 2001.
- [46] IEEE Standard for Information technology, IEEE Std 802.11: Wireless LAN Medium Access Control (MAC) and Physical Layer (PHY) Specifications - Amendment 4: Further Higher Data Rate Extension in the 2.4 GHz Band, IEEE Computer Society, 2003.
- [47] Available on-line (http://en.wikipedia.org/wiki/IEEE_802.11).
- [48] J. A. Gutierrez, IEEE Std. 802.15.4 Enabling Pervasive Wireless Sensor Networks, Eaton Corp. Innovation Center, 2005.
- [49] Luiz Fernando Gomes Soares, Guido Lemos, Sérgio Kolcher, Redes de Computadores: das LANs, MANs e WANs às Redes ATM, 7ª edição, Ed. Campus, 1995.
- [50] Elizabeth M. Royer, Chai-Keong Toh, A Review of Current Routing Protocols for Ad Hoc Mobile Wireless Networks, IEEE Personal Communications, April 1999.
- [51] Guido R. Hiertz, Rwth Aachen, Sebastian Max, Rakesh Taori, Javier Cardona, Lars Berlemann, Bernhard Walke, IEEE 802.11S: The Wlan Mesh Standard, IEEE Wireless Communications, February 2010.
- [52] Bilel NEFZI, Ye-Qiong Song, Performance Analysis and Improvement of ZigBee Routing Protocol, 7th IFAC International Conference on Fieldbuses & Networks in Industrial & Embedded Systems, Toulouse, France, 2007.
- [53] H. T. Friis, A Note on a Simple Transmission Formula, Proc. IRE, Vol 34, no 5, pp. 254-256, May 1946.
- [54] Yi Huang, Kevin Boyle, Antennas: from Theory to Practice, John Wiley and Sons, 2008.

- [55] Roger L. Freeman, Radio System Design for Telecommunications, Third Edition, John Wiley and Sons, 2007.
- [56] F. Nadeem, E. Leitgeb, O. Koudelka, T. Javornic, G. Kandus, Comparing the rain effects on hybrid network using optical wireless and GHz links. 2008 International Conference on Emerging Technologies IEEE-ICET 2008 Rawalpindi, Pakistan, 18-19 October, 2008.
- [57] T. Ogushi, Electromagnetic Wave Propagation and Scattering in Rain and Other Hydrometeors, Proceedings of the IEEE, Vol. 71, No. 9, September 1983.
- [58] Cisco Systems, Antenna Patterns and Their Meaning, Cisco white paper (www.cisco.com).
- [59] John D. Kraus and Ronald J. Marhefka, Antennas for all Applications, McGraw-Hill, 2002.
- [60] RFI Antennas, Vertical Collinear Antenna datasheet, (www.rfiantennas.com).
- [61] Electric Power Research Institute (EPRI), Sensor Technologies for a Smart Transmission System, December 2009.
- [62] D. T. Silva, J. L. Silvino, J. C. D. de Melo, Detection and location of direct lightning strokes to overhead power transmission lines by measuring currents from shield wires, 9th IEEE/IAS International Conference on Industry Applications, São Paulo, SP, Brazil, November 2010.
- [63] E. F. Koncel, Potential of a Transmission-Line Tower Top when Struck by Lightning, AIEE Winter General Meeting (1956), New York, N. Y., January 30-February 3, 1956.
- [64] Enrique Altman, Fabiano Magrin, Kennio Brito, Curto-Circuito de Altíssima Resistência de Falta em Linha de Transmissão de 525 Kv - um Relato de Caso, IX Seminário Técnico de Proteção e Controle, Belo Horizonte, Minas Gerais, Brasil, Junho de 2008.
- [65] Genscape Inc., Wireless Sensor Network for Electric Transmission Line Monitoring, available on-line (<http://www.genscape.com>).
- [66] D. T. Silva, J. L. Silvino, J. O. S. Paulino, J. C. D. de Melo, Fault Location on Overhead Power Transmission Lines by Measuring Currents from Shield Wires, 9th IEEE/IAS International Conference on Industry Applications, São Paulo, SP, Brazil, November 2010.

- [67] Akihiro Ametani, Yuji Hosakawa; EMTP simulations and theoretical formulation of induced voltages to pipelines from power lines; IPST Conference 2007; Lyon, France, 2007.
- [68] José Osvaldo S. Paulino, Influências de Curtos-circuitos nas Redes de Distribuição sobre Redes Telefônicas em Uso Mútuo de Posteação, Tese de Mestrado, Departamento de Engenharia Elétrica, Universidade Federal de Minas Gerais, Dezembro de 1987.
- [69] H. W. Dommel, Electromagnetic and electrostatic effects of transmission lines practical problems, safeguards and methods of calculation, IEEE Transactions on Power Apparatus and Systems, Volume PAS-93, Issue 3, pp:892 - 904, May 1974.
- [70] G. M. Amer, Novel technique to calculate the effect of electromagnetic field of HVTL on the metallic pipelines by using EMTP program, COMPEL: The International Journal for Computation and Mathematics in Electrical and Electronic Engineering Vol. 26 Issue 1, 2007.
- [71] H. Johnson and M. Graham, High Speed Digital Design: A Handbook of Black Magic, Prentice-Hall, Upper Saddle River, NJ, 1993.
- [72] Changhua He, John C Mitchell, Security Analysis and Improvements for IEEE 802.11i, The 12th Annual Network and Distributed System Security Symposium, San Diego, California.
- [73] Meshnetics, ZigBit 900 OEM Modules Ultra-Compact 868MHz/915MHz IEEE 802.15.4/ZigBee Modules for Wireless Networking Applications, Product Datasheet, March 2008 (www.meshnetics.com).
- [74] Iván Corredor Pérez, Ana-B García, José-F Martínez, Pedro López Bustos, Wireless Sensor Network-based system for measuring and monitoring road traffic, COLLECTeR Iberoamérica 2008, Madrid, Spain, 2008.
- [75] International Telecommunication Union, ITU-T Recommendation Z.120 - Message Sequence Chart (MSC), Apr 2004.
- [76] John Gibson, Geoffrey G. Xie, Yang Xiao, Performance Limits of Fair-Access in Sensor Networks with Linear and Selected Grid Topologies, In proceedings of GLOBECOM Ad Hoc and Sensor Networking Symposium, Washington DC, November 2007

- [77] The VINT Project, The NS Manual (formerly NS Notes and Documentation), UC Berkeley, LBL, USC/ISI, Xerox PARC, May 9, 2010 (<http://www.isi.edu/nsnam/ns/ns-documentation>).
- [78] IETF, RFC2501: Mobile Ad hoc Networking (MANET): Routing Protocol Performance Issues and Evaluation Considerations, January 2009.
- [79] Michel Burton, Channel Overlap Calculations for 802.11 Networks, Cirond Technologies Inc., available on-line (<http://www.eetimes.com/electrical-engineers/education-training/tech-papers/secure/cirond-technologies/4134127>).
- [80] OpenWrt documentation available on-line (www.openwrt.org).
- [81] Data sheets available on-line (www.broadcom.com).
- [82] Data sheets available on-line (www.atmel.com).
- [83] Data sheets available on-line (www.mikrotik.com).
- [84] Data sheets available on-line (www.ralinktech.com).
- [85] Data sheets available on-line (www.atheros.com).
- [86] D. T. Silva, J. L. Silvino, J. C. D. de Melo, Power harvesting from shield wire for monitoring apparatus on overhead transmission lines, 9th IEEE/IAS International Conference on Industry Applications, São Paulo, SP, Brazil, November 2010.
- [87] R. Kumar, M. Suresh, J. Nagaraju, Solar Array Capacitance on the Performance of Switching Shunt Voltage Regulator, IEEE Transactions on Power Electronics, Vol. 21, No. 2, March 2006.
- [88] Flex-Core Morlan & Associates, Inc., Catalog No. 2088 - Current & Potential Transformers, Transducers and Accessories, (www.flex-core.com).
- [89] Data sheets available on-line (www.maxim.com).
- [90] Data sheets on-line (www.microchip.com).
- [91] L. Prikler, H. K. Høidalen, ATPDraw version 3.5 for Windows 9x/NT/2000/XP User's Manual, Aug. 2002.
- [92] CIGRÉ Work Group 33-01, Guide to Procedures for Estimating the Lightning Performance of Transmission Lines, Cigré Monograph No. 63, October 1991.

- [93] R. Folkers, Determine current transformer suitability using EMTP models, available at Schweitzer Engineering Laboratories Web Site (www.selinc.com).
- [94] P. Chen, P. Ahammad, C. Boyer, S. Huang, L. Lin, E. Lobaton, M. Meingast, S. Oh, S. Wang, P. Yan, A. Yang, C. Yeo, L. Chang, D. Tygar, S. Sastry,,: Citric: A Low-Bandwidth Wireless Camera Network Platform, 2nd ACM/IEEE International Conference on Distributed Smart Cameras (ICDSC-08), Stanford, CA, USA, September 2008.
- [95] Available on-line (<http://www.loria.fr/~nefzi/downloads.html>).
- [96] Available on-line (masimum.inf.um.es/?Software:UM-OLSR).
- [97] Kaixin Xu, Mario Gerla, Sang Bae, How Effective is the IEEE 802.11 RTS/CTS Handshake in Ad Hoc Networks?, IEEE Globecom 2002, Taiwan, November 2002.
- [98] A. Ahmad, A. Riedl, Channel Access Comparison of IEEE 802.11-2007 and IEEE 802.15.4-2006, 2010 Seventh International Conference on Information Technology, IEEE Computer Society, 2010.
- [99] Anne Saaranen Carlos, Pomalaza-Ráez, Comparison of Reactive Routing and Flooding in Wireless Sensor Networks, Proceedings of The Nordic Radio Symposium, Oulu, Finland, 2004.
- [100] Agência Nacional de Telecomunicações (ANATEL), Resolução No 365 - Regulamento Sobre Equipamentos de Radiocomunicação de Radiação Restrita, 10 de Maio de 2004.
- [101] Vladimir V. Terzija, Djordje M. Dobrijevic, Short-circuit Studies in Transmission Networks Using Improved Fault Model, PowerTech 2007, Lausanne, Switzerland, 2007.
- [102] S. Visacro, Aterramentos elétricos: conceitos básicos, técnicas de medição e instrumentação, filosofias de aterramento, 2nd ed. São Paulo, Brazil, ArtLiber Edit., 2002.
- [103] S. Visacro, A Comprehensive Approach to the Grounding Response to Lightning Currents, IEEE Transactions on Power Delivery, Vol. 22, No. 1, pp. 381-386, January 2007.
- [104] A. Ametani, T. Kawamura, A Method of a Lightning Surge Analysis Recommended in Japan Using EMTP, IEEE Transactions On Power Delivery, Vol. 20, No. 2, pp. 867-875, April 2005.

Appendix A

The parameters of the fault simulation

Figure A.1 shows the dimensions of the tower modeled in the simulations and the position of each cable. Each tower is represented as a transmission line with surge impedance of 150Ω , calculated using the conical shape method [25] (35 m high and square base with 8 m of side) and the propagation velocity in the towers is 2.5×10^8 m/s [25]. The phase cables and ground wires are modeled by the Line/Cable objects (LCC) of ATPDraw program and the soil resistivity is $500 \Omega \cdot \text{m}$, which a reasonable value for the high resistivity soil in Brazil. The impedances of the supply network, including the short-circuit reactance of the transformer bank, are included in the simulations.

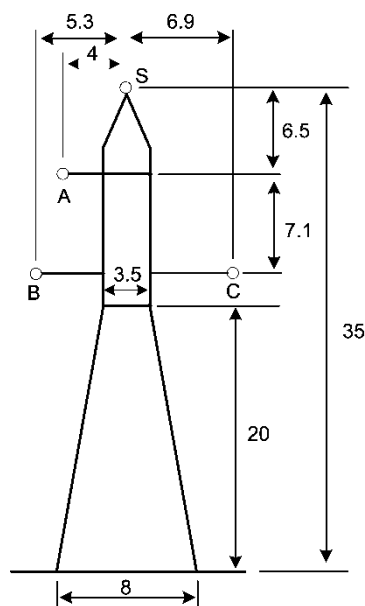


Figure A 1 - Tower dimensions (m) and the positions of the phase cables (A, B, and C) and the shield wire (S) (m).

The simulated homogeneous power transmission line has 11 towers spaced 500 m apart (5 km transmission line) plus a 50 km LCC section at each end as line terminations (total length of 105 km). The tower grounding resistances are 20Ω . The fault is simulated at 52.5 km from the source.

The simulated non-homogeneous power transmission line has 19 towers (5 km transmission line) plus a 50 km LCC section at each end as line terminations (total length of 105 km). Most of the span lengths are 300 m but the spans lengths between the 10th and 15th towers are 100 m, 300 m, 200 m, 400 m and 100 m, respectively. The tower grounding resistance for most of the towers is 20 Ω, except the resistances of 10th and 12th towers with 40 Ω and 10 Ω, respectively. The faults are simulated at 54 km from the source between the 10th and 11th towers.

All faults occur 6 ms after the beginning of a voltage cycle of phase A and the current in each phase is 600 A_{rms} (Figure A 1).

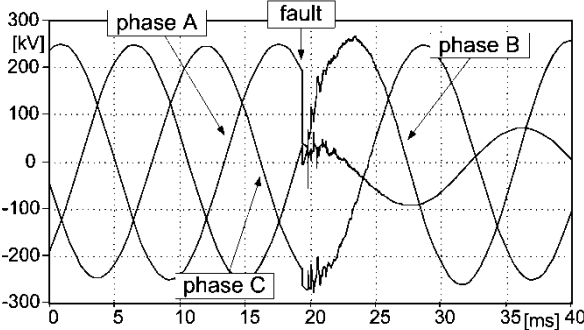


Figure A 2 - The instant of the fault within the voltage cycle.

The fault impedances of the phase-to-phase and phase-to-tower short-circuits are resistive. The fault impedances of the line-to-ground faults consist of a resistive component (value indicated in the tables) in series with an inductive component of 0.1 mH. This inductance is included to take into account the inductance of path of the current to earth, through a tree or other structure. The inclusion of a series inductance is a worst-case condition for the simulation because it reduces the di/dt and lowers the peak values of the transient currents.

Considering the short-circuit impedance of the phase-to-tower as resistive and constant, with the value of 1.5 Ω (used on handbooks), is a simplification that is conservative for the purpose of the simulations. In 80% of all faults, the arcing phenomenon occurs and the arc resistance is a nonlinear function of the arc/fault current and the arc length [101]. Nevertheless, its value is low (usually less than 1.5 Ω) and the arc resistance has little effect on the values of the currents of phase-to-ground and phase-to-tower short-circuits.

Appendix B

The parameters of the direct stroke simulation (one shield wire)

Figure B 3 shows the dimensions and the position of each cable of the lattice steel tower modeled in the simulations. The towers are represented as distributed parameter transmission lines with surge impedance of 150Ω , calculated using the conical shape method [25] (35 m high and square base with 8 m of side). The propagation velocity in the towers is 2.5×10^8 m/s [25]. The phase cables and shield wires were modeled by the Line/Cable objects (LCC) of ATPDraw program (Jmarti model).

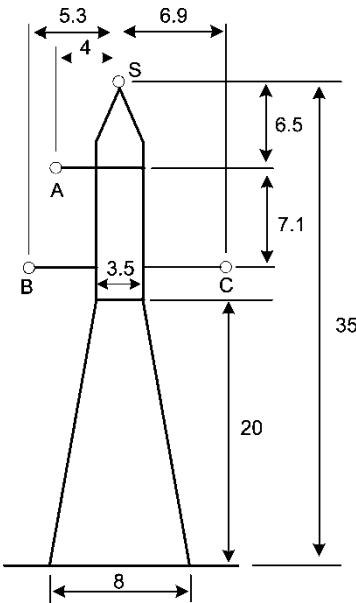


Figure B 1 - Tower dimensions (m) and the positions of the phase cables (A, B, and C) and the shield wire (S) (m).

This simulation has been done with 18 towers (5 km transmission line) shown in Figure B 2. From tower 1 to tower 8, and from tower 12 to tower 18, the spans are 300 meters each. From tower 8 to tower 12, the spans are 200 meters, 400 meters, 100 meters, and 200 meters, respectively. The tower grounding resistances of towers 1 to 8, and of towers 12 to 18, are 20 ohms. For towers 9, 10 and 11 they are 5 ohms, 30 ohms, and 5 ohms, respectively. The

stroke positions include the top of the tower and the shield wire at the middle of the span. A stroke position on the structure of tower 11, below the coil, was also included. Other stroke positions, between the top of the tower and the middle of the span, were simulated although they are not shown to simplify the table. However, they were used in the analyses. The value of soil resistivity was considered to be 2000 $\Omega\cdot\text{m}$, which is a typical value for the high resistivity soil in our State (Minas Gerais) [102].

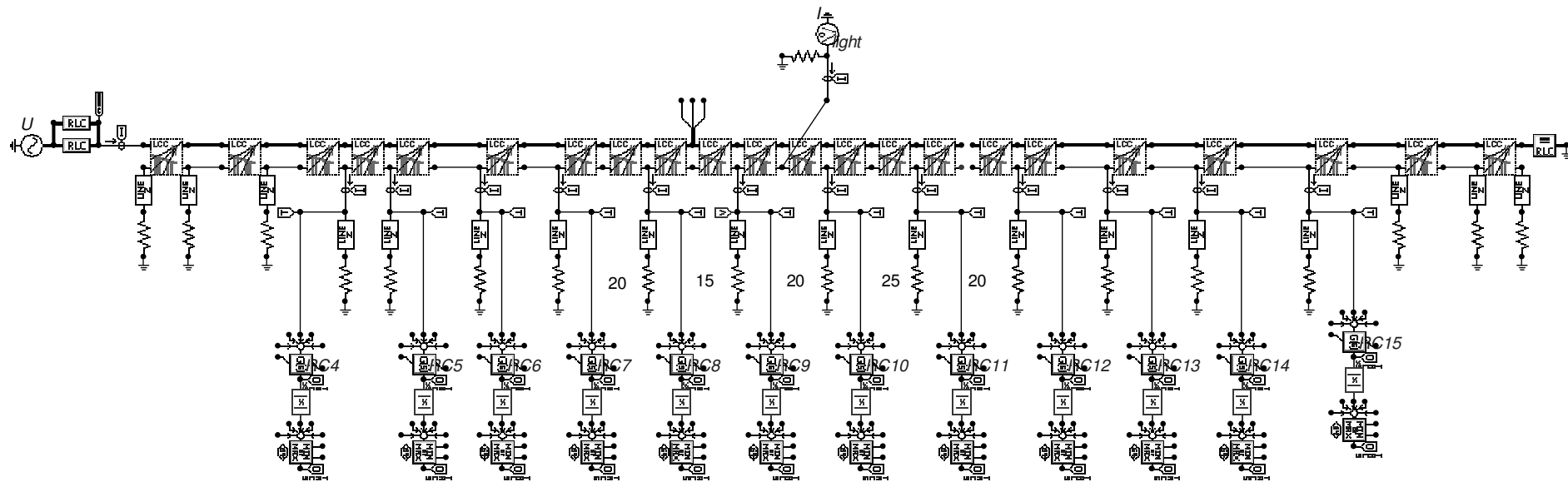


Figure B 2 - The simulation diagram of a direct stroke to shield wire.

The value of 20 ohms, used for most of the tower footing resistance, is a typical limiting value for the transmission lines in Brazil [103]. Tower footing impedance is modeled as a simple linear resistance as suggested in [104]. This is a reasonable simplification for the objective of our simulations. For the simulated lightning stroke, it was chosen the recommended waveshape by CIGRE guidelines with amplitude of 30 kA, with a front time of 2 μ s and a tail time of 50 μ s (Figure B 3).

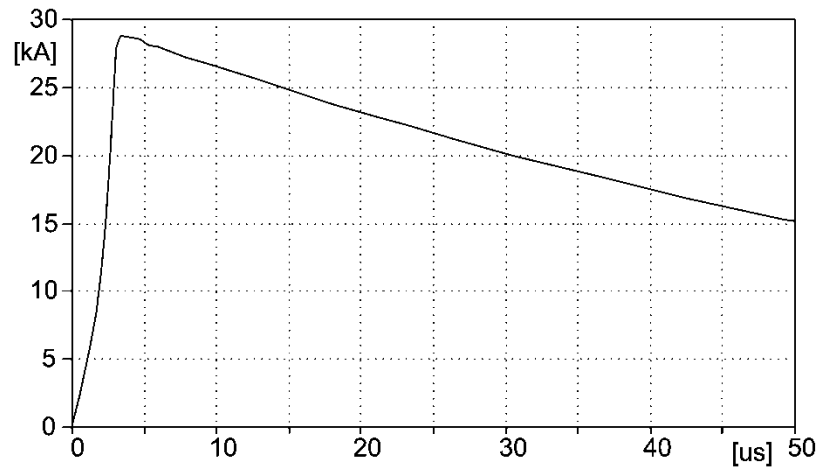


Figure B 3 – Shape of the lightning stroke current used in the simulations.

Appendix C

The parameters of the direct stroke simulation (two shield wires)

Figure C 1 shows the dimensions and the position of each cable on the lattice steel tower modeled in the simulations. The towers are represented as distributed parameter transmission lines with surge impedance of 135Ω , calculated using the method recommended by IEEE [26]. The propagation velocity in the towers is 2.5×10^8 m/s. The phase cables and shield wires were modeled by the Line/Cable objects (LCC) of ATPDraw program (Jmarti model).

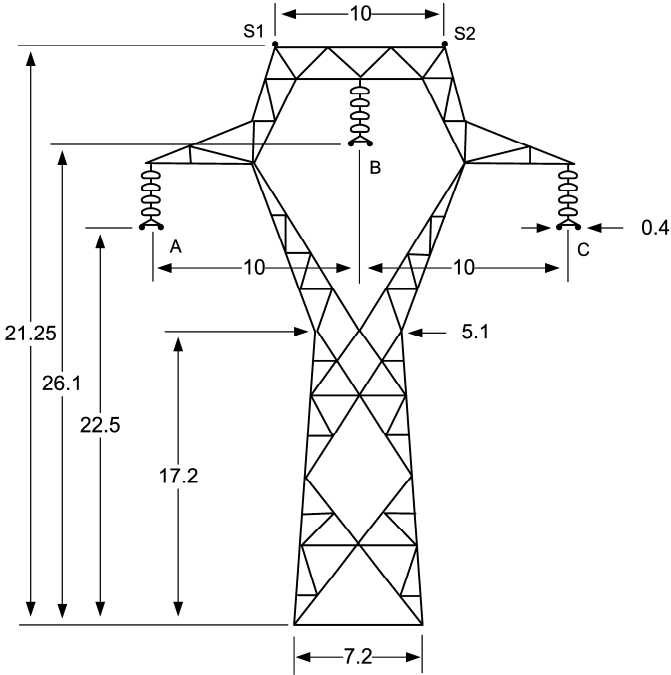


Figure C 1 - Tower dimensions (m) and the positions of the phase cables (A, B, and C) and the shield wires (S1 and S2) (m).

This simulation has been done with 42 towers (11 km transmission line) plus 20 km LCC sections at each end as line terminations (total length of 52 km). The currents were

analyzed on 16 towers at the middle of the simulated power line and we show only the result of eight towers numbered T1 to T8 in the tables.

The spans between all towers but T2 to T7 are 300 meters in length. The spans T2-T3, T3-T4, T4-T5, T5-T6 and T6-T7 are 200 meters, 400 meters, 100 meters, 200 meters and 100 meters in length, respectively. The tower grounding resistances of T2, T3 and T5 are 40 ohms, 5 ohms, 30 ohms and 15 ohms, respectively. All other towers have grounding resistance of 20 ohms. The value of soil resistivity was considered to be 1000 Ω .m, which is a typical value in Brazil [102].

Tower footing impedance is modeled as a simple linear resistance as suggested in [104]. This is a reasonable simplification for the objective of our simulations. For the simulated lightning stroke, it was chosen the recommended waveform by CIGRE guidelines [92] with amplitude of 40 kA, with a front time of 2 μ s and a tail time of 50 μ s.

Appendix D

The integrator of the fault simulation

In the simulations, the ATP equivalent circuit of the Rogowski coil is a TACS device simulating a coil with 300 turns, 7.5 cm toroid radius, 2 cm turn radius (K constant equal to 10^{-6}). The device includes the approximated frequency response in its transfer function. To integrate the signal, the output of the simulated coil passes through a low-pass first-order active filter with corner frequency of 1500 Hz and amplification factor equal to 20 (TACS device). The filter works as an integrator for frequencies well above 1500 Hz. The resulting integration restores most of the transient currents but attenuates the 60 Hz steady state currents and other low frequency components (Figure D 1).

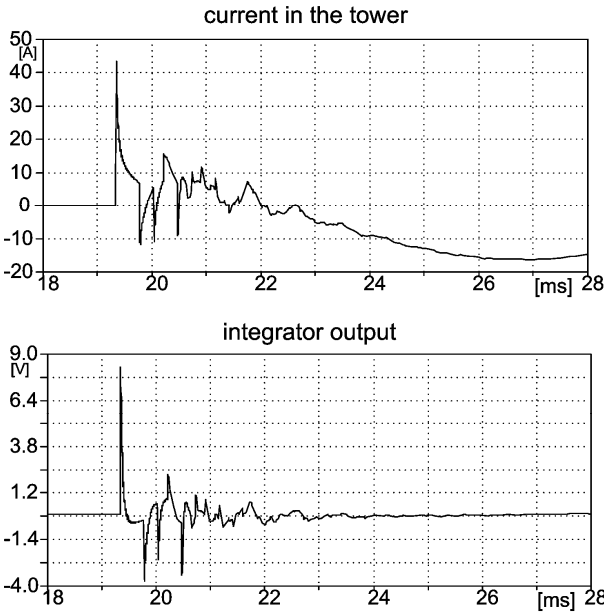


Figure D 1 - Current flowing in the tower and the corresponding output of the integrator.